GIULIA TORRIERI

DEVELOPMENT OF DRUG-LOADED ACETALATED DEXTRAN-BASED NANOPARTICLES FOR HEART TARGETING AND TREATMENT OF MYOCARDIAL INFARCTION

DRUG RESEARCH PROGRAM
DIVISION OF PHARMACEUTICAL CHEMISTRY AND TECHNOLOGY
FACULTY OF PHARMACY
DOCTORAL PROGRAMME IN DRUG RESEARCH
UNIVERSITY OF HELSINKI

Division of Pharmaceutical Chemistry and Technology
Faculty of Pharmacy
University of Helsinki
Finland

Development of Drug-Loaded Acetalated Dextran-based Nanoparticles for Heart Targeting and Treatment of Myocardial Infarction

by

Giulia Torrieri

ACADEMIC DISSERTATION

To be presented, with the permission of the Faculty of Pharmacy of the University of Helsinki, for public examination in Auditorium 2041, Biocenter 2, Viikinkaari 5, on November 4th, 2021, at 12 o'clock.

Helsinki 2022

Main supervisor	Professor Dr. Hélder A. Santos
	Drug Research Program
	Division of Pharmaceutical Chemistry and Technology
	Faculty of Pharmacy
	University of Helsinki
	Finland
Co-supervisors	Professor emeritus Dr. Heikki Ruskoaho
	Drug Research Program
	Department of Pharmacology and Pharmacotherapy
	Faculty of Pharmacy
	University of Helsinki
	Finland
	Professor and Vice-Rector Dr. Jouni Hirvonen
	Drug Research Program
	Division of Pharmaceutical Chemistry and Technology
	Faculty of Pharmacy
	University of Helsinki
	Finland
	Dr. Vimalkumar Balasubramanian
	Chemical and Pharmaceutical Development,
	Bayer Oy,
	Turku
	Finland
Reviewers	Dr. Pieter Vader
	University Medical Center Utrecht,
	Utrecht
	Netherlands
	Professor Maria J. Blanco Prieto
	University of Navarra
	Navarra
	Spain
Opponent	Professor Peter van der Meer
	Department of Cardiology
	University Medical Center Groningen
	Groningen
	Netherlands

The Faculty of Pharmacy uses the Ouriginal plagiarism checker to examine all doctoral dissertations.

Abstract

Cardiovascular diseases (CVDs), and in particular myocardial infarction (MI), represent a huge burden for society. Current therapies for MI are unfortunately unable to fully restore the lost function of the injured heart. In this regard, cell therapies and novel approaches, such as stimulation of cardiomyocytes proliferation and fibroblasts reprogramming, offer appealing alternatives, holding great potential for the regeneration of the infarcted heart. However, they suffer from degradation issues and poor pharmacokinetic properties. Nanomedicines can provide smart solutions to those challenges and have received increasing attention during the last decades. Moreover, they offer tools for minimally invasive treatments, an aspect that is very important for patient compliance and clinical translation. The ability of nanocarriers to target specific sites in the body is the most appealing feature of nanomedicines, which allows to increase the efficacy of treatments and reduce their systemic adverse effects. In the last decades, heart targeting was attempted by both passive strategies and conjugating different moieties on the surface of nanoparticles, *e.g.* angiotensin II type 1 (AT1) receptor and atrial natriuretic peptide (ANP). However, the constant pumping of the heart and the lack of selectivity of currently known heart targeting moieties, make heart targeting a challenging goal. Therefore, the aim of this thesis was to develop drug-loaded nanoparticles for improved targeting to the infarcted heart and its treatment. Acetalated dextran (AcDX) was chosen due to its pH-responsive properties, biocompatibility, biodegradability and ease of surface functionalization. Firstly, the heart targeting properties of ANP were improved by conjugating on the surface of putrescine modified-AcDX another peptide, lin-TT1. The conjugation of lin-TT1 peptide on the surface of the nanoparticles offered the ability to hitchhike the macrophages that are sequentially accumulating in the heart upon the onset of MI. *In vitro* studies showed the ability of the system to associate preferentially with M2-like macrophages, which have ant-inflammatory phenotype. Subsequent *in vivo* studies on a rat model of MI, confirmed the evidence of preferential accumulation of these particles in the infarcted heart after 7 days post-MI, and showed increased heart targeting ability compared to particles conjugated with only ANP peptide. Secondly, spermine-modified nanoparticles were developed and coated with a coordination complex, made of tannic acid (TA) and Fe^{3+} ions. TA was used for its proven heart targeting capability, which derives from its high affinity for components of the extracellular matrix, in particular collagen and elastin. *In vitro* studies proved the increased interaction of the system with cardiac cell cultures stimulated with transforming growth factor (TGF)-β, which induced higher collagen I production. The anti-fibrotic properties of TA were also confirmed by *in vitro* studies, showing the reduced expression of pro-fibrotic genes in cultured fibroblasts treated with the TA coated nanoparticles. Both systems demonstrated *in vitro* ability to induce cardiomyocytes proliferation due to the encapsulation of two small hydrophobic molecules, which stimulate cardiomyocytes to re-enter the cell cycle. Moreover, biocompatibility and pH-responsive release of the cargos were also evaluated. Overall, two AcDX-based nanoparticulate systems were developed for improved heart targeting and treatment of MI, bringing new insights about potential therapeutic advances in targeted delivery as a minimally invasive therapeutic approach for heart disease.

Acknowledgements

When I was a kid I have been asked multiple times what I wanted to became when adult. I remember having different answers and today I find some of them very funny. Once I remember I said I wanted to be a crazy scientist…..and apparently that's what I have been trying to achieve, even though I am still working on the scientist part.

Five and half years ago, when I was studying for my Master's in Italy at the University of Chieti I knew that one month after my graduation I would have gone to Finland for few months for the Erasmus traineeship program. I remember I was very excited, but scared at the same time and especially on the first day I arrived I felt completely lost, with no internet, no sense of orientation and with not so good English skills. I would have never thought that after the Erasmus I would have stayed in Finland to pursue a PhD and that I would fallen so much in love with the country! After almost five years, I am now in the end of the PhD journey. What an amazing, but challenging experience! Changing country allowed me to meet many different people and to get to know a new culture, quite different from my original one. I had many adventures, got new friends, lost some others, changed lovers, found new challenges and acquired new skills. Professionally, it was very stimulating and I got the opportunity to learn various techniques from different fields. However, research was not always easy. I have found myself multiple times dealing with failure, frustration, pressure for deadlines, uncertainty about the future. Many times I felt close to give up. Few times I cheered for successes. It certainly was a learning experience and I am sure I have changed and learnt some lessons through the years. Despite the toughness of some moments, I managed to go forward and reach the end. This would have not been possible without some determination from my side, but also, the help and support of the people that were close to me was fundamental to overcome obstacles. I am deeply thankful to all the people who helped me in the lab, but also outside, by simply making me smile during a bad day or by encouraging me when I was thinking I could not make it. Here, I want to express my gratitude to the ones who left a sign in my heart during these years and whose support was crucial for me.

I would like to start by acknowledging the Doctoral Program of Drug Research of the University of Helsinki, which granted me the possibility to pursue my doctoral degree. Thank you for giving me the opportunity to start this journey. Following, I would like to thank all the funding sources, that supported financially my studies: the EDUFI; the three years research grant from the University of Helsinki; the Paavo Nurmi Foundation and the Finnish Cultural Foundation.

Next, I want to express my deepest gratitude and admiration to my supervisor, Professor Hélder Santos, who accepted me in his lab for the first time in May 2017 as Erasmus student and then as doctoral candidate later in December of the same year. Your guidance and support were in many times crucial and I am profoundly grateful for all the times I needed you and you were there. Your passion and dedication for science are incredible and it is really impressive how you can handle so many things and people at the same time. Sometimes I ask myself if you are even human or if you have some secret super powers!

Then, I would like to thank my co-supervisors, Professor and Vice-Rector Jouni Hirvonen, Emeritus Professor Heikki Ruskoaho and Doctor Vimalkumar Balasubramanian. Professor Jouni, thank you for the recommendation letters for my grant applications, the useful scientific contributions to my manuscript and to this thesis, and for your support and positive attitude. Your encouragement helped me a lot during these years. Professor Heikki, I am deeply grateful for all the help, support and critical comments received during my PhD. Without you and Virpi all this work could have not been achieved. Thank you for having taught me so much about the heart and for being always encouraging. Vimal, thank you for supporting me since the

Acknowledgements

Acknowledgements

In Santos Lab we had many Erasmus studens and visiting PhDs coming and going during the years. Usually you never meet these people again once they leave and this is a bit sad. Luckily this is not always true. Special thanks to Sofia Moroni, Mattia Tiboni and Giulia Pallozzi for breaking the standard. When you were in the lab we shared many beautiful memories and I feel lucky that we still meet almost all the times I go back to Italy for my holidays.

I want to thank also the Masters's students I had the opportunity to supervise during my PhD. In particular, I would like to acknowledge Cláudia Carvalho. You did a great job in only three months and helped me a lot with the studies for my second manuscript. I will always remember your curiosity and diligence in the lab, as well as your cuteness and friendship.

Last Spring I had the opportunity to visit Professor Tambet Teesalu´s lab to learn phage display. Scientifically, it was a very stimulating and inspiring experience. I have learnt new things and got new ideas. Cherry on top of the cake, the lab mates were super nice. In particular,I would like to thank Maarja, Kaarel, Luca, Pablo and Lorena for giving me lot of wonderful memories (and Maarja was an awesome teacher). I really had fun with you guys and you made my thesis submission time less stressful. I am certain that the whole experience would have not been the same without you and I hope I will see you again (maybe in Tartu, who knows?).

After a day in the lab I love to release stress and frustration in the gym. One day I was there doing my stuff, when my at that time boyfriend came and introduced me to an Italian girl working in his neighboring lab. And that's how I met Anna. We became friends and since then we have had lot of fun, from playing board games to going to metal concerts and walks in nature. Our meetings are like a healing touch for me and I have always felt relieved after them. Thank you for being such a good friend to me. I extend my gratitude also to Francesco and Lyra. The three of you have often brightened my days.

Another friendship born semi-outside the lab was the one with Elena, my bubi. It is incredible that we have been studying in the same University and Faculty and that we have lived only 30 minutes apart, and we meet for the first time here in Helsinki. Your friendship has also healing powers and, especially in the last part of my PhD, you were a precious presence for me. You always listen to me and you understand me and don't judge me. Plus you are incredibly fun ☺ I love spending nights with you. I feel really lucky to have met you and I will always be there for you.

I want to thank also all the friends I have in Italy, whose friendship was able to erase kilometres of physical distance. In particular, I would like to thank my cousin Beatrice, Federica and Chiara, my companions of adventure, who are always ready to warmly welcome me back whenever I get back to Giulianova (my home town). Special thanks also to my childhood friend, Sara, who really was next to me since the beginning (if I am not wrong, we met for the first time when we were three years old). We have always been school mates until high school and we really shared lot of life experiences. University brought us in separate places and distance increased even more when I moved to Finland, but when I go home you always find time to see me, even multiple times and when we are together I always find the same Sara of my childhood. Now you became mother and I am extremely happy for you. I can´t wait to meet little Filippo when I am back. ☺

Another person that is very important for me and that I would like to thank now is Lucia (cutiii). We studied together at University and lived together under the same roof for more than three years. You became like a sister to me and know everything about me. We shared our secrets and we always understood each other. We also had plenty of adventures, starting from swimming lessons and spaghettate with people we just met to carnival trips to Offida. Despite the long distance and our busy lives, we still manage to be in touch and all the times we meet, it is like nothing has changed.

Acknowledgements

I would like to thank also my lovers for all the love and support they gave me in hard times and for all the lessons they taught me. I will always remember out times together, both good and bad ones. Thanks to you also I became stronger.

Last, but not least, I would like to thank my family, in particular my mom Claudia, my father Tiberio and my brother Lorenzo. Voi siete la mia unica certezza nella vita. Grazie per essermi stati sempre vicino anche quando ero in fase "Grinch" (lo so, a volte non è facile avere a che fare con me). Nonostante la distanza mi avete fatto sempre sentire il vostro amore e spero di essere anch'io riuscita a trasmettere il mio. Se oggi son qui è grazie a voi, a tutti i sacrifici che avete fatto, a tutti gli insegnamenti che mi avete dato e al supporto morale che avete fornito in questi anni. Non ci son parole per esprimere la mia gratitudine e il mio amore per voi. Spero solo che un giorno io possa ripagarvi e rendervi fieri di me. My family is the main reason that keeps me going forward. I would be lost without them.

Helsinki, October 2022

Giulia Torrieri

"Memento audere semper"

Gabriele D'Annunzio

"You have the power over your mind – not outside events. Realize this, and you will find strength"

Marcus Aurelius, *Meditations*

Table of contents

List of original publications

This thesis is based on the following publications, which are referred to in the text by their respective roman numerals (**I-III**).

I   **Torrieri G.**, Fontana F., Figueiredo P., Liu Z., Almeida Ferreira M., Talman V., Martins J. P., Fusciello M., Moslova K., Teesalu T., Cerullo V., Hirvonen J., Ruskoaho H., Balasubramanian V., Santos H.A., Dual-Peptide Functionalized Acetalated Dextran-Based Nanoparticles for Sequential Targeting of Macrophages during Myocardial Infarction, Nanoscale, 2020, 12, 4, 2350–2358.

II   **Torrieri G.**, Almeida Ferreira M., Shahbazi M-A., Talman V., Karhu T., Pohjolainen L., Carvalho C., Pinto J., Hirvonen J., Ruskoaho H., Balasubramanian V., Santos H.A., In vitro Evaluation of the Therapeutic Effects of Dual-Drug Loaded Spermine-Acetalated Dextran Nanoparticles Coated with Tannic Acid for Cardiac Applications, Advanced Functional Materials, 2021, 2109032.

III   **Torrieri G.**, Iqbal I., Liljenbäck H., Fontana F., Talman V., Teesalu T., Roivainen A., Saraste A., Hirvonen J., Ruskoaho H., Balasubramanian V., Santos H.A., In Vivo Evaluation of Macrophage Hitchhiking Nanoparticles for the Treatment of Myocardial Infarction, (submitted).

The publications are referred to in the text by their respective roman numerals (**I-III**). The papers are reprinted with kind permission from Royal Society of Chemistry (**I**), John Wiley & Sons, Inc (**II**).

List of additional publications

The list below presents additional manuscripts published during the doctoral studies, which are not included in the experimental section of this thesis:

I   Terracciano M., Fontana F., Falanga A.P., D'Errico S., **Torrieri G.**, Greco F., Tramontano C., Rea I., Piccialli G., De Stefano L., Oliviero G., Santos H. A.* & Borbone N.*, Development of Surface Chemical Strategies for Synthesising Redox-Responsive Diatomite Nanoparticles as a Green Platform for On-demand Intracellular Release of an Antisense Peptide Nucleic Acid Anticancer Agent, Small 2022, in press.

II   Liu Z., Lian W., Long Q., Cheng R., **Torrieri G.**, Zhang B., Koivuniemi A., Mahmoudzadeh M., Bunker A., Gao H., He H., Chen Y., Hirvonen J., Zhou R., Zhao Q., Ye X., Deng X. & Santos H. A., Promoting Cardiac Repair through Simple Engineering of Nanoparticles with Exclusive Targeting Capability toward Myocardial Reperfusion Injury by Thermal Resistant Microfluidic Platform, Advanced Functional Materials, 2022, 32, 36, 2204666.

III   Li J., Huang D., Cheng R., Figueiredo P., Fontana F., Correia A., Wang S., Liu Z., Kemell M., **Torrieri G.**, Makila E. M., Salonen J. J., Hirvonen J., Gao Y., Li J., Luo, Z., Santos H. A. & Xia B., Multifunctional Biomimetic Nanovaccines Based on Photothermal and Weak-Immunostimulatory Nanoparticulate Cores for the Immunotherapy of Solid Tumors, Advanced Materials, 2022, 34, 9, 2108012.

IV   Liu Z., Wang S., Tapeinos C., **Torrieri G.**, Känkänen V., Ibrahim N. E. A. A., Python A., Hirvonen J. & Santos H. A., Non-viral nanoparticles for RNA interference: Principles of design and practical guidelines, Advanced Drug Delivery Reviews, 2021 174, p. 576-612.

V   Figueiredo P., Lepland A., Scodeller P., Fontana F., **Torrieri G.**, Tiboni M., Shahbazi M-A., Casettari L., Kostiainen M., Hirvonen J., Teesalu T. & Santos H. A., Peptide-guided resiquimod-loaded lignin nanoparticles convert tumor-associated macrophages from M2 to M1 phenotype for enhanced chemotherapy, Acta Biomaterialia, 2021, 133, p. 231-243.

VI   d'Avanzo N., **Torrieri G.**, Figueiredo P., Celia C., Paolino D., Rebelo Correia A. M., Moslova K., Teesalu T., Fresta M. & Santos H. A., LinTT1 peptide-functionalized

liposomes for targeted breast cancer therapy, International Journal of Pharmaceutics, 2021, 597, p. 120346.

VII   Cheng R., Fontana F., Xiao J., Liu Z., Figueiredo P., Shahbazi M-A., Wang S., Jin J., **Torrieri G.**, Hirvonen J. T., Zhang H., Chen T., Cui W., Lu Y. & Santos H. A., Recombination Monophosphoryl Lipid A-Derived Vacosome for the Development of Preventive Cancer Vaccines, ACS Applied Materials & Interfaces, 2020, 12, 40, p. 44554-44562.

VIII   Li Y., Liu Z., Li L., Lian W., He Y., Khalil E., Makila E., Zhang W., **Torrieri G.**, Liu X., Su J., Xiu Y., Fontana F., Salonen J., Hirvonen J., Liu W., Zhang H., Santos H. A. & Deng X., Tandem-Mass-Tag based proteomic analysis facilitates analyzing critical factors of porous silicon nanoparticles in determining their biological responses under diseased condition, Advanced Science, 2020, 7, 15, p. 2001129.

IX   Vergallo C., **Torrieri G.**, Provenzani R., Miettinen S., Moslova K., Varjosalo M., Cristiano M. C., Fresta M., Celia C., Santos H. A., Cilurzo F. & Di Marzio L., Design, Synthesis and Characterization of a PEGylated Stanozolol for Potential Therapeutic Applications, International Journal of Pharmaceutics, 2020, 573, p. 118826.

X   Fontana F., Martins J. P., **Torrieri G.** & Santos H. A., Nuts and Bolts: Microfluidics for the Production of Biomaterials, Advanced Materials Technologies, 2019, 4, 6, 1800611.

XI   Martins J. P., **Torrieri G.** & Santos H. A., Expert Opinion on Drug Delivery, 2018, 15, 5, p. 469-479.¨

XII   Ferreira M. P. A., Talman V., **Torrieri G.**, Liu D., Marques G., Moslova K., Liu Z., Pinto J. F., Hirvonen J., Ruskoaho, H. & Santos H. A., Advanced Functional Materials, 18, 28, 15, 1705134.

Abbreviations and symbols

AcDXSp	Spermine modified-acetalated dextran
ACE	Angiotensin converting enzyme
ACK	Ammonium-chloride-potassium
ACN	Acetonitrile
AKT	Protein kinase B
Ang II	Angiotensin II
ANP	Atrial natriuretic peptide
APC	Allophycocyanin
ARB	Angiotensin receptor blockers
ARNI	Angiotensin receptor/neprilysin inhibitors
ATP	Adenosine triphosphate
BMDMs	Bone marrow derived macrophages
BMNC	Bone marrow mononuclear cells
BMP	Bone morphogenic protein
BSA	Bovine serum albumin
CAR	Chimeric antigen receptor
CCR2	C-C chemokine receptor type 2
CD	Cluster of differentiation
Cdc	Cell division cycle
CDK	Cyclin-dependent kinase
CDKi	Cyclin-dependent kinase inhibitor
CH_2Cl_2	Dichloromethane
CHIR	CHIR99021
CMs	Cardiomyocytes
CO_2	Carbon dioxide
CRISPR-Cas9	Clustered regularly interspaced short palindromic repeats associated protein 9
CRT	Cardiac resynchronization therapy
CSFM	Complete serum free medium
CSCs	Cardiac stem cells
CTGF	Connective tissue growth factor
cTnT	Cardiac troponin T
CVDs	Cardiovascular diseases
DAMPs	Damage-associated molecular patterns
DAPI	4',6-Diamidino-2-phenylindole
DGC	Dystrophin–glycoprotein complex
DMEM	Dulbecco's Modified Eagle's Medium
DLS	Dynamic light scattering
DMAP	4-Dimethylaminopyridine
DMEM	Dulbecco's Modified Eagle's Medium
DMSO	Dimethyl sulfoxide
DNA	Deoxyribonucleic acid
DOTA	S-2-(4-aminobenzil)-1, 4, 7, 10-tetraazacyclododecane-1,4,7,10-tetrater-butyl acetate
DRP-1	Dynamin-1 like protein
ECG	Electrocardiogram

ECM	Extracellular matrix
EDA-FN	Extra domain-A-containing fibronectin
EDC	1-Ethyl-3-(3-dimethylaminopropyl)carbodiimide
EDTA	Ethylenediamine tetraacetic acid
EE	Encapsulation efficiency
e.g.	For example
ELS	Electrophoretic light scattering
EPCs	Endothelial progenitor cells
EPR	Enhanced permeation and retention
ErbB	Epidermal growth factor receptor family
ESCs	Embrionic stem cells
EVs	Extracellular vesicles
FAM	5(6)-Carboxyfluorescein
FBs	Fibroblasts
FBS	Foetal bovine serum
FDG	Fluorodeoxyglucose
Fe	Iron
Fe_3O_4	Iron oxide
FGF	Fibroblast growth factor
FITC	Fluorescein isothiocyanate
Fox3p$^+$	Forkhead box P3 positive
FOXO	Forkhead box O
FR-β	Folate receptor β
FTIR	Fourier transform infrared spectroscopy
g	Relative centrifugal force
GSK3β	Glycogen synthase kinase 3 β
G-CSF	Granulocyte-colony stimulating factor
GM-CSF	Granulocyte-macrophage colony stimulating factor
HBSS	Hanks' balanced salt solution
HCAEC	Human coronary artery endothelial cells
HCl	Hydrochloric acid
H&E	Hematoxylin & Eosin
HEPES	4-(2-Hydroxyethyl)-1-piperazineethanesulfonic acid
HER	Human epidermal growth factor receptor
HF	Heart failure
HFrEF	Heart failure with reduced ejection fraction
HIF	Hypoxia-inducible factor
hiPSC	Human induced pluripotent stem cells
HPLC	High-pressure liquid chromatography
IFN-γ	Interferon gama
Ig	Immunoglobulin
IGF1	Insulin-like growth factor 1
IL	Interleukin
IMDM	Iscove's Modified Dulbecco's Medium
IMTP	Ischemic myocardium-targeted peptide
iNOS	Inducible nitric oxide synthase
I/R	Ischemia/reperfusion
i.v.	intravenous

KBr	Potassium bromide
KHCO$_3$	Potassium bicarbonate
LCA	Left coronary artery
LD	Loading degree
lin-TT1	AKRGARSTA
LNPs	Lipid nanoparticles
LPS	Lipopolysaccharides
LSD/KDM1	lysine demethylase 1
LV	Left ventricle
LVADs	Left ventricular assist devices
LVEF	Left ventricular ejection fraction
MAPK	Mitogen-activated protein kinase
MAPKAPK2	Mitogen-activated protein kinase-activated protein kinase
M-CSF	Macrophage colony-stimulating factor
MCP-1	Monocyte chemotactic protein 1
MECG	MesoEndo Cell Growth Medium
MES	2-(*N*-Morpholino)ethanesulfonic acid
MFI	Median fluorescence intensity
MI	Myocardial infarction
miRNA	Micro ribonucleic acid
MMPs	Matrix metalloproteases
MPS	Mononuclear phagocytic system
MRA	Mineralcorticoid receptor antagonists
MRI	Magnetic resonance imaging
MSCs	Mesenchimal stem cells
m-UNO	CSPGAK
Mw	Molecular weight
N$_2$	Nitrogen
NaBH$_4$	Sodium borohydride
NaCl	Sodium chloride
Na$_2$EDTA	Di-sodium ethylenediamine tetraacetic acid
NaF	Sodium fluoride
NEAA	Non-essential amino acids
NETs	Neutrophil extracellular traps
NH$_4$Cl	Ammonium chloride
NHS	*N*-Hydroxysuccinimide
NPs	Nanoparticles
NPR-A	Natriuretic peptide receptor-A
NRF2	Nuclear factor erythroid 2–related factor 2
O$_2$	Oxygen
OPA-1	Optic atrophy-1
o/w	Oil-in-water
P2	CSTSMLKAC
P3	CRSWNKADNRSC
PBMCs	Peripheral blood mononuclear cells
PBS	Phosphate buffered saline
PDI	Polydispersity index
PDK1	Phosphoinositide-dependent protein kinase 1

PE	Phycoerythrin
PEG	Polyethylene glycol
PerCP	Peridinin chlorophyll protein
PET	Positron emission tomography
PFA	Paraformaldehyde
PGE2	Prostaglandin E2
PHF	Perfluorohexane
PLA	Polylactic acid
PLGA	Poly(lactic-co-glycolic acid)
PPARδ	Peroxisome proliferator-activated receptor delta
PS	Phosphatidylserine
Putre-AcDX	Putrescine-modified acetalated dextran
PVA	Poly(vinyl alcohol)
R848	Resiquimod
RAAS	Renin angiotensin aldosterone
RBCs	Red blood cells
RGD	Arginine-Glycine-Aspartic acid peptide
ROS	Reactive oxygen species
RPMI	Roswell Park Memorial Institute
RT-qPCR	Real time quantitative polymerase chain reaction
RXFP	Relaxin family peptide
SB	SB203580
s.d.	standard deviation
SGLT2	Sodium-glucose co-transporter 2
SI	Supporting information
SORT	Selective organ targeting
SPECT/CT	Single photon emission computed tomography
SPIO	Superparamagnetic iron oxide nanoparticles
SSR-2	Somatostatin receptor subtype 2
TA	Tannic acid
TAMs	Tumor associated macrophages
TB	Trypan blue
TEA	Triethylamine
TEM	Transmission electron microscopy
TGF-β	Transforming growth factor beta
TIMPs	Tissue inhibitors of metalloproteinases
TNF-α	Tumor necrosis factor alpha
TSPs	Thrombospondins
Un-P-D	Undecylenic acid thermally hydrocarbonized PSi NPs modified with PEG and DOTA
USPIO	Ultrasmall superparamagnetic iron oxide nanoparticles
V2	Vasopressin 2
VEGF	Vascular endothelial growth factor
vs	versus
v/v	volume per volume
Wnt	Wingless-related integration site
w/v	weight per volume
YAP-TEAD	Yes-associated protein-transcriptional enhanced associate domain

Abbreviations and symbols

α-SMA	Alpha smooth muscle actin
ζ	Zeta

1   Introduction

The limited regenerative potential of human adult cardiomyocytes (CMs) makes cardiovascular diseases (CVDs) the leading cause of death worldwide, accounting for nearly 18 million deaths in 2019, corresponding to 32% of all global deaths.[1] Among the CVDs, ischemic heart disease represents the one with biggest incidence, causing over one third of all casualties.[1] The proliferative ability of the heart is lost in adult life, and thus, the massive cell loss caused by a myocardial infarction (MI) cannot be tackled, leading to an unfunctional remodeling of the cardiac muscle.[2,3] In this remodeling phase, the typical contractile tissue of the heart is replaced by a fibrotic scar, resulting in ventricular wall dilation, thinning and hypertrophy. This pathological state, known as heart failure (HF), can be tackled by current therapies, which are able to delay the progression of the disease and increase the survival rate of patients.[4]

However, conventional pharmacological treatments and chirurgical interventions are not able to fully restore the lost function of the heart, leaving millions of patients without an ultimate cure.[5,6] Hence, there is a urgent need for more efficient cures. Besides conventional pharmacological medicines and chirurgic interventions, the discovery of new therapeutic targets has opened new frontiers and challenges for the treatment of MI and HF, with new approaches being investigated and developed. Among the most novel and promising approaches there are cell therapies, stimulation of CMs proliferation, fibroblasts reprogramming, cardiac tissue engineering and nanomedicines.[7,8]

Cell therapies gave hope for the rehabilitation of the cardiac function, by potentially replacing the loss of cells after a MI. However, despite the initial enthusiasm generated by promising preliminary results, clinical trial showed their controversial inefficacy in producing a significant benefit in the restoration of the cardiac function.[9–12] Cardiac tissue engineering approaches instead, include the design of scaffolds or patches to be applied directly on the heart. Even though these approaches are advantageous because of the mechanical support they offer to the myocardium, their application requires invasive procedure and there is question if their direct contact with the heart can cause problems in the long term.[13–16] Nanoparticulate carriers have attracted increasing interest and they can be administered by minimally invasive routes, such as intravenously (i.v.) or orally, meeting requirements for a better patience compliance and potentially clinical translation. Moreover, the possibility to tune different properties of nanoparticulate carriers in order to achieve specific targeting and loading of different payloads, makes them multifunctional platforms for the imaging and therapeutic treatment of various diseases.[17] In particular, the most appealing property of nanoparticles (NPs) is their ability to target specific areas in the body. In recent years, different approaches have been proposed to achieve heart targeting, exploiting both passive and active strategies.[18,19] However, targeting the infarcted myocardium still represent a challenge because currently, a specific CMs marker, which could be used as targeting moiety selective enough to avoid potential dangerous adverse effects, has not been found yet.[20] Also, the constant pumping of the heart prevents the retention of the nanocarriers *in situ*, representing a mechanical obstacle for heart targeting NPs.[20]

In this thesis, both passive and active targeting approaches to improve the heart homing properties of nanoparticulate systems are explored. The heart targeting abilities of atrial natriuretic peptide (ANP) have been extensively exploited in the past.[19,21] However, it is known that ANP receptors are not exclusively in the heart, but they have been found also in other organs, such as kidneys, lungs, brain, testes, adipose tissue, adrenal gland tissues and vascular smooth muscle cells.[22] Among the different types of NPs, polymeric acetalated dextran-based NPs have been chosen due to their ability to deliver hydrophobic payloads,

safety profile and pH-responsiveness.[23] As passive targeting strategy, spermine-modified acetalated dextran (AcDXSp) NPs were coated with tannic acid (TA) because TA has showed heart targeting capability due to its affinity for components of the extracellular matrix (ECM), such as collagen and elastin, which are abundant in the infarcted myocardium.[24] The biocompatibility of the system was investigated in cardiac cells and interaction in cultures stimulated with transforming growth factor β (TGF-β) characterized by increased production of ECM. The pH responsive release of two small hydrophobic compounds for the stimulation of CMs proliferation, CHIR99021 and SB203580, was also evaluated at pH 7.4, mimicking the physiological environment, and pH 5, mimicking the endosomal space. Also, the anti-fibrotic properties of the TA coating were determined, as well as the ability of the system to induce proliferation of CMs *in vitro*.

An active targeting strategy was used here to improve the heart targeting ability of ANP. Considering the important role of inflammation in MI and the massive recruitment of inflammatory cells in the infarcted myocardium,[25,26] the surface of putrescine-AcDX (Putre-AcDX) NPs was modified with both ANP and linear-TT1 peptide. Lin-TT1 was chosen because of its ability to target tumor associated macrophages, as well as macrophages associated to the atherosclerotic plaques,[27–29] with the aim to hitchhike on macrophages and improve the heart targeting properties of ANP. The biocompatibility and cell−NP interactions of the system was evaluated *in vitro* in both macrophages and CMs of different origin. Then the ability of the compounds encapsulated, CHIR99021 and SB203580, to stimulate cardiac proliferation *in vitro* was investigated. Finally, *in vivo* biodistribution studies for assessment of the ability of the system to reach the infarcted heart were performed.

2   Literature overview

2.1. Coronary heart disease and therapeutic approaches

2.1.1. Cardiovascular diseases and their prevalence

CVDs are the leading cause of death worldwide. They consist of a group of disorders of the blood vessels and heart. Within this group there are coronary heart disease, hypertension, cerebrovascular disease, HF, peripheral vascular disease, congenital heart disease and rheumatic heart disease.[1] Official reports classify them as the main cause of death globally, causing an estimated 17.9 million deaths in 2019, and representing 32% of all global deaths.[1] Among these 17.9 deaths, 85% were due to heart attack and stroke, which are caused by a blockage that prevents blood from flowing to the heart or brain.[1] The most important risk factors at the base of CVDs are unhealthy diet, physical inactivity and excess use of tobacco and alcohol, which are result of the improved health conditions acquired in the 20th century.[1] In Europe, numbers are still astonishing, with 85 million people living such burden and 11.3 million new cases of CVDs recorded in 2015.[30] Also in Europe, CVDs account every year for approximately 45% of deaths and the overall costs to the EU economy are estimated to be up to €210 billion a year.[30] In Finland, despite the substantial decrease of incidence, CVDs still represent the main cause of death in 2020, accounting for around 30% of the total deaths.[31]

2.1.1.1   Limited regenerative potential of adult human heart

The heart functions as a pump and it has the important role of maintaining the circulation and supplying the other organs with blood. Although the function of the heart is crucial for life, the adult human heart has limited capacity to restore its function when insults occur.[2,3] This deficiency accounts for the high morbidity and mortality of ischaemic heart diseases. When MI occurs in mammals, there is either death or repair mechanisms, characterized by different phases.[3,32] If there is survival after MI, the massive death of cardiomyocytes (CMs), which consist of 1 billion of cells dying, generate an acute inflammatory response with recruitment of inflammatory cells and fibroblasts.[2] After few weeks, a large, collagen-rich scar tissue forms, with the aim of solving the loss of cardiac cells and preventing rupture of the cardiac wall.[2] This fast solution thoug is causing weakening of the cardiac tissue and initiating a compensatory pathologic remodeling of the heart.[2]

These injury-induced repair processes differ between species and in some animals can actually lead to regeneration of the tissue.[3] Indeed, while mammals have poor cardiac regenerative abilities, certain amphibian and fish species, like the zebrafish (Danio rerio), have shown robust regenerative capacity post heart injury.[3,33–39] Interestingly, the regenerative capacity not only differs between species, but also between genetically identical organisms at different life stages. For example, it is known that mice retain some ability of regenerating the heart within 7 days post birth,[40,41] with some evidences that this capacity is actually restricted to the first 2 days after birth.[42] Similarly to rodents, there have been reports of new-born humans recovering after infarction.[43,44] Adult mammals and zebrafish, as well as new-borns, share the same repair process, but there are differences, that lead adult mammals to form scar tissue, while zebrafish and new-borns are able to regenerate the heart. In **Figure 1** the main differences between regenerating and non-regenerating hearts are summarized. When MI occurs, adult mammals prevent heart rupture and direct death by deposition of an extracellular matrix (ECM) network.[32] This process can be divided into three phases: the

inflammatory phase (which will be discussed in detail in the next paragraph); the proliferative phase and the maturation phase.[32] During the inflammatory phase, the necrotic tissue is cleared away by the activity of matrix metalloproteases (MMPs) and the recruited inflammatory cells,[45,46] while the enhanced permeability of blood vessels close to the damaged area allow the accumulation of fibrinogen, forming a provisional fibrin-based matrix network.[47,48] In the following proliferative phase, the proliferating (myo)fibroblasts, together with macrophages, replace the fibrin-based network with fibronectin and collagenous type-III filaments.[49–51] Finally, in the maturation phase, type-I collagen filaments, which are highly cross-linked and provide robust structural integrity, replace the type-III collagen fibers, creating a permanent stiff scar.[52,53]
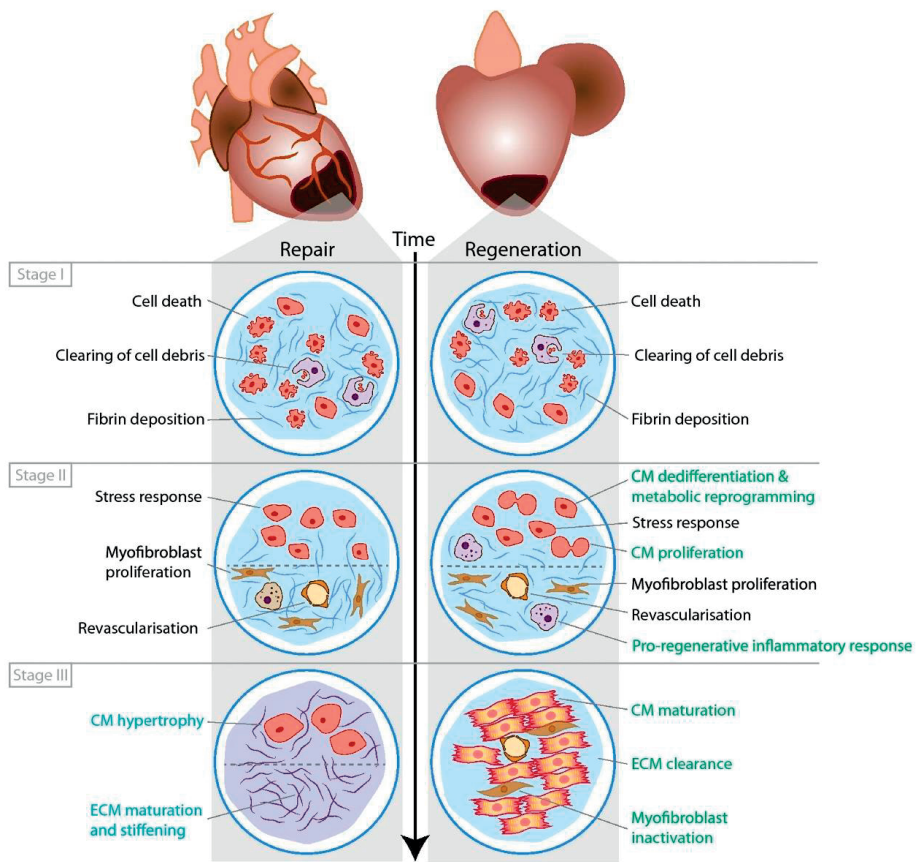
Figure 1. Comparison between repair and regenerative responses. Copyright© 2021 Springer Nature. Reprinted with permission from ref.[3]

The (myo)fibroblasts of the regenerating zebrafish heart not only arise from resident fibroblasts, but are also derived by trans-differentiation of epicardial[54,55] and endocardial cells.[56] These fibroblasts are gradually de-activated as regeneration progresses to prevent excessive

fibrosis.[55] Differences in the ECM composition, early deposition and clearance kinetics in the zebrafish need still to be elucidated. Another difference between zebrafish and adult mammals in the heart regenerative process is that zebrafish has shown the recruitment of a Wt1^{+} macrophage sub-population, which displays a pro-regenerative transcriptomic signature.[57] Also, there is evidence that in the zebrafish, the adaptive immune system plays an important role in the regenerative process.[58] Revascularization also differs between regenerating and repairing tissues. While in adult mammals angiogenesis starts as early as the inflammatory phase, but the new vessels become obsolete when scar is forming,[59,60] in zebrafish the vessels are maintained and support the newly formed CMs.[3] Another difference resides in the way CMs counteract the reduced function of the heart after MI. In the non-regenerating heart, CMs tend to grow in size, initiating an hypertrophic response.[61,62] While hypertrophy represent a fast solution, it transforms into a problem later, resulting in HF.[61,62] The CMs populating the border zone go instead towards a dedifferentiation program, activating a stress response.[63,64] The regenerative heart instead, tackles the reduced functionality of the heart with an hyperplastic response.[65,66] Also in this case, CMs in the border zone go towards a more pronounced dedifferentiation, activating an embryonic gene program and switching from a fatty acid metabolism towards glycolysis dependent ATP production.[67,68] Finally, another characteristic responsible for the regeneration of the zebrafish heart is in the properties of the CMs nuclei. Indeed, zebrafish CMs are diploid and mononuclear, characteristics that are fundamental for the successful heart regeneration.[69–71] In adult humans the CMs are instead polyploid, while in murine species they are multinucleated.

In summary, despite there are many similarities between regenerating and non-regenerating hearts, distinct differences can be found. Precise management of these differences could hopefully one day unlock the regenerative potential of human adult heart.

2.1.1.2   Role of inflammation in MI

As discussed above, the inflammatory response taking place after MI has a huge impact on the outcome of MI. After MI the repair is taking place by a sequential recruitment and activation of different cell types.[25,26] Three different phases can be distinguished: An inflammatory phase; a reparative and proliferative phase; and a maturation phase.[25] A scheme of the different phases can be found in **Figure 2**.

The hypoxia occurring during ischemia affects the vascular permeability and facilitates leukocyte infiltration, while causing the massive death of cardiac cells by necrosis and apoptosis.[26,72] Despite that restoration of the blood circulation seems to be solution to the necrotic process, it might result in further damage, known as ischemia reperfusion (I/R) injury, as a result of abrupt reoxygenation, reactive oxygen species (ROS) generation, and activation of the complement pathway.[26,72–75] Necrotic cells release danger signals, called danger-associated molecular patterns (DAMPs), activating the innate immune pathways and triggering inflammation.[75–78] The first cells that are recruited in the infarcted area are the neutrophils,[26,79] reaching the infarcted area in the first 24 h, attracted by DAMPs, cytokines, chemokines, endogenous lipid mediators (*e.g.*, prostaglandin E2, leukotriene B4), histamine and complement components.[80–82] The extravasation of neutrophils across the microvasculature is mediated by binding of leukocyte integrins to endothelial adhesion molecules.[83] Once infiltrated, the neutrophils release proteolytic enzymes, contributing to the clearance of the wound from dead cells and matrix debris. They might also amplify the immune response by secreting inflammatory cytokines.[84] Shortly after the neutrophils recruitment, monocytes are attracted to

the infarction site. Monocytes are recruited in two waves.[85] The first wave of recruitment in mice is characterized by accumulation of pro-inflammatory Ly6C^{hi} monocytes, mediated by activation of the monocyte chemotactic protein 1 (MCP-1)/CCR2 axis.[85,86] These pro-inflammatory monocytes peak at day 3 post-MI and give rise to macrophages and dendritic cells.[87,88] They exert proteolytic and inflammatory actions by secretion of tumor necrosis factor alpha (TNF-α), interleukin (IL)-1b, myeloperoxidase, MMPs, cathepsins and plasminogen activator urokinase, and phagocyting dead cells and debris.[25,87] The second wave of monocyte recruitment is characterized by increasing accumulation of anti-inflammatory Ly6C^{low} monocytes, peaking around day 7 post-MI.[25,85] In this second phase tissue repair is promoted, by secretion of anti-inflammatory, pro-fibrotic and angiogenic factors (*e.g.*, IL-10, transforming growth factor (TGF)-β, and vascular endothelial growth factor (VEGF)).[25,85] A well coordinate bi-phasic monocyte response is necessary for successful healing.[25,87]
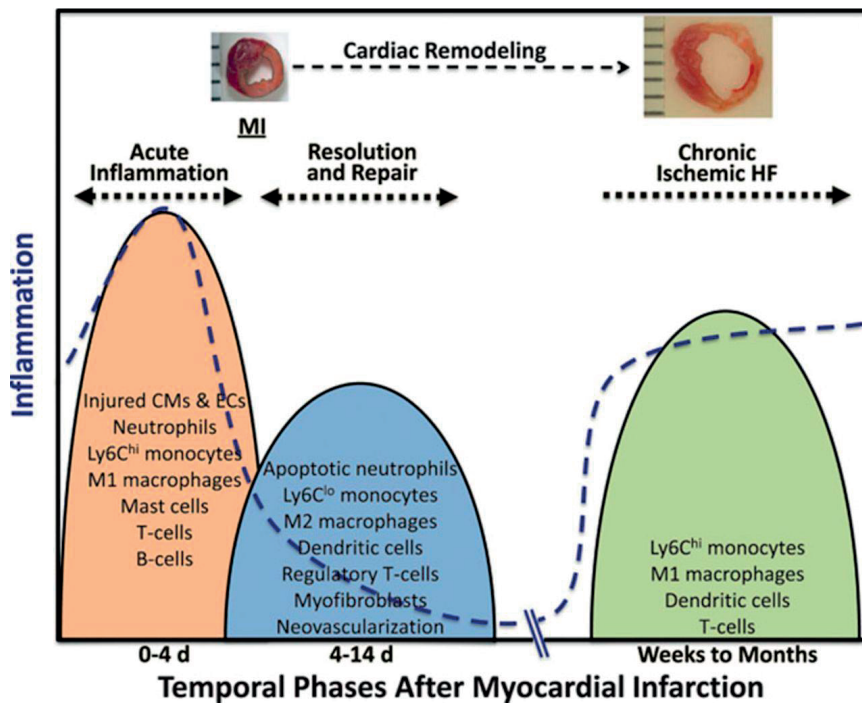
Figure 2. Phases of the repair process in mice after MI with correspondent description of the different inflammatory states. Copyright© 2016, Wolters Kluwer Health. Reprinted with permission from ref.[25]

Moreover, both phases derive from Ly6C^{hi} monocytes. They are first recruited in the infarct site during the pro-inflammatory phase and then they switch phenotype to Ly6C^{low} and proliferate during the reparative anti-inflammatory phase.[85,89] T cells are also recruited in the infarcted site, but their mechanism of action and contribution to the resolution or worsening of the function of the infarcted heart is still not very clear. T-lymphocytes, including CD4^{+} and CD8^{+} T-cells, Foxp3^{+} regulatory cells, invariant natural killer T cells, and γδT-cells, infiltrate the heart after MI, peaking during the reparative phase, around day 7 post MI.[90–94] Studies have demonstrated that CD4 helper T cells are activated in MI as response to autoantigens and take

part in wound healing, resolution of the inflammation and scar formation, limiting adverse remodeling.[90,95] However the type and nature of the autoantigens still remains to be elucidated. Regarding the role of CD8^{+} T-cells, recent findings show that CD8^{+} T-cells are recruited into the myocardium following MI, are activated and release Granzyme B.[96] In this way, CD8^{+} T cells fostered adverse ventricular remodeling with their pro-apoptotic functions.[96] Interestingly, studies with a Cd8[atm1mak] mice, a genetically modified mouse model characterized by CD8^{+} T-cell deficiency, CD8^{+} T-cells have been shown to play a dual and contradictory role.[97] Indeed, animals lacking functional CD8^{+} T-cells had increased cardiac rupture despite having better overall survival after MI.[97] Other evidences instead, describe the presence of a subset of CD8^{+} T-cells expressing the type 2 angiotensin II (AngII) receptor, which might be protective.[98] The proliferative phase of cardiac repair is followed by scar maturation, characterized by cross-linking of the extracellular matrix, and deactivation of reparative cells, which may undergo apoptosis.[25] After healing, in both humans and animal models with MI, a subset of those afflicted will exhibit late progressive ventricular dilatation and HF, a state characterized by chronic inflammation.[99] Histopathology studies of failing hearts showed increased presence of tissue macrophages and T-lymphocytes, and augmented adhesion molecule expression in endothelial cells.[100] Discovering the precise roles and mechanism of action of the different protagonists taking part in the inflammation following MI, could provide new therapeutical targets to find a cure for MI and save the lives of millions of people.

2.1.1.3 Heart failure and fibrosis

HF is a major health and socio-economical burden, affecting over 23 million people around the world[101,102] – a number expected to increase due to the aging population.[103] HF is the main consequence of MI, caused by persistent activation of fibrotic processes and remodeling of the myocardium, including areas not directly affected by the MI. After MI, the mammalian heart is unable to replace the huge loss of CMs and instead, starts forming a scar. While the initial replacement fibrosis is aimed at forming a scar and prevents the rupturing of the ventricular wall after an ischemic insult,[104,105] in HF the activation of reactive fibrotic processes in the infarct border zone and in the remote uninjured myocardium, leads to increased ventricular stiffness, altered chamber compliance and impaired function of the cardiac tissue.[4,106] Moreover, scar formation and interstitial fibrosis also interfere with the normal electrical function of the heart thus predisposing to arrhythmia.[107]

HF is characterized not only by excessive fibrosis, but also hypertrophy of CMs, infiltration of inflammatory cells and chronic activation of pro-inflammatory signals, increased ROS production, endothelial dysfunction and renin-angiotensin-aldosterone (RAAS) pathways activation.[106] As described above, CMs go towards hypertrophy in response to damage with the aim to compensate the loss of cells following MI. However, this response might progress to a degeneration state with induction of structural changes in CMs, such as loss of myofibrils, disorganization of cytoskeletal and membrane-associated proteins, enlargement of the cytoplasm and nuclei, grouping of small-sized mitochondria, and proliferation of T tubules.[108–110] All these features have shown to have a key role in the pathogenesis of cardiac contractile dysfunction.[109,110] Concomitantly with the hypertrophy of CMs, after MI there is an intensive remodeling of the ECM. The ECM consists of a highly dynamic microenvironment composed by a network of fibers, different cell types, matrix proteins, and signaling molecules that play a fundamental role in maintaining the heart function and propagating the electrical contractile forces throughout the heart.[111–113] Collagen is the main structural component of the ECM.

There are different types of collagen, but the cardiac ECM is mainly composed by collagen I and III (over 80 and 10% respectively).[114] Type I collagen is characterized by tensile strength and provides rigidity, determining the cardiac stiffness.[115] Type III collagen, instead, confers elasticity to the ECM by forming a fine network of distensible fibers.[116] After MI, there is alteration in the concentration of collagen with increase of collagen I abundance, alteration of the ratio between type I and type II collagen, crosslinking and increased rigidity, and changes in the fibers alignment.[114,117–119] All these features contribute to the establishment of fibrosis and scar formation and they take place both in the site of injury (with scar formation) and in areas of the heart not directly affected by the MI, that undergo towards interstitial fibrosis. The main producers of ECM are (myo)fibroblasts, a specific type of fibroblast with contractive properties due to expression of alpha-smooth muscle actin (α-SMA) microfilaments (**Figure 3**).[120–122]
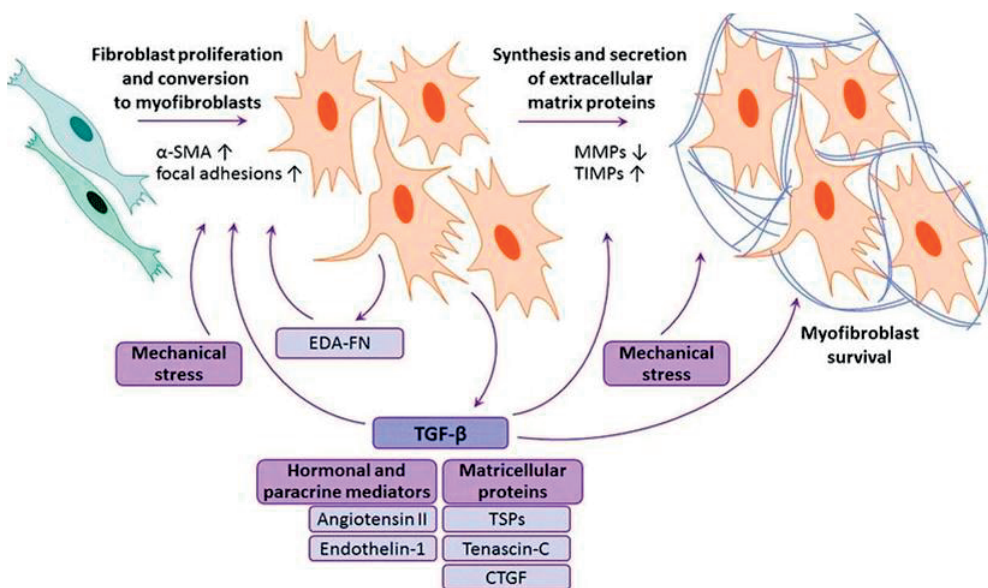
Figure 3. Activated (myo)fibroblasts can contract due to expression of α-SMA and they are the responsible for ECM deposition. Abbreviations: TSPs, thrombospondins; TIMPs, tissue inhibitors of metalloproteinases; CTGF, connective tissue growth factor; EDA-FN, extra-domain-A-containing fibronectin. Copyright© 2016 Springer Nature. Reprinted with permission from ref.[4]

They are activated and recruited in the infarct site after 3-4 days post-MI by expression of TGF-β_1.[123] TGF-β is in turn up-regulated by mechanical stress, Ang II and endothelin I, revealing the pro-fibrotic roles of RAAS and endothelial dysfunction in the cardiac remodeling.[123–125] Pro-inflammatory cytokines, like TNF-α, IL-1, and IL-6, also play an important role in the remodeling of the ECM and they exert either beneficial or detrimental effects depending on their concentration and on the acuteness versus chronicity of the primary insult.[99,126–129] In particular, TNF-α alters the function of matrix MMPs and their inhibitors (TIMPs) causing imbalance between deposition and synthesis of ECM.[123,130,131] IL-1, IL-6, and IL-18 have a role in the hypertrophic growth response of cardiac myocytes.[132–135] Left ventricular (LV) remodeling is characterized by fibrillar collagen degradation, ECM remodeling, progressive ventricular

dilatation, and wall thinning, as a result of the upregulation of MMPs and down regulation of TIMPs.[123] Production of ROS (including superoxide anions, hydrogen peroxide, and the hydroxyl radical) may cause CMs necrosis, consequently boosting the inflammation and the scar tissue formation.[136–138] Altogether, chronic inflammation, hypertrophy of myocytes, formation of scar tissue and development of interstitial fibrosis in non-infarcted areas, all contribute to LV remodeling and impaired cardiac function.

2.1.2 Developed therapies for the treatment of myocardial infarction and heart failure

To date the pharmacological treatment of MI and HF is unsuccessful in restoring completely the function of the myocardium.[5,6] The first aid treatment after MI usually consists in chirurgical interventions aimed at restoring the blood circulation to the heart. There are established guidelines telling how to proceed according to the patient situation.[139,140] Once the patient is stabilized, administration of pharmacological treatment will start. At the same time, novel approaches, such as cell therapies, cellular engineering, fibroblasts reprogramming, stimulation of CMs proliferation and the development of materials, have been developed.[7,8] In the next paragraphs I will explore the current therapies that are clinically approved, as well as the novel strategies that are being developed, but not yet clinically translated and on the market.

2.1.2.1 Clinically approved therapies and pharmacological and surgical treatments current in use

As previously stated, the therapeutic options clinically available for MI patients are aimed at contrasting the LV remodeling and preventing the recurrence of ischemic events, while trying to improve the contractility of the cardiac muscle and reduce the congestion.[5] Current therapies have been developed with the aim to alter the processes causing LV remodeling, such as upregulation of different paracrine, neuroendocrine and autocrine factors, hemodynamic imbalance and LV wall stress.[5,6] In clinical practice, the best treatment for patients affected by HF with reduced ejection fraction (HFrEF) consist in the administration of an angiotensin receptor/neprilysin inhibitor (ARNI), a mineralcorticoid receptor antagonist (MRA), a beta blocker and a sodium-glucose co-transporter 2 (SGLT2) inhibitor.[141,142] Different types of diuretics are also used to keep fluids from collecting in the body and reduce congestion.[142–144] Digoxin may be considered in patients with symptomatic HFrEF in sinus rhythm despite treatment with an angiotensin-converting enzyme (ACE) inhibitor (or ARNI), a beta-blocker and an MRA, to increase the strength of the heart contractions and reduce the risk of hospitalization..[142–144] Hydralazine and isosorbide dinitrate can be used as combination in patients who cannot tolerate any of ACE inhibitors, ARNI or angiotensin receptor blocker (ARB), to relax the blood vessels and thus reduce the blood pressure and risk of death.[142–144] Ivrabadine, an inhibitor of the I_f channel in the sinus node, is used to slow the heart rate in patients in sinus rhythm, with a left ventricular ejection fraction (LVEF) <_35% and with a heart rate >_70 b.p.m..[142] Changing life style, with adoption of a healthy diet and exercise, is also recommended to patients in order to prevent the disease from worsening. When the disease reaches advanced stages, the use of mechanical support devices is considered and, ultimately, heart transplantation.[145,146] Common implantable devices include pacemakers, cardiac resynchronization therapy (CRT), cardioverter defibrillators and left ventricular assist devices (LVADs).[146] A pacemaker is usually installed when the heart of the patient beats too slowly,

and it works by constantly monitoring the heart rate, while sending electrical pulses to the heart in order to achieve a regular beating.[146] CRT is a particular type of pacemaker instead, adopted when the walls of the LV chamber contract asynchronically.[146] Cardioverter defibrillators are also a type of pacemaker and they send an electrical impulse to the heart when it start beating too fast.[146] LVADs are instead battery-operated, mechanical pump-like devices that are implanted in the patient body and help the heart to maintain pumping ability.[146] It is often used when the HF is severe and the patient is waiting for heart transplant. Ultimately, heart transplant is the last resource for patient suffering from HF. However, limited availabilities of hearts and organ rejection issues make this approach not suitable and/or available for all the patients and a high-risk procedure.

2.1.2.2 Novel therapeutical approaches

To date there is no cure for MI and HF and these burdens kill millions of people each year. The current therapies listed above leave an unmet need and give reason for research of new therapeutic approaches aimed at restoring the lost function of the heart. Increasing knowledge of the complex pathophysiological mechanisms responsible for the loss of contractility of the cardiac muscle have helped finding new therapeutical targets and strategies. Besides the discovery of new small molecules, research is focusing also in the investigation of the efficacy of biologics, cell therapies, biomedical engineering approaches, gene therapy, nanoparticulate systems and combination of them.

Table 1 summarizes the main therapeutic approaches under development for the treatment of MI and HF, with the exception of cell therapies and nanoparticulate systems, which will be described respectively, in brief here and in detail in the next section.

Cell therapies have been developed during the years with the aim to replenish the loss of CMs, and have been validated by promising pre-clinical results. Among the different cell sources, skeletal myoblasts, bone marrow mononuclear cells (BMNCs),[147] hematopoietic stem cells (HSCs),[148] endothelial progenitor cells (EPCs),[149] mesenchymal stem cells (MSCs),[149] and pluripotent stem cell (PSC)-derived CMs (PSC-CMs) have been used. However, despite the number of past and ongoing clinical trials, the desidered results have not yet being achieved. Moreover, there have been multiple clinical trials showing paradoxical result, and different hurdles hinder the clinical translation of such therapies.[11,12] Among those, poor cell engrafment and survival, the immaturity of the cell types used for transplant and the risk of teratoma formation and engrafment rejection, are the most important ones.[11,12] As showed also in the table below, biomedical engineering approaches have been developed also to improve the engrafment of cells to the heart, but further investigations on the therapeutical outcomes and possible long-term risks are still needed.

In recent years, also chimeric antigen receptor (CAR) T cells have been used[150] or generated in vivo[151] to reduce the fibrosis in the infarcted area, representing a novel promising approach for the treatment of HF. However, further studies are needed to determine doses of such therapies, improve the targeting and minimize the possible toxic effects.

Table 1. Novel therapeutic approaches for the treatment of MI and HF.

Class	Drugs/cell types/materials	Mode of action	Efficacy	Refs.
Small molecules drug and biologics	• Omecamtiv mecarbil	• Cardiac myosin activator; increases stroke power	• Approved in February 2022	152
	• Pirfenidone	• Anti-fibrotic	• Phase 2	153,154
	• Carbacyclin	• Increases PPARδ activity, which activates β-cat via PDK1/AKT/GSK3β pathway	• *In vitro* proliferation of adult CMs	155
	• TT-10	• enhances YAP-TEAD activities and Wnt/β-catenin signaling, and activates NRF2 transcription factor	• *In vitro* stimulation of CMs proliferation and antioxidant properties	156,157
	• NRG-1	• Activates ErbB2-4 tyrosin kinase signaling	• *In vitro* stimulation of CMs proliferation	158
	• BIO, CHIR99021	• GSK-3 inhibitors.	• Induces proliferation of mammalian CMs	159,160
	• 5-azacytidine	• Induces CM differentiation of glycolytic cardiac progenitors	• Stimulation of CMs proliferation	161
	• SAG, NBI-31772, SB-203580, and CHIR99021	• Drive CMs proliferation	• Stimulation of CMs proliferation	162
	• Dorsomorphin	• Inhibits the BMP signaling and induces CM differentiation in mouse ESCs	• Stimulation of CMs proliferation	163
	• Sulfonyl-hydrazone	• Induces cardiac differentiation in murine PBMCs	• Stimulation of CMs proliferation	164
	• CHIR 99021 SB431542, parnate, forskolin and transcription factor Oct4	• Respectively GSK3β inhibitor, TGF-β signaling inhibitor, LSD1/KDM1 inhibitor, adenylyl cyclase activator, and reprogramming transcription factor	• FBs reprogramming into CMs	165
	• SB203580	• p38 MAPK inhibitor	• stimulation of CMs proliferation *in vitro* adult rat CMs	160,166
Gene therapy and RNA therapeutics	• miR-199a KO and miR-590 KO	• Hopx, Homer1c	• CMs proliferation	167
	• miR-204	• Jarid2	• CMs proliferation	168
	• miR-210	• APC	• CMs proliferation	169
	• miR-25	• FBXW7	• CMs proliferation	170
	• miR-1, miR-133, miR-208, miR-499	• HSP60, SREPB-1c, MYH7 and MYH7b respectively	• *In vitro* and *in vivo* FBs reprogramming	171,172
	• miR-1/miR-133a	• Osmr, Fgfr1	• CMs proliferation	173
	• OSKM (Oct4, Sox2, Klf4, c-Myc)	-	• *In vitro* reprogramming of FBs into CMs	174,175
	• GMT (Gata4, Mef2c, Tbx5)	-	• *In vitro* reprogramming of FBs into CMs	176
	• GHMT (Gata4, Hand2, Mef2c, Tbx5)	-	• *In vitro* reprogramming of FBs into CMs	177,178
	• miR208b-3p, ascorbic acid and Bmp	-	• *In vitro* reprogramming of FBs and implant of the tissue in MI area	179
Biomedical engineering	• Injectable fibrin biomatrix	• Transplantation of bone marrow mononuclear cells in the heart	• *In vivo* improved LV function recovery post-MI	180
	• Injectable fibrin scaffold	• Transplantation of skeletal myoblasts in the heart	• Decrease of infarct size in rats and induced	181

		neovasculature formation	
• Alginate microspheres	• Transplantation of human mesenchymal stem cells	• Preservation of LV function, increase of angiogenesis and improvement of cell survival.	[182]
• Chitosan-based injectable hydrogel	• ROS scavenging effect	• Suppression of oxidative stress injury	[183]
• Collagen-based matrices	• Transplantation of circulating progenitor cells	• Efficient transplantation	[184]
• Nanocellulose, poly(glycerol sebacate), and polypyrrole scaffold	• Delivery of cardioprotective drug and NPs	• Potential application for MI treatment	[185]
• Elastin-like recombinamers-based injectable hydrogel	• ECM mimic	• Reduced fibrosis, increased angiogenesis in ischemic region and improved cardiac function	[186]
• Collagen-based hydrogel	• Delivery of stem cells-derived EVs	• Improved cardiac function, decreased CM apoptosis, and reduced infarct size	[187]
• *In situ* forming fibrin scaffold	• Delivery of mesenchymal stem cells-derived EVs	• Improved cardiac function, reduced fibrosis and promotion of endogenous angiomyogenesis	[188]

Abbreviations: NPR-A: Natriuretic peptide receptor-A. NO: nitric oxide. V2: vasopressin 2. RXFP: relaxin family peptide. PPARδ: peroxisome proliferator-activated receptor delta. PDK1/AKT/GSK3β: 3-Phosphoinositide-dependent protein kinase 1/ protein kinase B/ glycogen synthase kinase 3 β. YAP-TEAD: Yes-associated protein-Transcriptional enhanced associate domain. NRF2: Nuclear factor erythroid 2–related factor 2. ErbB: Epidermal growth factor receptor family. BMP: Bone morphogenic protein. LSD1/KDM1: Lysine demethylase 1. FBs: Fibroblasts. MAPK: Mitogen-activated protein kinase. BMNC: Bone marrow mononuclear cells. EVs: extracellular vesicles.

2.1.2.2.1 Stimulation of cardiomyocytes proliferation

Mammalian hearts are fully differentiated organs with limited regenerative capacity, confined mainly to fetal and early postnatal stages of life.[2] Shortly after birth there is a transition from hyperplastic to hypertrophic growth, with CMs not anymore able to complete cytokinesis and becoming bi-nucleated cells.[189,190] Yet, recent evidence has shown that there is a CMs turnover in human adult heart ranging between 0.3% and 1% per year.[191] This turnover, despite promising, is not sufficient to generate a number of CMs of clinical relevance in case of injury. Hence, potential approaches to achieve meaningful CMs proliferation at injury sites consist in removal of cell cycle blocks and/or administration of drugs boosting CMs proliferation.[9]

The cell cycle consists of four phases (G1, S, G2 and M phases) and it is tightly regulated by cyclins, cyclin-dependent kinases (CDK) and cyclin-dependent inhibitors (CDKi). In particular, CMs proliferation is promoted by expression, complex formation and activation of various cyclins and CDKs (cyclin E, A B1 and D1, and CDK1, 2 and 4), while it is inhibited by increased expression of CDKi, including Cip/Kip (p21Cip1, p27Kip1, p57Kip2) and Ink4 family members (p15Ink4b, p16Ink4a, p18Ink4c, p19Ink4d).[9] For instance, immuno-depletion of p21Cip1 or deletion of CDKi p27Kip1 resulted in S phase progression in CMs.[192] Expression and activation by phosphorylation of FOXO transcription factors (Foxo1 and Foxo3) by IGF1/PI3K/AKT and fibroblast growth factor (FGF) 1 signaling pathways, promotes CMs cell cycle re-entry and proliferation.[193194] Similar cell cycle activation can be obtained also with growth factors and cytokines, such as periostin, neuregulin, FGF1, and oncostatin-M, as well

as induction of Hippo pathway.[158,166,195–197] Concentration of O_2 and metabolism also play a role in CMs proliferation, with hypoxia and glycolysis promoting CMs dedifferentiation and proliferation.[197] Another factor affecting the differentiation and ability of CMs to proliferate is the ECM composition. While adult CM are tightly connected between each other and they are organized in a relatively rigid scaffold composed mainly by collagen I,[198] fetal and early neonatal ECM is enriched in fibronectin and periostin and it favors CMs de-differentiation and proliferation.[195,199] Moreover, recent reports discovered that a major component of the fetal ECM is Agrin, which promotes cell proliferation through the disassembly of the dystrophin–glycoprotein complex (DGC) that sequesters YAP into the cytoplasmic compartment, thus inducing the activation of a YAP-related signaling mechanism.[200,201] Small drug molecules have also been investigated for the stimulation of CMs proliferation. Compared to growth factors and nucleic acids, these molecules possess various advantages, such as better diffusion through cell membranes, flexibility, ease of production and storage, and lack of immune response against them.[202]

Hence, in this thesis, I investigated the pro-proliferative effect of two small hydrophobic molecules, CHIR99021 and SB203580, which have shown synergistic ability to stimulate CMs proliferation.[160] CHIR99021 (for simplicity shortened as CHIR in the following text), is a Wnt activator. Wnt/β-catenin signaling has an essential role during the neonatal heart development and, in particular, despite it leads to cardiac differentiation at early developmental stages, it has the opposite effects in later stages.[203] Degradation of β-catenin in the cytoplasm is prevented by inhibition of the GSK3, which is achieved by activation of the Wnt pathway.[204] β-catenin is then able to translocate in the nucleus and once there, it regulates the expression of target genes. CHIR was identified as the most potent molecular inducer of human CMs proliferation, able to activate the cell cycle, as marked by the increased expression of Ki67, as well as to increase the CMs number.[205] SB203580 (for simplicity shortened as SB in the following text) instead, is a p38 MAPK inhibitor.[166] Activation of p38 resulted in differentiation of CMs and repression of cell cycle re-entry.[206] Inhibition of p38 instead, exhibited an up-regulation of cell cycles specific genes, such as cyclin A, and genes involved in mitosis and cytokinesis, including cyclin B, cdc2, and aurora B.[206] Moreover, it regulates neonatal CMs karyokinesis by increasing of almost 4-fold the percentage of phospho-histone H3 positive CMs.[206] Besides the ability to stimulate cell cycle entry in CMs, CHIR and SB have shown also ability to modulate inflammatory responses.[207,208] In particular, GSK3 inhibition by CHIR in a murine obesity model resulted in a decrease in the visceral adipose tissue of pro-inflammatory M1 macrophages and an increase of anti-inflammatory M2 macrophages, while reducing also the levels of circulatory inflammatory monocytes.[207] The anti-inflammatory effects of CHIR were partly driven by inactivation of STAT3, which was then followed by reduced production of free fatty acids, chemokines and apoptosis inhibitor of macrophage.[207] Inhibition of the p38 MAPK by SB instead, results in decreased production of pro-inflammatory cytokines, including TNFα, IL-1β, IL-6, and IL-8, and less induction of key inflammatory enzymes, including COX-2 and inducible nitric oxide synthase.[208]

Albeit the discovery of various therapeutics able to stimulate proliferation of resident CMs has created great excitement for the development of new treatments for MI and HF, it brings up questions regarding their involvement in tumor formation. Such treatments are designed to be short-term and thus have a transient effect. However, long-term exposure together with exposure to mutagens, as well as accumulation in off-target tissues, could lead to accumulation of mutations in different cell types and uncontrolled growth, and eventually formation of tumors.[7,202] Other issues related with the abovementioned therapeutics are their hydrophobicity (especially for small drug molecules), poor pharmacokinetics and possible

degradation inside our bodies.[7] Novel approaches and technologies are then needed to promote the clinical translation of these therapies.

2.2   Nanomedicines

2.2.1   Engineering nanoparticles for drug delivery

Despite the recent advances in MI treatments, the patience life expectancy is still relatively low, and novel approaches, such as stimulation of CMs proliferation, have difficulties to find a way to clinical translation, due to their potential side effects, instability of the active ingredients and poor pharmacokinetic profile.[7,202] In this regard, the advent of nanomedicines has brought excitement and hope for the establishment of efficient regenerative medicines therapeutics. Since Paul Ehrlich's definition of the "magic bullet" as drugs that go straight to their intended cell-structural targets,[209] there has been an increasing effort in the scientific community to create advanced drug delivery systems, aimed at curbing the drawbacks of conventional and developing drug therapies. In particular, nanoparticulate systems have been increasingly used over the years for both treatment and diagnostics/imaging of MI.[210,211] The main advantages brought by nanomedicines in the field are: (1) Targeting to the injured myocardium with reduction of potentially adverse effects of the payloads; (2) Possibility of less invasive administration routes; (3) Protection of degradation and short half-life of biologics; ability to deliver one or combination of drugs; and (4) Improvement of solubility and stability of cargos.[8,212]

The extreme versatility of nanoparticulate system offers researchers a wide variety of options for the engineering of carriers aiming at specific sites of the body or possessing particular features. NPs can be made of different materials and consequently, each nanoparticle type possess specific characteristics. NPs composition can influence their stability and biodistribution, as well as their optical and magnetic properties. In principle, nanocarriers can be classified as organic or "soft" (*e.g.*, lipid based and polymeric NPs) and inorganic or "hard" (*e.g.*, gold NPs, carbon nanotubes, porous silicon/silica NPs).[17,213] There are also biologically-derived nanoplatforms in which cell membranes (*e.g.*, cancer cell or red blood cell membranes) are used to prepare vesicles or coat other materials.[214–216] Combination of different materials are also reported in the formation of composites or hybrid platforms.[217–220] The main types of nanosystems are summarized in **Table 2** together with their correspondent advantages and disadvantages. In addition to composition, the physicochemical features of NPs, such as size, shape, surface chemistry and charge, can influence the NP−cell interactions and uptake, pharmacokinetics, biodistribution and half-life in the bloodstream upon administration.[221]

Size of NPs affects the biodistribution and fate of the NPs inside the body. Small NPs (< 5.5 nm) are rapidly excreted from the body by renal clearance, while NPs larger than 200 nm tend to accumulate in liver and spleen. If particles aggregate and their size is larger than 2 μm, they will accumulate instead in the lungs.[17,221–224] Extravasation through the vasculature is consequently achieved by NPs, whose size is between 20 and 200 nm. This effect, known as enhanced permeability and retention (EPR) effect has been exploited for both cancer and cardiovascular applications.[225,226] In addition, size of NPs determines also the way in which NPs are internalized by cells. Small NPs (60−200 nm) are usually internalized by different mechanisms, including clathrin- and caveolin-mediated endocytosis and clathrin and caveolin-independent endocytosis. NPs with size < 1 μm can be internalized non-specifically by micropinocytosis. Finally, large NPs are usually taken up by phagocytosis.[17,227–229]

As for the morphology, the most common NP's shape is spherical, but different kind of shapes have been produced, such as rods, stars, cubes, prisms, fibers. The shape of the NPs can influence their interaction with cells and hemorheological dynamics.[221,224,228,230,231] For instance, rod-shaped NPs showed tendency to marginate towards the vessel wall, and thus, had increased predisposition to extravasation compared to spherical counterparts.[17,221,224,231] Moreover, the aspect ratio (ratio between the height and width of the particle) of NPs, can influence their cellular uptake. Particles with higher aspect ratio, like rod-shaped NPs, exhibited higher contact area with cells compared to lower aspect ratio NPs (spherical NPs), and thus, they were taken up more by the cells.[232]

The surface charge of the NPs has also an influence on the NP−cell interactions. Compared to NPs with negative or neutral charge, positively charged NPs showed higher interaction with the negatively charged cell membranes, as a result of their electrostatic attraction.[228,233] In addition, positively charged NPs can successfully escape endosomes and avoid premature delivery of cargos due to their "proton sponge effect".[234] However, despite these advantageous features, positively charged NPs can cause cytotoxicity due to increased mitochondrial and lysosomal damage, and disruption of plasma membrane integrity.[233]

Finally, elasticity, hydrophobicity and roughness of NP can also affect NPs fate inside the body and interaction with cells. For example, softer NPs are taken up more by the cells compared to stiffer ones.[235,236] Surface roughness instead, can increase loading of payloads and favors cellular uptake.[237,238] Cellular uptake is also increased by the NPs hydrophobicity.[239] However, hydrophobic NPs present shorter circulation times compared to hydrophilic counterparts, as well as increased toxicity.[240,241]

Overall, by fine tuning of all these features, particles with specific characteristics can be engineered to satisfy different therapeutical needs.
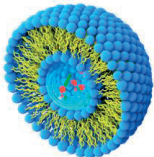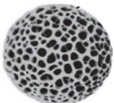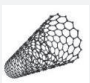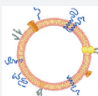
2.2.1.1 Acetalated dextran for the fabrication of drug delivery systems

In this thesis, acetalated dextran polymer was used for the fabrication of drug delivery systems. This polymer derives from the acetalation of dextran's hydroxyl groups, which endow the polymer with pH-responsive properties.[242] Dextran is both biocompatible and biodegradable, which makes it suitable material for drug delivery applications.[243] Upon acetalation, dextran not only acquire pH-responsive properties, but it becomes also hydrophobic, making it able to encapsulate hydrophobic payloads during NPs preparation by nanoprecipitation or emulsion techniques.[242,244] Moreover, acetalated dextran can be further functionalized to achieve polymers with different characteristics. For instance, conjugation with spermine or putrescine enabled the synthesis of positively charged polymers, used for the synthesis or NPs aimed at intracellular delivery of nucleic acids.[245–248] Conjugation with glucose sensitive moieties, give birth also to a polymer sensitive to hyperglycemic microenvironment, used for wound-healing treatment.[249] As stated above, acetalated groups are responsible for the pH-responsiveness of the polymer. During the acetalation reaction, bot cyclic and acyclic acetals are forming, with the former ones being thermodynamically favourable and replacing the acyclic ones when reaction time is prolonged.[250] Consequently, modifying the reaction time can tune the ratio of cyclic and acyclic acetals present in the polymer.[250]

Table 2. Nanoparticulate systems classified by their composition with correspondent advantages and disadvantages

Type of nanosystem	Advantages	Disadvantages	Refs.
Organic / "soft" NPs			
Lipid based NPs (Liposomes, lipid NPs, solid lipid NPs, emulsions)	- High bioavailability - Biocompatibility - Formulation simplicity and high versatility - Encapsulation of hydrophilic, lipophilic and imaging agents - Controllable drug-release kinetics - Possibility to functionalize surface	- Low encapsulation efficiency - Difficult purification methods	17,251–254
Polymeric NPs (Polymerosomes, polymeric micelles, dendrimers, nanospheres)	- Good stability - Biocompatibility - Possibility to use stimuli-responsive polymers - Encapsulation of both hydrophilic and lipophilic agents - Precise control of NPs characteristics - Controllable drug-release kinetics	- Difficult purification methods - Difficult to scale-up - Poor storage conditions - Possibility of aggregation and toxicity	17,255–261
Inorganic / "hard" NPs			
Porous silicon/silica NPs	- High porosity - High loading degree - Intrinsic adjuvant properties - Biocompatibility - Biodegradability	- Poor stability in physiological conditions - Fast release of cargoes (if not functionalized) - Short circulation time (if not functionalized)	262–266
Iron oxide NPs	- Low toxicity - Chemically inert - Superparamagnetic behaviour - Contrast agent for computed tomography - Hyperthermia agent - Easy to functionalize and modify surface properties	- Limited colloidal stability (if surface is not coated) - High opsonisation by macrophages	267–269
Gold NPs	- Optical properties (for photothermal therapy and photoimaging) - Bioinert - Easy functionalization and tuning of phisico-chemical characteristics	- Long-term toxicity - Non-biodegradable	270–272
Carbon nanotubes	- Large surface area - Easy functionalization - Optical properties (for photothermal and photodynamic therapy)	- Lack of size uniformity - Long-term cytotoxicity (if not functionalized)	273–275
Quantum dots	- Higher photostability compared to fluorophores - High quantum yield and long life time - Tuneable size and shape-dependent optoelectronics properties	- Toxicity - Low aqueous solubility - Colloidal instability in the bloodstream - Incomplete elimination from the body	276,277
Biologically-derived NPs			
Cell membrane-based NPs	- Long circulating properties - Surface is source of antigens - Possibility of stimulating both humoral and cell-mediated immune responses	- Poor colloidal stability - Difficulty of loading proteins	215–217,278

Considering that cyclic acetals degrade slower compared to acyclic, the reaction time is crucial to control the polymer degradation half-time and pH-sensitivity.[250]Acetalated dextran is relatively stable at physiological pH (pH=7.4), but degrades faster at acidic pH (pH=5.0), being an optimal feature for the delivery of drugs intracellularly at endosomal level or in tissues presenting lower pH (*e.g.*, cancer, infarction, and intestinal inflammation).[247,279–281] Acetalated dextran can be used to form scaffolds, fibers, micro- and nano-structures, representing a material used for a wide range of biomedical applications. It has been successfully used for the development of vaccines against infective disorders as well as cancer vaccines, cancer treatment, treatment for cardiovascular and infectious diseases and immunomodulators for autoimmune diseases.[246,247,250,282–289]

2.2.1.2 Strategies to improve the stability and increase the circulation time of drug delivery systems

Once in the bloodstream, nanoparticulate systems have to face one of the greatest barriers, which influences their ability to reach their target site, and it is known as protein corona formation. The protein corona consists in the association of biomolecules (usually proteins) on the NPs surface.[290–294] This association of bloodstream components on the surface of drug delivery systems, can lead to formation of an "hard corona" and a "soft corona". The former one consists of a layer of proteins with high affinity for the NPs surface, which might bind irreversibly to it; the latter instead, is a layer of low affinity binding molecules, adhering to the NPs surface by reversible bonds.[294,295] The formation of protein corona alters the composition of the NPs, hindering their stealth properties and ability to reach and interact with their target cells, thus limiting their therapeutic efficacy and clinical translation.[293,296] If the corona is composed of opsonin molecules (*e.g.*, complement factors, immunoglobulin (Ig) G or other proteins), the system is recognized, phagocyted and cleared by cells of the mononuclear phagocytic system (MPS), which consists of a system of phagocytic cells, predominantly resident macrophages, in the spleen, lymph nodes and liver. This process is known as opsonization.[221,241,297,298]

The protein corona formation depends on the characteristics of the NPs surface. Modification of the surface properties can then prevent or at least reduce protein corona formation. One of the mainstream strategies is grafting poly(ethylene glycol) (PEG), or PEGylation on the NPs surface.[299–301] The ethylene glycol units prevent protein interaction with the NPs by forming an hydrated layer.[301] Moreover, the flexibility of PEG chains makes the interpenetration of other molecules in the PEG layer thermodynamically unfavorable.[302,303] Molecular weight, length of the chain and density of PEG engrafted are all parameters that influence the circulation time of NPs in the bloodstream.[301] The most famous example of enhanced circulation time by PEG is the FDA approved nanomedicine Doxil®, in which doxorubicin loaded liposomes gained an increased lifetime in the blood from minutes to hours.[304] Since then, PEGylation has been extensively used to stabilize and increase the blood circulation time of different drug delivery systems. Although other materials presenting similar stealth properties, such as poloxamers, poly(vinyl alcohol), poly(amino acids) and polysaccharides, have been investigated,[305] PEG still remains the most used material.

Alternatively, use of "self" peptides, like the "don't eat me" marker CD47, have been used to decorate the surface of NPs, as studied by Disher *et al*.[306] In their study, attachment of computationally designed "self" peptides on the surface of 160 nm beads,

significantly reduced they clearance by liver and spleen, prolonging their circulation time and increasing their accumulation in the tumor site.[306]

Coating with red blood cells (RBCs) or leukocytes membranes also showed reduced opsonization and enhanced circulation times.[216,307] The prolonged circulation time is guaranteed by "self" moieties present on the cell membranes.

Recently, TA, a polyphenol derived from plants, has also been used for the development of drug delivery systems or used as coating to impart different properties to the NPs. Reports have shown that the abundant presence of hydroxyl groups in the TA structure prevents non-specific protein binding when NPs are in plasma, thus enhancing the circulating time of TA-modified NPs.[308] Similarly, Shin *et al.* complexed proteins and peptides with TA to achieve increase blood circulation and heart targeting.[24] Taking account these considerations, in this thesis besides PEGylation, the properties of TA as NPs coating were also explored.

2.2.2 Nanomedicines for the treatment and imaging of myocardial infarction

As discussed above, current therapeutic treatments are able to improve the quality of life of patients affected by MI and HF, but unable to fully restore the lost function of the heart, leaving millions of patients without an ultimate cure. Despite the discovery of new therapeutic targets and novel approaches to tackle the loss of CMs and regenerate the cardiac tissue, there is little of no clinical translation, due to invasiveness of administration, limited efficacy and harmful adverse effects of new therapeutics.[7] In this regard, nanomedicines offer a great opportunity to translate the abovementioned approaches into clinics. Thanks to their high versatility, nanoparticulate materials have received increasing interest over the years for CVDs applications.[19,210,211,247,248] While microparticles for MI therapy have also been fabricated with the intention of being administered locally, NPs were developed with the aim to avoid such invasive procedures and improve patient compliance.[309,310] Since NPs can encapsulate imaging agent or have optical properties by themselves, they have been used also for imaging and diagnostic purposes.[311,312] In **Table 3** there is a summary of the main micro- and nano-particulate systems developed for imaging or treatment of MI and HF.

2.3 Targeting strategies

2.3.1 Passive targeting strategies in drug delivery applications

The most appealing feature of drug delivery systems is their ability to reach specific sites in our body, characteristic that makes them advantageous compared to conventional therapies. Accumulation of NPs in different sites of our body can be achieved in two ways: passive or active targeting.[313] Here, the description is limited to passive targeting, while active targeting will be described in detail in the next section. Passive targeting is defined as the natural accumulation of NPs in particular sites of the body by leveraging physiological features encountered by the NPs in their journey. It can include exploitation of leaky vasculature in different sites of our bodies, and use of materials or systems which have a particular tropism for particular organs.

The first example of passive targeting was described by Matsumura and Maeda in 1986 and it was demonstrating accumulation of nanomedicines in tumor site due to some characteristic of the tumor microenvironment.[314] The effect was called EPR effect and was attributed to the leaky vasculature present in some tumor sites.[315,316] The fenestrations in the blood vessels constituting the tumor microenvironment range between 100 and 780 nm,

allowing accumulation of nanocarriers of size up to several nanometers.[315,316] The EPR effect can be enhanced also by the extensive angiogenesis and lack of lymphatic drainage.[315,316] Tuning the physicochemical features of nanocarriers with the aim of prolonging their circulation time in the bloodstream can increase their passive accumulation on tumor sites. Moreover, leaky vasculature has been found not only in tumor sites, but also in ischemic and inflammatory sites[317–319] and could thus be exploited for different applications.

Recently, the development of lipid NPs for tissue-specific mRNA delivery and CRISPR-Cas9 editing, revealed the possibility to achieve particular organ accumulation by modulating the lipid composition of the NPs and their charge.[320] Lipid NPs (LNP) are carriers traditionally used for the delivery of ribonucleic material and they are usually composed of ionizable cationic lipids, amphipathic phospholipids, cholesterol and PEG lipids. In their work, Cheng *et al.* demonstrated that addition of a specific lipid, named selective organ targeting (SORT) lipid, could determine NPs tropism for either lungs, spleen or liver.[320] They explained the specific organ targeting as a process called endogenous targeting.[321] In this process, LNPs after desorption of PEG lipids from their surface, bind to specific endogenous proteins in the blood circulation according to the chemical nature of the SORT lipid and achieve selective organ targeting by protein binding to cognate receptors highly expressed in specific tissues.[321]

The EPR effect theory has been recently challenged by Warren[322–324] and Weissleder[325,326] groups, who demonstrated that the primary entry mechanism of NPs into tumor sites is not occurring by passive diffusion, but it is an active process mediated by endothelial cells[323,324] and tumor associated macrophages (TAMs).[322,325,326] By imaging the tumor vessel with intravital confocal microscopy, Warren et al. demonstrated that 20% of the TAMs in their videos contained NPs and were migrating. TAMs penetrate into the tumor and then redistribute the NPs to cancer cells. Moreover this TAM mediated transport is size-dependent.[322] Future studies will elucidate how the different physico-chemical characteristics (*e.g.* chemistry, surface charge, shape) of NPs influence this active transport mechanism. These and future findings will revolutionize the way cancer nanomedicines are designed and open possibilities to explore novel strategies to enhance NPs tumor accumulation. Moreover, similar mechanisms could take place in different pathologies, like ischemic and inflammatory sites, and could be exploited to increase the NPs accumulation in such districts.

2.3.1.1 Passive targeting strategies developed to reach the infarcted myocardium

The discovery of the existence of leaky vasculature in the infarcted myocardium[317] has paved the way to the development of nanosystems able to extravasate through them and accumulate in infarction sites by passive targeting. Evidence suggested that the optimal size for NPs to be able to accumulate in the infarcted myocardium via this mechanism range between 20 and 200 nm.[226] Keeping in mind these findings, researchers have been developed different systems for the treatment and imaging of MI. For example, the passive delivery of porous silica NPs containing adenosine, resulted in reduction of infarct size in a rat model of I/R injury. Moreover, the adverse effect of adenosine (hypotension) was attenuated by encapsulation in the silica NPs.[18] Recently, Bejerano *et al.* delivered miRNA-21 to macrophages accumulating in the infarcted heart in order to induce their phenotype modulation towards an anti-inflammatory, reparative state.[327]

Table 3. Summary of micro- and nanoparticulate systems for treatment and imaging of MI.

Micro- and nanosystems	Purpose	Administration route	Targeting	Refs.
Liposomes	Therapeutics delivery	i.v.	active	[328]
Porous silicon NPs	Therapeutics delivery	i.v.	active	[19]
Protein complexes with TA	Potential application in CVD treatment	i.v.	passive	[24]
PLGA MPs	Therapeutics delivery	intramyocardial	-	[329]
PLGA NPs	Therapeutics delivery	intramyocardial	-	[330–332]
Chitosan hydrogel NPs	Therapeutics delivery and imaging	intramyocardial	-	[333]
Chitosan-alginate NPs	Therapeutics delivery	intramyocardial	-	[334]
Hyaluronan-sulphate NPs	Therapeutics delivery	i.v.	passive	[327]
RGD-PEG-PLA NPs	Therapeutics delivery	i.v.	passive	[335]
Calcium phosphate NPs	Therapeutics delivery	inhalation of NPs	passive	[336]
Lipid NPs	Therapeutics delivery	i.v.	active	[21]
IMTP-Fe$_3$O$_4$-PFH NPs	Imaging	i.v.	active	[337]
MnO NPs	Potential imaging and therapeutic applications	i.v.	passive	[338]
PLGA NPs	Therapeutics delivery	i.v.	passive	[339]
Gold NPs	Therapeutics delivery	oral gavage	-	[340]
Silica NPs	Therapeutics delivery	i.v.	passive	[18]
Iron NPs	Therapeutics delivery and imaging	i.v	active	[341,342]
USPIO NPs	Therapeutics delivery and imaging	bolus	active	[343,344]
SPIO NPs	Imaging	i.v.	active	[345,346]
Gold NPs	Imaging	i.v.	active	[347]

They used hyaluronan-sulfate NPs assembled with the micro ribonucleic acid (miRNA)-21 through calcium ion bridges, which had a size of approximately 100 nm.[327] These NPs were in the perfect range (10–300 nm) to be efficiently taken up and accumulate in diseased tissues into which macrophages are usually recruited and reside (*e.g.*, ischemic myocardium).[348] With this treatment they achieved improved heart function especially in the remote myocardium.[327]

Alternatively, calcium phosphate NPs have been administered via inhalation to move from the pulmonary circulation straight to the heart via the pulmonary vein. The NPs accumulated in the heart according to previous evidence showing how combustion-derived NPs and ultrafine particulates inhaled through polluted air were present in the heart and causally associated with cardiac arrhythmia and dysfunction.[349,350]

Recently, modification of protein with TA in a process called as TANNylation, resulted in prolonged circulation and stability of such proteins and their accumulation in the heart.[24] The reason at the base of the heart targeting properties of TA, lies in its high affinity for components of the extracellular matrix, in particular collagen[351] and elastins (rich of proline residues),[352] which are abundant in the heart and further produced (especially collagen) during ECM remodeling following MI. This modification allowed for efficient delivery of basic fibroblast growth factor in a murine model of I/R injury, resulting in a significant reduction of infarct size and increased cardiac function.[24] This approach has been investigated also in this thesis to develop a system for the delivery of pro-proliferative compounds to the infarcted myocardium.[248] Examples of passive targeting are summarized in **Table 3**.

2.3.2   Active targeting strategies in drug delivery applications

The other targeting strategy that allow NPs homing to specific organs is active targeting and consists in using ligands which recognize receptors expressed by cells of particular organs. These ligands can be peptides, proteins, antibodies, sugars, and aptamers.[353] The design of actively-targeted nanocarriers is not easy and various aspects can influence the targeting efficacy. For instance, the types of ligand available, the way the ligand is bound on the NPs' surface, the density of the targeting moiety all affect the efficacy of the targeting strategy.[354–357] Moreover, the administration route and the formation of protein corona have also a big impact on the ability of NPs to target specific sites in the body.[358] Indeed for an efficient active targeting, the NPs still have to meet the requirements to achieve a prolonged circulation in the blood stream, since targeting moieties can recognize their receptors only when in proximity.[359] This means that active targeting without working on extending the circulation times of the NPs will not improve the targeting ability of the nanosystem. In cancer therapy active targeting is indeed considered as a complimentary strategy to the EPR effect.[313] For instance, liposomes with anti-human epidermal growth factor receptor (HER)2 targeting antibodies could significantly increase the NPs uptake in HER2-expressing cancer cells, compared to un-targeted liposomes which accumulated in perivascular and stromal space and were taken-up mainly by macrophages.[360]

Always in cancer therapy, immunomodulation of the tumor microenvironment was achieved by active targeting mediated by m-UNO peptide and delivery of R848, a small molecule for the reprogramming of M2-like macrophages into the pro-inflammatory phenotype M1.[361] Administration of vinblastine as anticancer drug had a synergistic effect in reducing tumor size in mice.[361]

2.3.2.1 Active targeting strategies developed to reach the infarcted myocardium

Active targeting strategies have been exploited also in the realization of systems able to target the infarcted heart. Efficient targeting is fundamental to maximize the effects of the delivered payloads and to reduce their potential side effects generated by off-target biodistribution.[362] Especially for therapies aimed at stimulation of CMs proliferation, there is a risk of inducing tumors in other body districts, if NPs are not properly selective for the infarcted tissue and despite treatment is meant to be transient.[7,202] However, efficient targeting of the infarcted heart is challenging due to the constant pumping of the organ, which pones a mechanical obstacle to the NPs retention.[24] Also, to date, a specific CMs marker that can be used as targeting moiety has not been found yet.[20] Current research focuses on the exploitment of some receptors overexpression, as well as targeting inflammatory cells that are recruited in the myocardium after MI.[19,327,328] Simultaneously, discovery of new targeting peptides ligands is done by phage display.[363] Examples of active targeting NPs are listed in **Table 3**.

For instance, liposomes able to target the infarcted heart were designed by Dvir *et al.* by chemical conjugation with antibodies against the AngII type 1 receptor, which is overexpressed in the heart post-MI.[328] In this work, they just focused on showing the heart targeting abilities of such approach, without delivering any therapeutic or imaging agent.[328] One of the most explored peptide for heart targeting applications is the ANP, which targets its own receptors upon overexpression in MI. Ferreira *et al.* demonstrated its efficacy in delivering cardioprotective compound 3i-1000, encapsulated in PEGylated porous silicon NPs, in a rat isoprenalin model of myocardial ischemia.[19] Results showed increased biodistribution in the cardiac tissue upon functionalization with ANP (**Figure 4**).[19] In another work, the same group compared the heart targeting abilities of ANP and other two peptides, designated as P2 and P3, which were identified by a phage display-based approach as potential molecules to target the ischemic myocardium.[364] In particular, P2 is a cyclic 9 amino acid sequence (CSTSMLKAC) that mimics endogenous peptide sequences, such as titin, optic atrophy-1 (OPA-1) or the dynamin-1 like protein (DRP-1),[365] while P3 has 12 amino acids (CRSWNKADNRSC) in a cyclic structure and has also shown alone a 5-fold selective targeting to the ischemic heart.[366] Their investigation demonstrated that there were no significant differences in *in vivo* biodistibution between the NPs conjugated with the three different peptides; however, *in vitro* studies demonstrated an increased uptake of porous silicon NPs when they were conjugated with ANP compared to P2 and P3.[364] Interestingly, besides its heart targeting abilities, ANP has demonstrated also anti-fibrotic and immunomodulatory effects.[367,368] In particular, ANP has shown anti-inflammatory properties by inhibiting the lipopolysaccharide (LPS)-induced expression of inducible nitric oxide synthase (iNOS) and secretion of TNF-α in macrophages. Furthermore it reduced the release of IL-1β and did not affect the secretion of the anti-inflammatory cytokines IL-10 and IL-1 receptor antagonist (IL1ra).[368] This potential anti-inflammatory effect exerted by ANP, could be beneficial in attenuating the inflammation taking place after MI, which has shown negative influence on the remodeling of the heart.

Nguyen *et al.* instead, developed micelles targeting the infarcted heart via a stimuli-responsive peptide that activated in the presence of MMP-2 and 9, which are overexpressed in the heart after MI.[369] Upon activation in the infarcted site, the peptide induced conformational changes to the NPs, which shifted from spherical to network-like assemblies. This conformation showed retention in the myocardium up to 28 days.[369]

Alternatively, macrophages, that are recruited in the heart after MI, can be targeted by NPs to reach the infarcted heart. For instance, Harel-Adar *et al.* achieved accumulation of liposomes in the infarcted heart, by injecting phosphatidylserine (PS)-presenting liposomes in a rat model of MI.[370] The accumulation in the heart took place upon uptake of PS-liposomes by pro-inflammatory macrophages, which are recruited in the infarcted site.[370] The uptake of the PS-liposomes by the pro-inflammatory macrophages had effect on their polarization, which switched towards an anti-inflammatory type and promoted improvement of the cardiac function.[370]

Coating NPs with cell membranes can also be considered a particular type of active targeting. Indeed, cell membranes present on their surface particular ligands which can be recognized and guarantee their accumulation in particular organs.[215] This strategy has been exploited also to target the infarcted heart, as different cell types are known to accumulate in the myocardium after MI. For instance, Su *et al.* have developed PLGA NPs cloaked in platelet membranes modified with prostaglandin E2 (PGE2) for homing in the myocardium in a model of I/R injury.[371] The platelet inspired nanocell showed 14.9-fold higher radiance efficiency (*i.e.*, a measure of photon flux from the fluorescently labelled NP in the organ of interest, normalized by the area of emission, the exposure time, and the solid angle of the detector) than those treated with bare uncoated NPs, as well as 3.4- and 8.6-fold higher than the liver and kidney, respectively.[371] The validated accumulation in the injured heart was achieved because of the platelet recruitment taking place after a MI,[372] as well as the overexpression of PGE2 receptors.[373,374] Furthermore, delivery of resident cardiac stem/stromal cells (CSCs) secretome, together with the PGE2 signaling, augmented the cardiac function and reduced the heart remodeling concomitantly with increased presence of cycling CMs, activation of endogenous progenitor cells, and promotion of angiogenesis.[371]

With a similar approach, recruitment of neutrophils immediately after MI, has been employed as shuttle for NPs homing to the infarcted heart.[375] In that work, neutrophils were loaded *ex vivo* with liposomes and then were injected in animal models of I/R injury.[375] Biodistribution studies showed accumulation of the liposomes in the injured myocardium according with the neutrophils recruitment in the inflamed damaged heart tissue.[26,375] Release of the liposomes in inflammatory sites was mediated by formation of neutrophil extracellular traps (NETs) within few hours.[375]

Altogether, research work in the nanomedicine field has led to the development of various strategies to address NPs to infarcted sites, ranging from peptide and antibody based approaches to explotaition of endogenous ligands by cell membrane cloaking. However, the lack of clinically available solutions still underlines the urgent need for efficient strategies.
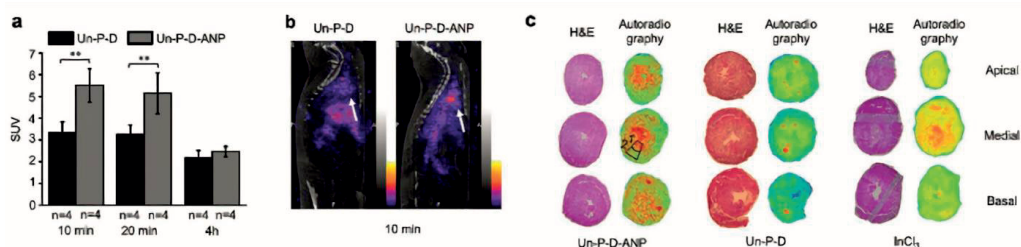
Figure 4. Quantification of the standardized uptake values (SUVs) in the rat heart at 10 min, 20 min, and 4 h after i.v. administration of NPs and Single photon emission computed tomography (SPECT/CT) imaging (**a**). Representative sagittal SPECT/CT images showing the

biodistribution of the NPs at 10 min after i.v. administration. Heart location is indicated by white arrows (**b**). Representative H&E stainings and autoradiograms of apical, basal, and medial rat heart sections (from a single heart for each treatment: Un-P-D-ANP, Un-P-D, and $^{111}InCl_3$ control) showing the localization of radioactivity 10 min after the injection of NPs or the control (**c**). Abbreviations: SPECT/CT, single photon emission computed tomography/computed tomography; H&E, hematoxylin and eosin staining; Un-P-D: Undecylenic acid thermally hydrocarbonized PSi (UnTHCPSi) NPs modified with PEG and DOTA; Un-P-D-ANP: Un-P-D NPs further modified with ANP peptide. Copyright© 2017 WILEY- VCH Verlag GmbH & Co. KGaA, Weinheim. Adapted and reprinted with permission from ref.[19]

2.3.3 Cellular hitchhiking

Besides passive and active strategies, using cells as piggy back carriers to reach specific organs has also been used in a process called cellular hitchhiking. RBCs have been explored as first cellular shuttle for NPs, taking inspiration from preclinical studies showing the improved delivery and therapeutic effects of drugs coupled to RBCs surface.[376–378] Mitragotri's group has largely demonstrated the use of RBCs as cellular shuttles to increase the NPs circulation time and accumulation in organs different from liver and spleen.[379] Non-covalent absorption of polystyrene NPs on the surface of RBCs exhibited ~3-fold increase in blood circulation time and ~7-fold higher accumulation in lungs, while it improved lung/liver and lung/spleen nanoparticle accumulation by over 15-fold and 10-fold, respectively.[379] The accumulation in the lungs was attributed to mechanical transfer of particles from the RBC surface to lung endothelium.[379] Surface modification of polystyrene NPs with anti-ICAM-1 antibody further increase their accumulation in the lungs.[379,380] Successively they improved and generalized the system, by testing the absorption of different NPs types and studying the biodistribution upon administration through different routes.[381] For instance, the i.v. injection of liposomes hitchhiking RBCs resulted in increased uptake in the first downstream organ, lungs, by ~40-fold compared with free liposomes.[381] Alternatively, intra-carotid artery injection delivered >10% of the injected NP dose to the brain, ~10× higher than that achieved with affinity moieties.[381] Moreover, they demonstrated that this strategy works in mice, pigs, and *ex vivo* human lungs without causing RBC or end-organ toxicities.[381] In particular, since insertion of an arterial catheter is standard of care in acute MI, the intra-arterial administration of such a system can be used and promote the cardiac accumulation of nanocarriers, thus bringing benefits in the treatment of MI.

In another study, leukocytes (monocytes and neutrophils) accumulating in the brain after ischemic stroke, have been used as "Trojan horse" for the delivery of liposomes in the ischemic region.[382] Hitchhiking on leukocytes was achieved by modifying liposomes with cyclic-RGD peptide,[382] which bound to $\alpha_v\beta_1$ integrins, highly expressed on the leukocytes' surface.[383–385] Liposomes were then successfully transferred from the immune cells to the neuronal cells with a mechanism involving formation of bridges between the cells, membrane transfer, deformation of immune cells and secretion of exosomes,[382] similarly to what was observed in other reports.[386]

Recently, monocytes have been used as shuttle to achieve heart targeting of liposomes modified with the J10 aptamer.[387] The study showed increased liposome accumulation in the infarcted heart at day 4 post-MI, in concomitance with the peak of monocytes recruitment.[387] The system was used for the delivery of IOX2, a potent and selective hypoxia-inducible factor (HIF)–1α prolyl hydroxylase–2 inhibitor, in a murine model if I/R injury and resulted in improved

cardiac function, reduced infarct size and apoptosis, and promoted cardioprotection and angiogenesis.[387]

In this thesis, the design of dual targeted dextran-based NPs was inspired by the inflammatory cells hitchhike strategies developed to target inflammatory sites with the aim to exploit the recruitment of such cells to the infarcted heart and improve the heart targeting abilities of ANP peptide. For this purpose, the surface of the NPs was conjugated with ANP and lin-TT1 peptide, which has been used to target TAMs and macrophages associated to the atherosclerotic plaques.[27–29] The lin-TT1 peptide, binds to the mitochondrial chaperone protein p32, which is normally expressed at the intracellular level, but translocated on the surface of TAMs, tumor endothelial cells and atherosclerotic plaques.[27,28] Similar to integrin-binding arginine–glycine–aspartic acid (iRGD) and LyP-1 peptides, lin-TT1 contains a cryptic basic sequence motif (C-end Rule or CendR motif), that is, following cell surface recruitment of the peptide by the p32-dependent mechanism, proteolytically processed to activate the CendR element and allow interaction of the peptide with the secondary receptor neutropilin-1 (NRP-1). This interaction initiates an uptake process similar to classical endocytosis.[388] Considering the bi-phasic recruitment of inflammatory cells after MI,[25] it was important to assess which cells were targeted by these NPs, in order to know which time-frame could result in maximal hitchhike effect and subsequent optimal accumulation in the infarcted hearts.

Compared to published literature, the dual targeted dextran-based NPs presented in this thesis make the combination of active targeting and hitchhiking effect, aiming at synergistic effect and improved accumulation of NPs in the infarcted heart. Increased heart targeting achieved through the combination effect, may reduce side effects and translate into a safer and more efficient administration of chemicals stimulating cell proliferation, with superior recovery of the cardiac function.

3   Aims of the study

In the past decades, there has been an increasing interest in the development of nanocarriers for the therapeutic treatment of MI. Despite the numerous advances in the field, heart targeting still represent a challenge and there is need for the discovery of better heart-homing systems. Also, there is lack of improved regenerative strategies aimed at repairing the damage caused by MI.

The overall aim of this thesis was to evaluate the potential of dextran-based NPs as platforms to deliver therapeutics for enhanced cardiac drug delivery. In addition, the cytocompatibility and cell–NP interactions of bare and functionalized NPs were investigated, and their *in vivo* biodistribution and therapeutic efficacy were also assessed.

More specifically, the aims of the present study were:

1. To investigate the cytocompatibility of different dextran-based NPs towards cardiac cell and macrophages, and to evaluate the drug loading ability into the NPs (**I-III**).

2. To estimate the hitchhiking potential of Putre-AcDX-PEG-TT1-ANP NPs by studying their *in vitro* interaction with M1– and M2–like macrophages of different origin (**I**).

3. To study the *in vitro* ability of AcDXSp-TA NPs to stimulate CMs proliferation and reduce fibrosis (**II**).

4. To investigate the *in vivo* biodistribution of Putre-AcDX-PEG-TT1-ANP NPs and see if the hitchhiking effect of macrophages can improve the heart targeting abilities of ANP (**III**).

4 Experimental

This section summarizes the experimental methods used for the studies described in the thesis. Detailed description of the materials, instrumentation and methods can be found in the original publications (**I–III**). The *in vivo* studies presented in publication **III** were performed in collaboration with the PET Center and the University of Turku, Finland.
The detailed description of the materials used in this thesis can be found in the materials and methods section of each original publication.

4.1 Preparation and characterization of spermine and putrescine-modified acetalated dextran NPs (AcDXSp and Putre-AcDX NPs respectively) (I–III)

4.1.1 Synthesis of AcDXSp and Putre-AcDX

Dextran (5 g, MW 9–11 kDa; Sigma-Aldrich) was dissolved in 20 mL of Milli-Q water, followed by addition of sodium periodate (1.1 g; Sigma-Aldrich). Partially oxidized dextran was obtained after stirring the mixture at room temperature for 5 h and it was then washed and lyophilized. Freeze-dried partially oxidized dextran (3 g) was then modified with 2-methoxypropene (10.6 mL, Sigma–Aldrich) and pyridinium p-toluenesulfonate (46.8 mg; Sigma–Aldrich) in anhydrous dimethyl sulfoxide (30 mL, Sigma–Aldrich) during 3 h under a N_2 atmosphere to obtain the partially oxidized AcDX. Reaction was quenched with triethylamine (TEA, 1 mL; Sigma–Aldrich) and the resulting AcDX was precipitated by addition of water. A series of centrifugation (10 min, 68320g) steps and washings followed. The pellet was dried under vacuum at 40 °C to yield partially-oxidized AcDX powder. The partially oxidized AcDX (2.0 g) was dissolved in 20 mL of DMSO and spermine (4.0 g, Sigma-Aldrich) was added to the solution and kept stirring for 24 h at 50 °C. Reduction reaction was carried out by addition of sodium borohydride ($NaBH_4$, 1.0 g; Sigma-Aldrich) and the mixturewas left to stirr at room temperature during at least 24 h. Water (80 mL) and methanol (10 mL) were added to the flask to precipitate the polymer and to dissolve the excess $NaBH_4$. The obtained polymer was centrifuged, washed and finally lyophilized, to obtain AcDXSp as a white powder.[245,250] For the synthesis of Putre-AcDX instead, the partially oxidized AcDX (2.0 g) was then dissolved in 10 mL of methanol and putrescine (4.0 g, Sigma-Aldrich, USA), dissolved in other 10 mL of methanol, was added to the solution, which was kept stirring for 24 h at room temperature. The reduction, stopping, centrifugation and drying steps are the same used for the synthesis of AcDXSp.[246]

4.1.2 Preparation of Putre-AcDX and AcDXSp NPs (I–III)

The Putre-AcDX and AcDXSp NPs were prepared by a standard single oil-in-water (o/w) emulsion method, as previously reported.[247] Briefly, Putre-AcDX or AcDXSp polymer (6.5 mg) was dissolved in CH_2Cl_2 (0.125 mL). The compounds CHIR99021 (300 µg, Tocris) and SB203580 (500 µg, Sigma) (CRIH99021 + SB203580, CHIR and SB) were added to the polymer solution. An aqueous solution of poly(vinyl alcohol) (PVA, MW: Experimental 31000-50000 g/mol, Sigma–Adrich) (0.25 mL, 2.0%, w/v) was further added to the AcDXSp solution, and the mixture was mixed thoroughly and emulsified by sonication during 30 sec on ice, with an output setting of 5 and a duty cycle of 40%, using a probe sonicator (Sonics VCX 750). The

resulting single emulsion was transferred immediately to another solution of PVA (0.75 mL, 0.05% w/v) and stirred for 3 h for solvent evaporation. The resulting drug-loaded NPs were obtained as a pellet by centrifugation (16100g, 5 min), washed twice with Lutrol® F127 0.5 % pH 8 (BASF) and once with sucrose 2% (w/v) pH 8. All supernatants were kept for the detection of CHIR and SB contents by high-performance liquid chromatography (HPLC). Empty NPs were prepared similarly.

4.1.3   Surface functionalization of Putre-AcDX NPs (I, III)

Putre-AcDX NPs were functionalized with a branched PEG (N-Mal-N-bis(PEG$_2$-acid); MW 488.5 g/mol, BroadPharm, USA) using 1-ethyl-3-(3-dimethylaminopropyl) carbodiimide hydrochloride/N-hydroxysulfosuccinimide (EDC/NHS, Sigma-Aldrich, USA) crosslinking chemistry. Briefly, a EDC/NHS solution was prepared by adding EDC (8 µL) and 2 mg of NHS to 2 mL of 10×10^{-3} M of 2-(N-morpholino)ethanesulfonic acid (MES, Sigma-Aldrich, USA). The pH was adjusted to 7.4, and the branched PEG and Putre-AcDX NPs were, respectively, dissolved and re-suspended in the EDC/NHS solution. The EDC/NHS solution:NPs ratio was 1:3, while the ratio branched PEG:Putre-AcDX NPs was 1:4. Ethylenediaminetetraacetic acid (EDTA) was added at a concentration 5×10^{-2} M to decrease the reactivity of activated carboxylic groups and prevent formation of bridges between different NPs. First, the branched PEG was dissolved in EDC/NHS solution and put to stir. Immediately after, the NPs' suspension was added dropwise to the PEG solution and finally EDTA was added to the suspension. The mixture was let to stir for 1 h at room temperature in dark. PEGylated NPs were pelleted by centrifugation (16100g, 5 min), washed once with 2% w/v of sucrose (pH < 8) and then conjugated with carboxyfluorescein (FAM)–labelled Lin–TT1 peptide (AKRGARSTA), through formation of a thioether bond between the thiol group of a cysteine residue of the peptide and the maleimide group on the functionalized particles. The reaction occurred in a solution of 10×10^{-3} M of MES (pH 7.8). The NPs:peptide ratio was 60:1 (w/w), whereas the NPs:MES ratio was 3:1 (w/w),. The peptide was dissolved in 1:10 of MES and added dropwise to the NPs suspension. EDTA was added to the suspension at a concentration 5×10^{-2} M to increase the stability of thiol groups.[389] The mixture was left to stir for 2h at room temperature in dark. Particles were collected by centrifugation (16100g, 5 min), washed once with 2% w/v of sucrose (pH < 8) and then re-suspended in a solution of ANP (MW 3080 g/mol, United BioSystems Inc, USA) in EDC/NHS pH 7.4 (3.6 mg/mL), and kept under stirring during 2 h at room temperature in dark. EDTA was added also in this last step. Fluorescently labelled NPs without any peptide or containing only ANP, were prepared by forming a thioether bond between the thiol group of the cysteine residue of FAM-Cys and the maleimide group on the functionalized particles, as described above for the conjugation of Lin-TT1.

4.1.4   Surface functionalization of AcDXSp NPs (II)

The particles were coated with tannic acid (TA), similarly to what reported in literature.[390] Briefly, 0.5 mg of NPs were re-suspended in 490 µL of Milli-Q water pH > 8. Then, 5 µL of a TA solution 40 mg/mL were added and vortexed vigorously for 10 seconds. Right after that, 5 µL of an Iron III solution 6 mg/mL were added to the suspension and vortexed for other 10 sec. Particles were then collected by centrifugation for 5 minutes at 13400g and washed once with

MilliQ water pH > 8. All supernatants were kept for detection of the drugs, CHIR and SB, using HPLC, as described below. For fluorescence labelling of AcDXSp NPs, the AcDXSp were activated using EDC/NHS chemistry and the addition of AlexaFluor® 488 (AF488, Life Technologies) was at a ratio of 500:1 (w/w) (AcDXSp:AF488) during 1 h.

4.1.5 Physicochemical characterization of dextran NPs (I–III)

The hydrodynamic diameter, polydispersity (PDI) and ζ-potential of the NPs were measured in a Zetasizer Nano ZS instrument (Malvern Instruments Ltd, UK). KBr–Fourier Transformer Infrared Spectroscopy (FTIR) was performed using a Bruker VERTEX 70 series FTIR spectrometer (Bruker Optics, Germany) to determine the surface chemical composition of the dry NPs. The FTIR spectra were recorded in the range of 4000–650 cm^{-1} with a resolution of 4 cm^{-1} , using an OPUS 8.1 software. The amount of ANP covalently conjugated onto the NPs was determined by elemental analysis using a vario MICRO cube CHNS analyzer (Elementar AnalysenSystem) using dry samples. The percentages of carbon, hydrogen, and nitrogen were recorded. The amount of ANP conjugated onto the NPs' surface was calculated based on the percentage of N content and the chemical structure of the peptide.

4.1.6 Stability of dextran NPs in different media (II, III)

Stability of the NPs was evaluated by incubating the nanocarriers in DMEM/F-12 supplemented with 10% FBS (Gibco, Thermo Fisher), human plasma and a solution 5.4% (w/v) of glucose. Briefly, 0.6 mg of NPs were re-suspended in 200 µL of Milli-Q water and immediately added to 1.6 mL of stability medium. The suspension was kept under stirring at 37 ºC. Aliquots of 200 µL were taken at different time points, diluted in 800 µL of Milli-Q water and measured by dynamic light scattering (DLS), using a Zetasizer Nano ZS instrument (Malvern Instruments Ltd, UK).

4.1.7 Drug loading, encapsulation efficiency, loading degree and release studies (I, II)

The compounds encapsulated in the NPs were quantified by using an Agilent 1100 series HPLC system (Agilent Technologies, Germany). The column used was a Discovery 5 µm C18 reversed phase column (100 × 4.6 mm, Supelco, USA). The mobile phase was Na_2HPO_4:citric acid (2:1) (pH 6.0) and acetonitrile (ACN) (50:50, v/v). The injection volume was 5 µL, while the flow rate was 1.4 mL/min and the wavelengths were set at 274 ± 20 nm and 304 ± 20 nm for CHIR and SB, respectively. For determination of EE (ratio between the amount of drugs encapsulated and the total amount of drugs) and LD (ratio between mass of loaded drugs and total mass of drug encapsulated NPs), a known amount of loaded NPs was dissolved in ACN. The CHIR and SB contents were measured by HPLC from the resulting solution, and all the supernatants resulting from the NP preparation. *In vitro* release studies were performed in sink conditions, in phosphate-buffered saline (PBS) (pH 7.4), acetate buffer (pH 5) and DMEM 10% FBS, to simulate both the extracellular (pH 7.4) and intracellular (pH 5) microenvironments, as well as the conditions encountered in cell cultures. The drug-loaded NPs were immersed in the appropriate release medium, stirring at 150 rpm and 37 ± 1 °C. Free drugs were used as controls. At specific time points, aliquots of 200 mL were taken from samples, replaced with the same volume of fresh preheated medium and analyzed by HPLC.

4.2 *In vitro* studies (I–III)

4.2.1 Cell lines and cell culturing (I–II)

RAW 264.7 and KG-1 macrophages (ATCC® TIB-71™ and ATCC® CCL-246™, respectively) were used for biocompatibility and uptake studies **(I)**. RAW 264.7 and KG-1 macrophages were cultured with Dulbecco's Modified Eagle's Medium (DMEM) and Iscove's Modified Dulbecco's Medium (IMDM), respectively, supplemented with 10% heat inactivated fetal bovine serum (FBS), 1% non-essential amino acids (NEAA), 1% L-glutamine and 1% penicillin-streptomycin. HCAEC (ATCC® PCS-100-020™) were used for biocompatibility studies **(II)**, since those are the first cardiac cell type encountered by the NPs once reaching the heart. Cells were growth according to ATCC® guidelines in MesoEndo Cell Growth Medium (MECG, Sigma-Aldrich, USA), supplemented with 10% FBS and 0.1% VEGF. Cells were kept in an incubator (BB 16 gas incubator, Heraeus Instruments GmbH) at 37 °C, 5% CO_2 and 95% relative humidity.

4.2.2 Isolation of primary rat and murine cardiomyocytes (II–III)

Primary cardiac cells were isolated as previously described.[247] Neonatal Wistar rats (1–3 d old) were sacrificed by decapitation, the hearts were taken, and atrial tissues were discarded. The ventricles were cut into small pieces and enzymatically digested by incubating at 37 °C with gentle mixing for 1 h and 45 min in a collagenase/pancreatin (2 mg/mL) solution. The cells in suspension were collected by centrifugation at 160g for 5 min. The supernatant and the top layer containing damaged cells were discarded, and the remaining cells were suspended in DMEM/F-12 (Gibco) supplemented with 2.5×10^{-3} M L-glutamine, 1% of penicillin-streptomycin (Gibco, Thermo Fisher), and 10% FBS. The cells were pre-plated for about 90 min to separate CMs from non-myocytes,[391] and after that the unattached CMs were seeded at a desired density for experiments **(II–III)**. For murine cardiac cultures, neonatal Balb C57BL/6JRcc mice (1–3 d old) were sacrificed by decapitation, hearts taken, and atrial tissues were discarded. Hearts were dissociated with the Neonatal Heart Dissociation Kit (Miltenyi, Biotech, GmBH, USA), according to the manufacturer's instructions. CMs were then isolated with the Neonatal Cardiomyocyte Isolation Kit (Miltenyi, Biotech, GmBH, USA), following the manufacturer's instructions. Cells were finally counted and seeded at a desired density for following applications **(III)**. After 24 h, for both rat and murine derived cells, the CMs medium was replaced with complete serum free medium (CSFM, DMEM/F-12, 2.5 mg/mL bovine serum albumin (BSA, Sigma), 1×10^{-6} M insulin, 2.5×10^{-3} M l-glutamine, 32×10^{-9} M selenium, 2.8×10^{-3} M sodium pyruvate, 5.64 µg/mL transferrin, 1×10^{-9} M T3, and 1% penicillin-streptomycin). Non-myocytes were cultured in complete DMEM/F-12 until confluent and plated for the experiments **(II–III)**. The cells were maintained at 37 °C with 5% CO_2 and 95% air in a humidified atmosphere.

4.2.3 Human induced pluripotent stem cell-derived cardiomyocytes (II–III)

The iPS(IMR90)-4 line[392] was purchased from WiCell (Madison, Wisconsin, USA). The stem cells were cultured in on six-well plates coated with Matrigel® (1:50) (Corning, Bedford, Massachusetts, USA) by using Essential 8™ medium (E8) (Gibco). For sub-culturing, the cells were dissociated with Versene® and re-suspended in E8 containing 10 µM ROCK inhibitor Y-

27632 (Tocris Bioscience, Bristol, UK). The cells were grown until 80–95% confluent. The human induced pluripotent stem cells (hiPSCs) were stimulated with small-molecules to obtain CMs, as described earlier.[393–395] Differentiation was started by adding 6 µM CHIR99021 (Tocris Bioscience, Bristol, UK) in Roswell Park Memorial Institute (RPMI) 1640 medium supplemented with B-27 without insulin (RB-ins) to the cells (day 0). After 24 h, CHIR99021 was removed and replaced with fresh RB-ins (day 1). On day 3, the medium was changed to RB-ins containing 2.5 µM Wnt-C59 (Tocris Bioscience, Bristol, UK) for 48 h. From day 5 to 11, the cells were maintained in RB-ins. Purification of the CM cultures, on day 11 9 and 13, was obtained by feeding the cells were with RPMI 1640 without glucose with B-27 supplement. From the 15th day, the cells were maintained in RPMI 1640 supplemented with B-27 (RB + ins). Between days 15 and 17, dissociation of beating hiPSC-CMs was achieved by incubating them in cell dissociation solution containing 40% enzyme-free cell dissociation buffer (Gibco), 40% RPMI 1640 (Gibco) and 20% trypsin–EDTA (Gibco) (final trypsin concentration 0.01%) for 7–8 min. Trypsin was inactivated with RB + ins supplemented with 10% FBS. Cells were then centrifuged and suspended in RB + ins with 10% FBS containing 10 µM ROCK inhibitor Y-27632 and seeded at 2.5×10^4 cells per well on gelatine-coated 96-well plates. The obtained CMs cultures were almost pure (> 95%), indicating high differentiation efficiency. The cells were let to attach for 2 days, after which they were maintained in RB + ins (without FBS) until the NP treatments on day 20. Treatments (NPs and drugs) were administered to the cells in RB + ins (without FBS).

4.2.4 Isolation of monocytes from human peripheral blood mononuclear cells (PBMCs) and polarization in M1- / M2-like macrophages (I)

Isolation of monocytes was performed, as described elsewhere with some modifications.[396] Briefly, PBMCs were isolated on Ficoll-Paque (1.077 g/mL density) gradients, according to the manufacturer's instructions (GE Healthcare Bio-sciences, Piscataway, NJ) from buffy coats obtained from unknown healthy anonymous donors from the Finnish Red Cross. Once counted, CD14+ monocytes were isolated from PBMCs by magnetic labelling using MAb CD14 conjugated microbeads (Miltenyi, Biotech, GmBH, USA), according to the manufacturer's instructions. They were then grown in Petri dishes at a density of 2×10^5 cells per mL in RPMI 1640 medium (Gibco, Grand Island, NY, USA), supplemented with 10% FBS, 1% NEAA, 1% L-glutamine and 1% PS. Once isolated, PBMCs were cultured in complete RPMI 1640 medium further supplemented with Granulocyte-Macrophage Colony-Stimulating Factor (GM-CSF) (20 ng/mL) or Macrophage Colony-Stimulating Factor (M-CSF) (20 ng/mL), depending on whether monocytes were destined to M1 or M2 polarization. After three days, the medium was changed and monocytes were left to mature until day six. Then, cells were kept for 48h in medium supplemented with 100 ng/mL of lipopolysaccharide (LPS) or 20 ng/mL IL-4 to obtain, respectively, M1 and M2–like macrophages.

4.2.5 Isolation of murine bone marrow derived macrophages (BMDMs) and polarization in M1–/M2–like macrophages (I–III)

Female 6-8 week old BALB/c mice were sacrificed with CO_2 and cervical dislocation. The femur and tibia bones were collected, cleaned from extra tissues and rinsed in sterile PBS (pH 7.4) at 4 ºC. The bones were then cut open, without losing the bone marrow, which was then flushed with a syringe, equipped with a 27G needle, in a Petri dish containing cold PBS.

Clumps were broken by pipetting, and the cell suspension was transferred to a 15 mL Falcon and centrifuged at 500g for 5 min. The pellet was then gently dispersed into 1 mL of Ammonium-Chloride-Potassium (ACK) lysing buffer (150 × 10^{-3} M of NH_4Cl, 10 × 10^{-3} M of $KHCO_3$, and 0.1 × 10^{-3} M of Na_2EDTA) and incubated for 1 min to remove RBCs. After this passage, 9 mL of complete RPMI medium were added and the cell suspension centrifuged again at 500g for 5 min. Cell were counted, dispersed in complete RPMI medium at density of 1 × 10^7 cells per mL and 200 µL of cell suspension were added in Petri dishes, containing 10 mL of complete RPMI medium supplemented with GM-CSF or M-CSF (20 ng/mL), depending on whether cells were destined for M1-/M2-like polarization. After three days, the medium was changed and monocytes were left to mature until day six. Then, cells were kept for 48h in medium supplemented with 100 ng/mL of LPS and 20 ng/mL INF-γ or 20 ng/mL IL-4 to obtain, respectively, M1- and M2-like macrophages.

4.2.6   Flow cytometry study of the expressed markers (I–III)

In publication **(I)**, human-derived M1- and M2-like macrophages were stained with allophycocyanin (APC)-CD86 and fluorescein isothiocyanate (FITC)-CD206 (Miltenyi, Biotech, GmBH, Germany) for 15 min at 4 ºC in the dark. Analogously, murine-derived matured and 48 h stimulated MØ macrophages were treated instead with cocktails made, respectively, of APC–F4/80 and phycoerythrin-Cy7 (PE-Cy7)-CD11b, and APC-CD206 and FITC-CD11c. Fluorescence was detected by a LSR II flow cytometer (BD Biosciences, USA), and the data were analyzed with FlowJo software (Tree Star, Inc., USA). In publications **(II)** and **(III)** the phenotype of M1– and M2–like macrophages was assesses by evaluating their markers' expression. After blocking unspecific staining by incubating for 10 min with 1% (w/v) BSA, cells were stained with APC-CD206 (BioLegend, USA) and Peridinin chlorophyll protein(PerCP)-Cyanine5.5-CD86 (BioLegend, USA) for 15 min at 4 ºC in the dark. Fluorescence was detected by a BD Accuri C6 Plus (BD, USA) flow cytometer, and the data were analyzed with FlowJo software (Tree Star, Inc., USA).

4.2.7   Cytocompatibility studies (I–II)

In publication **(I)** the cell viability was tested on both human and murine primary macrophages, while in publication **(II)** the biocompatibility was tested with both the HCAEC cell line and primary rat cardiac cells. In publication **(III)** cellular viability was tested on both primary murine and rat CMs, primary rat fibroblasts and hiPSC-CMs. Cells were seeded in white bottom 96-well plates (Corning, USA) at a density of 2 × 10^4 cells per well and left to attach overnight. NP-suspensions were prepared in the corresponding media at different concentrations (10, 25, 50, 100, 250 and 500 µg/mL) and incubated respectively for 6 h and 24 h with HCAEC and 24 and 48h with primary cardiac cells. The cell viability of TA, Fe^{3+} and TA- Fe^{3+} were also tested. A solution of 9% (v/v) of Triton X-100, cell medium, and CellTiter-Glo® reagent were used as negative, positive and blank controls, respectively. After incubation, cells were let to stabilize at room temperature for 30 min and then washed twice with Hanks' Balanced Salt Solution−(N-[2- hydroxyethyl]piperazine-N´-[2-ethanesulfonic acid]) (HBSS−HEPES, pH 7.4). Thereafter a solution (50:50) of HBSS–HEPES and assay reagent (CellTiter-Glo®, Promega, USA) was added to the cells for 2 min. The cell viability was finally determined by luminescence, which was measured using a Varioskan Flash Multimode Reader (Thermo Fisher Scientific).

4.2.8 Cellular association and internalization studies (I–III)

The NP–cell interactions were evaluated both quantitatively by flow cytometry and qualitatively by confocal imaging. In publication **(I)** we evaluated the interaction between Putre-AcDX NPs and RAW 264.7 and KG-1 cell lines, as well as M1– and M2–like macrophages of both human and murine origin, while in publication **(III)** we extended the investigation to cardiac cells of murine, rat and human origin. In publication **(II)** the uptake of AcDXSp-TA NPs was evaluated in both rat cardiac cells and murine derived M1– and M2–like macrophages. Macrophages and primary rat cardiac cells were seeded onto 6–well plates at a density of 5×10^5 and 1.5×10^5 cells per well for macrophages and CMs, and non-myocytes, respectively, and let attach overnight at 37 ºC. Cells were then incubated with 50 µg/mL of fluorescent-labelled NPs for 1 h and 2 h, respectively, for macrophages and cardiac cells. In publication **(II)** the incubation between murine macrophages and AcDXSp-TA NPs was 2h. Competition studies **(III)** on the uptake of Putre-AcDX-PEG-TT1-ANP NPs, were performed by pre-treating the cells for half an hour with ANP at a concentration 1×10^{-4} M. After incubation, RAW 264.7 and cardiac cells were washed twice with PBS-EDTA, collected by trypsinization and then washed again. KG-1 were pelleted and washed twice with PBS-EDTA. Both human and murine macrophages were washed twice with PBS–EDTA and then kept for 15 min on ice with PBS–EDTA solution (3×10^{-3} M of EDTA). All the cells were finally dispersed in PBS–EDTA and quantitative uptake was evaluated by an LSR II flow cytometer (BD Biosciences, USA) **(I, III)** and by a BD Accuri C6 Plus (BD, USA) flow cytometer **(II)**. In order to quantify the cellular uptake, external fluorescence was quenched by incubation for 4 min with trypan blue (TB; 0.005% v/v). Cells were then pelleted by centrifuging, dispersed in fresh PBS–EDTA and samples were run again. All the data were analyzed with FlowJo software (Tree Star, Inc., USA) and results were reported as bare median fluorescence intensity (MFI) values or normalized to the control.

The endocytosis mechanism adopted by cells to uptake AcDXSp-TA NPs and Putre-AcDX-PEG-TT1-ANP NPs was studied for both primary CMs and FBs **(II)**, and M1– and M– like macrophages of both human and murine origin **(I)**, respectively. Before incubation with the NPs, cells were treated with the compounds listed in **Table 4**, in order to inhibit specific uptake pathways, and thus, evaluate the mechanism of internalization of the NPs. Incubation with the compounds was performed for 30 min, followed by the addition of AcDXSp-TA NPs or Putre-AcDX-PEG-TT1-ANP. After incubation, cells were washed, detached, dispersed in PBS–EDTA and analyzed by flow cytometry, as described above.

The qualitative intracellular uptake of the NPs was evaluated by confocal microscopy with a Leica TCS SP8 STED 3X CW 3D inverted microscope (Leica Microsystems, Germany) **(I–III)**. RAW 264.7 and primary macrophages were seeded at a cell density of 7×10^4 cells per well into 8-well chambers (Lab TekTM, Thermo Fisher Scientific, USA) and let attaching overnight **(I)**. For primary rat and mouse CMs and hiPSC-CMs, cells were seeded in 8-well chambers pre-coated with gelatine **(III)**. Cells were then incubated with Putre-AcDX NPs at concentration of 50 µg/mL for 1 h. After incubation, macrophages were washed twice with PBS and then stained with CellMask Deep Red (Thermo Fisher, USA), followed by fixation with 4% paraformaldehyde (Sigma-Aldrich, USA), and nuclear staining with DAPI (Thermo Fisher, USA). After staining steps and fixation, cells were washed three times with PBS. Images were captured by using a 63× water objective and then processed with Leica AS software (Leica Microsystems, Germany).

Table 4. Compounds used to inhibit the different mechanisms of endocytosis

Compound	Uptake mechanism inhibited	Concentration
Cytochalasin D (SigmaAldrich, USA)	Macropinocytosis (actin polarization/depolarization)	5-10 µM
Nocodazole (Sigma-Aldrich, USA)	Macropinocytosis (microtubule disruptor)	20 µM
Genistein (Sigma-Aldrich, USA)	Caveoline-mediated endocytosis	200 µM
Chlorpromazine (TCI, Japan)	Clathrin-mediated uptake	10 µg/mL
Sodium azide (SigmaAldrich, USA)	Active transport	100 mM
Protamine sulfate (TCI, Japan)	Adsorptive-mediated endocytosis	1 mM

The qualitative uptake studies were performed also on primary CMs, FBs, and co-cultures, both with and without TGF-β stimulation **(II)**. Cells were seeded in 8-well chambers pre-coated with gelatine. Cell co-cultures were settled up by seeding directly the cell suspension obtained after tissue digestion. After seeding, cells were let attach overnight and then they were treated with TGF-β at a concentration 3 ng/mL for 48 h. Subsequently, cells were incubated with 50 µg/mL of fluorescently labelled AcDXSp-TA NPs for 2 h. After treatment with AcDXSp and AcDXSp-TA NPs, cells were washed 2 × 5 min with PBS, fixed for 20 min with a solution of paraformaldehyde (PFA) at a concentration of 4% (v/v) and then washed again 3 × 5 min with PBS. After fixation, immunostainings were carried out. Some wells were left untreated to characterize the three different cell cultures. First, cells were permeabilized with 0.1% (w/v) Triton X-100, then washed 2 × 5 min with PBS and blocked with 4% (v/v) FBS in PBS for 45–60 min. Incubation with primary antibodies for 60 min at room temperature, shaking at 300 rpm was then following. Different cells were treated with different antibodies according to the scheme presented in Table 5. Afterward, cells were washed 3 × 5 min with PBS and then secondary antibodies (anti-rabbit 546 (1:250, A-11035), anti-mouse 488 (1:250, A11029), anti-rat 647 (1:200, A-21247) (all from Invitrogen, USA), and DAPI, (1:250, Vector Laboratories) were added to each well and incubated for 45 min at room temperature, shaking at 300 rpm. Cells were washed 3 × 5 min with PBS and stored in darkness at +4 °C in Ibidi glycerol-based mounting media until imaging (Ibidi, Germany). Images were captured and then processed as described above.

Table 5. Primary antibodies used in qualitative uptake studies.

	Cardiomyocytes	Fibroblasts	Co-culture
Uptake samples	Rabbit anti-Collagen I (1:500, ab34710, Abcam)	Rabbit anti-Collagen I (1:500, ab34710, Abcam)	Rabbit anti-Collagen I (1:500, ab34710, Abcam)
Characterization samples	Rabbit anti-Collagen I (1:500, ab34710, Abcam), mouse anti-cTnT (1:500, MS_295, ThermoFisher Scientific)	Rabbit anti-Collagen I (1:500, ab34710, Abcam), rat anti-Vimentin (1:250, MAB2105, Rndsystem)	Rabbit anti-Collagen I (1:500, ab34710, Abcam), mouse anti-cTnT (1:500, MS_295, ThermoFisher scientific), rat anti-Vimentin (1:250, MAB2105, Rndsystem)

4.2.9 Repolarization studies (III)

Murine M1– and M2–like macrophages were differentiated from precursor cells isolated from the bone marrow of mice as described above. For the studies on the phenotype change

upon treatment with NPs, MØ macrophages were seeded on 12-well plates at a density of 3 × 10^5 cells per well and treated with different cytokines for 48h to obtain M1– and M2–like macrophages. After 48h, cells were treated with different NPs suspensions at a concentration of 50 µg/mL for 30, 60 or 120 min. After the different time-points, cells were detached as described above and the cells were blocked with a solution 1% (w/v) of bovine serum albumin (BSA) for 10 min. After blocking, cells were incubated for 20 min in the dark at + 4 °C with a cocktail of antibodies constituted by APC–CD206 (BioLegend, USA) and PerCP-Cyanine5.5-CD86 (BioLegend, USA). Fluorescence was detected by a BD Accuri C6 Plus (BD, USA) flow cytometer, and the data were analyzed with FlowJo software (Tree Star, Inc., USA).

4.2.10 Immunostainings and high content cell imaging and analysis (II, III)

The CMs proliferation was assessed by Ki67 **(II)**, BrdU **(III)**, phospho-histone H3 **(II)**, β-catenin **(III)**, phospho-mitogen-activated protein kinase-activated protein kinase 2 (MAPKAPK2) **(III)** and aurora B immunostainings **(II)**. Primary rat **(II, III)** and murine **(III)** CMs were seeded in transparent 96-well plates (Corning, USA) at a cell density of 2.5 × 10^4 cells per well and left to attach overnight. Ki67, BrdU, β-catenin and phosphor-MAPKAPK2 immunostainings were performed also on hiPSC-CMs and in that case, cells were seeded at a cell density of 2.5 × 10^4 cells per well. hiPSC-CMs were obtained, as described above, and they were at day 20 post-differentiation when treated with the NPs. Cells were then treated with different concentrations of empty and loaded Putre-AcDX, Putre-AcDX-PEG-TT1-ANP, AcDXSp and AcDXSp-TA NPs corresponding to concentrations of CHIR99021 of 1 × 10^{-6}, 3 × 10^{-6}, 5 × 10^{-6} and 10 × 10^{-6} M (calculated according to LD values). Compounds alone, were used as positive controls, while medium alone and medium containing 1% (v/v) DMSO, were used as controls for empty and drug-loaded NPs. For murine primary CMs and hiPSC-CMs we chose the concentration of CHIR 5 × 10^{-6} M in BrdU, β-catenin and phosphor-MAPKAPK2 immunostainings **(III)**, since it was the one showing the better results for compounds loaded in Putre-AcDX-PEG-TT1-ANP NPs for rat CMs and was corresponding to still safe concentration of NPs. After 24 h, cells were placed on ice to block all cellular actions, washed twice with PBS pH 7.4 and then fixed for 20 min with a solution of PFA at a concentration of 4% (v/v). After fixation, cells were washed 3 × 5 min with PBS and then permeabilized for 10 min with 0.1% (w/v) Triton X-100. Then cells were washed 2 × 5 min with PBS and blocked with 50 µL of 4% (v/v) FBS in PBS for 45–60 min. For BrdU immunostainings, before blocking with FBS, the DNA was denatured by addition of 50 µL of a solution of sodium borate 1 × 10^{-1} M pH 8 for 30 min, followed by neutralization by addition of 50 µL of HCl 2 × 10^{-1} M. FBS was removed and cells were incubated with 30 µL of primary antibodies (Rabbit Anti-Ki67 antibody [SP6] (1:200, ab16667, Abcam), Rabbit Anti-Phospho-Histone H3 (Ser10) (1:500, 9701S, Cell Signaling Technology), Rabbit Anti-Aurora B (1:500, ab2254, Abcam), Rat Anti-BrdU (1:250, abcam ab6326), Rabbit Anti-β-catenin (1:250, abcam ab32572), Rabbit Anti-Phospho-MAPKAPK2 (Thr334) (1:200, Cell Signaling, 3041S),and Mouse Anti-troponin T, cardiac (1:500, MS_295, ThermoFisher scientific)) for 60 min at room temperature, shaking at 300 rpm. Aurora B and phospho-histone H3 immunostainings were performed by incubating cells with primary antibodies overnight at +4 °C. Primary antibodies were washed away 3 × 5 min with PBS and 30 µL of secondary antibodies (goat anti-mouse IgG H+L Alexa-546 (1:250, A-11030, Life Technologies; donkey anti-rabbit IgG H+L Alexa-647 (1:250, A-31573, Life Technologies), goat anti-rabbit IgG (H+L) Alexa-546 (1:250, Life technologies, A-11035); goat anti-rat IgG H+L Alexa-647 (1:250, Life technologies, A-21247) and DAPI (1:250, Vector Laboratories) were

added for 45–60 min at room temperature, shaking at 300 rpm. Wells were also treated with medium and used as a secondary antibody control. Cells were finally washed 3 × 5 min with PBS and stored in darkness at +4 °C until imaged. Plates were then imaged with an ImageXpress Nano (Molecular Devices, USA) high content imaging system **(II)** or with a Cellomics CellInsight high-content analysis platform (Thermo Scientific) **(III)**, using a 10× objective. Analysis was conducted with a MetaXpress 6.6.1.42 software (Molecular Devices) **(II)** or with the Cellomics CellInsight simultaneously, using a protocol based on Compartmental Analysis bioapplication **(III)**. For quantification, the cells were first identified based on DAPI fluorescence, which defined the nuclear area. Non-myocytes were excluded based on the absence of cardiac troponin T staining (cTnT). The threshold for cardiac troponin T fluorescence intensity was set manually in each experiment to allow optimal exclusion of non-myocytes. The data were collected only from cardiac troponin T-positive cells. The intensities of Ki67, phospho-histone H3 and aurora B stainings were analyzed within the nucleus. The threshold for Ki67, phospho-histone H3, and aurora B positive cells was set manually in each experiment to adjust for minor variation in staining intensity. For aurora B immunostainings, analysis of the surface area of CMs by identifying and quantifying the area of cTnT staining was also run. The percentage of CMs in telophase was obtained by manually counting in a blinded experiment the number of cells that were presenting the aurora B staining between the two dividing cells. Percentages were then calculated referring to the total amount of CMs present in each well (calculated by the MetaXpress 6.6.1.42 software). The quantification of percentage of BrdU positive cells, Phospho-MAPKAPK2 and β-catenin intensities was done instead by high content imaging choosing regions of interest corresponding to the nucleus and the cytoplasm (DAPI staining was used to define the nuclear area and a 5-pixel ring immediately outside the nucleus was considered to represent cytoplasm).

4.2.1   Real-time quantitative polymerase chain reaction (RT-qPCR) Studies (II)

The anti-fibrotic effect of TA and the proliferative effect of drug-loaded NPs were evaluated by RT-qPCR. Primary rat FBs and CMs were seeded in six-well plates (Corning, USA) at a cell density of 2.5×10^5 and 5×10^5 cells per well, respectively, and let to attach overnight. Empty and loaded NPs, as well as compounds alone, were added to the cells in order to achieve a concentration of CHIR99021 of 3×10^{-3} M, based on the LD of the NPs. Cells were treated also with medium and medium containing 1% (v/v) of DMSO as controls. After 24 h incubation, RNA was isolated from cells using TRIzol reagent (Invitrogen), following the manufacturer's protocol by using the Phase Lock Gel system (Eppendorf AG). The cDNA was synthesized from total RNA with a First-Strand cDNA Synthesis Kit (GE Healthcare Life Sciences), following the manufacturer's instructions. Finally, the RNA was analyzed by RT-PCR on a LightCycler 480 qPCR machine (GE Healthcare Life Sciences) using TaqMan chemistry. The results were quantified using ΔΔCT method and normalized to housekeeping gene 18S quantified from the same samples. The following pre-designed TaqMan probes from Thermo Fisher Scientific were used in the assay: 18S (4352930E), Col1a1 (Rn01463848_m1), Spp1 (Rn00681031_m1), Tgfb1 (Rn00572010_m1), Tnfa (Rn01525859_g1), Myc (Rn07310910_m1) Fos (Rn02396759_m1), Ccna2 (Rn01493715_m1), Ccnb1 (Rn01494180_g1), Ccnd1 (Rn00432359_m1) and Ccne1 (Rn01457762_m1).

4.3   *In vivo* studies (III)

4.3.1   Experimental model of MI and NPs injection (III)

Male Sprague-Dawley rats (Central Animal Laboratory, University of Turku, Turku, Finland) (283 ± 29 g) were anesthetized and infarction was induced by a permanent ligation of the left coronary artery (LCA) as previously described. Ligation was confirmed visually as pale appearance of the myocardium at risk. The sham operation consisted of all the same protocols except that the suture was not tightened around the LCA. MIs were further confirmed by hematoxylin and eosin (H&E) stainings, which were scanned with a digital slide scanner (Pannoramic 250 Flash, 3DHistech Ltd., Budapest, Hungary). Animals were kept under isoflurane anaesthesia (Attane Vet., ScanVet Animal Health, Finland) in air/oxygen carrier at 0.4/0.6 (L/min) during sucrose or NPs administration. 2mg of NPs were injected in the tail vein after being re-suspended in 100 μL of isotonic sucrose, followed by a flush of 0.1 mL of sterile 0.9% NaCl. The animals were sacrificed at specific time points with an overdose of isoflurane followed by cervical dislocation.

4.3.2   *Ex vivo* biodistribution studies

The biodistribution of the NPs was studied at 3 days (n = 5 for each group) or 7 days (n = 5 for each group) after coronary ligation or at 3 days (n = 5 for each group) or 7 days (n = 5 for each group) after the sham operation. The rats were divided into four groups: (1) isotonic sucrose; (2) Putre-AcDX-PEG NPs; (3) Putre-AcDX-PEG-ANP NPs; and (4) Putre-AcDX-PEG-TT1-ANP NPs. One hour post NPs injection, animals were sacrificed and different organs were collected. For the study of *ex vivo* NPs biodistribution, hearts, livers, and spleens were collected and sliced into 8 and 20 μm sections. Sections deriving from all the above mentioned organs, except hearts, were fixed with 4% PFA and stained with DAPI. Hearts sections were blocked with 1% BSA for 1h after fixation and then stained with anti-CD86 (1:200, from BioRad, MCA2874GA) and anti-CD163 (1:200, from Invitrogen, PA5-78961) primary antibodies overnight at 4 °C. After overnight incubation, sections were washed 3 times for 5 min with PBS ant then incubated with secondary antibodies (Goat anti-mouse IgG H+L Alexa-546 (1:250, Life technologies A-11030); donkey anti-rabbit IgG H+L Alexa-647 (1:250, A-31573, Life technologies)) and DAPI (1:250, Vector Laboratories) for 1 h. Sections were then washed again 3 x 5 min with PBS and slides were mounted with a non-hardening mounting media. Slides were then imaged using a 63× water objective in a Leica TCS SP8 STED 3X CW 3D inverted microscope (Leica Microsystems, Germany) and images were then processed with Leica AS software (Leica Microsystems, Germany) to check the presence of NPs in the different organs.

4.3.3   Immunoprofiling

For each experimental group of the *in vivo* studies, spleen and blood were collected to study the immunoprofiling of the animal upon NPs injection. Spleens were smashed onto 70 μm strainers. White cells from blood were instead separated by Ficoll-Paque (1.077 g/mL density) gradients according to the manufacturer's instructions (GE Healthcare Bio-sciences, Piscataway, NJ). White cells derived from blood and cells suspensions derived from spleens, were then blocked with a solution 1% (v/v) of BSA for 10 minutes. After that, they were incubated with a cocktail of antibodies for 20 min, at 4 ºC in the dark, to study the population

of macrophages and T cells: APC anti-rat CD3, PE anti-rat CD8 and PerCP anti-rat CD4 (all from BioLegend) were used to study the T cell population; PerCP anti-rat CD11b, AlexaFluor647 anti-rat CD86 and PE anti-rat CD163 (the first two from BioLegend and the last one from Novus Biologicals) were used to study the macrophages population. Stained cell suspensions were then washed with PBS and flow cytometry analysis was performed using a BD Accuri 6 plus (BD Biosciences) and analyzed by FlowJo software (Tree Star, Ashland, OR, USA).

4.4   Statistical analysis

Statistical analysis was performed using a GraphPad Prism 7 (GraphPad Software, Inc., La Jolla, CA, USA). The statistical methods used to analyze the data from each experiment are described in each figure caption.

4.5   Ethics

For the primary cell cultures for *in vitro* experiments in all the publications **(I–III)**, the animals were used after an internal license was authorized and approved by the Laboratory Animal Centre, University of Helsinki. In publication **(III)**, experimental protocols with animals were approved by the national Animal Experiment Board in Finland and the Regional State Administrative Agency for Southern and Eastern Finland, and they were carried out in compliance with the European Union directive.

5 Results and Discussion

Nanotechnology has brought great innovation and advantages in the biomedical field and it has helped to overcome the drawbacks of conventional therapies.[17,221] Current treatment of MI and HF is still unsuccessful in completely restoring the function of a damaged heart and leaves millions of patients without proper treatment.[5,6] Nanomedicine can push regenerative therapies towards clinic use. However, selective targeting of the infarcted heart, which is fundamental to avoid the systemic and potentially dangerous adverse effects of regenerative therapies, still represents a challenge.[24]

In this thesis, two approaches to improve the heart targeting abilities of AcDX-based NPs were explored (**Figure 5**). In the first approach, the macrophage recruitment to the infarcted heart[85] was exploited to improve the heart targeting abilities of ANP peptide. For that purpose, the NPs were further modified with lin-TT1 peptide, which is able to target tumor associated macrophages, as well as macrophages associated to the atherosclerotic plaques (**Figure 5A**).[27–29] In the second approach, TA was used to coat AcDXSp NPs, as TA has shown heart targeting abilities due to affinity for components of the ECM (**Figure 5B**).[24] Both systems were physico-chemically characterized and their drug release profile was studied. Then, *in vitro* biocompatibility, cell–NP interactions and bioactivity of the compounds encapsulated were investigated on secondary cell lines and different primary cells. Finally the biodistribution and safety upon administration of the first system were assessed *in vivo* on a rat model of MI.

A. Putre-AcDX-PEG-TT1-ANP NPs
B. AcDXSp-TA NPs

CHIR99021   Putre-AcDX NPs

SB203580   ANP

Lin-TT1

CHIR99021   AcDXSp NPs

SB203580   TA coating
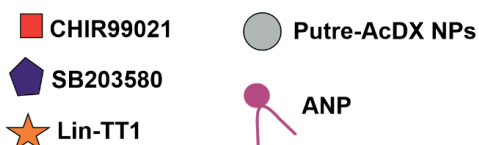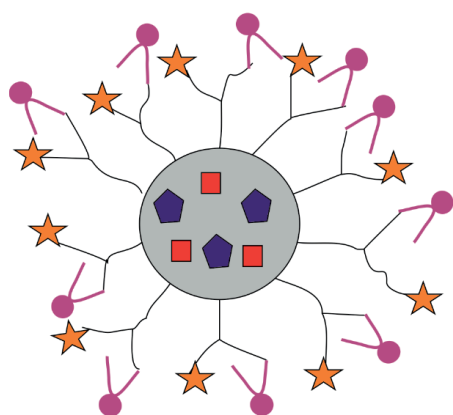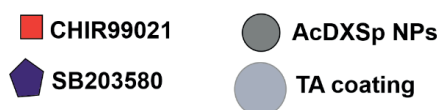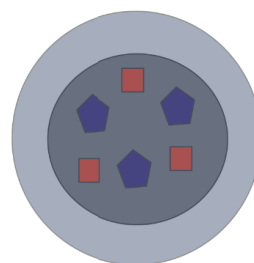
Figure 5. Schematic representation of the NPs developed in this thesis. (**A**) Putre-AcDX-PEG-TT1-ANP NPs: Putrescine-modified acetalated dextran based NPs, modified with a branched PEG through EDC/NHS coupling and further conjugated with lin-TT1 and ANP peptides **(I,III)**.

(**B**) AcDXSp-TA NPs: spermine-modified acetalated dextran NPs, coated with a coordination complex made of TA and Fe^{3+} ions (**II**).

5.1 Physicochemical characterization of the NPs and investigation of their drug release profile (I, II)

Nanocarriers are seen as versatile tools for the delivery of therapeutical or imaging agents. The fine tuning of different characteristics, such as size, charge, shape, composition, surface roughness, *etc.*, influences their accumulation in specific sites of the body, their interaction with cells, as well as their safety, drug loading and release profiles.[17] It is then of utmost importance to design NPs in order to satisfy specific cues and study their characteristics before testing them *in vitro* and *in vivo*. Here, acetalated dextran-based NPs have been chosen because of their biocompatibility, pH-sensitive properties and ability to encapsulate hydrophobic compounds.[23] Their design was optimized in order to obtain carriers with determined features. In publication (**I**), putrescine-modified acetalated dextran NPs, abbreviated as Putre-AcDX NPs, were modified with a branched PEG to allow the surface conjugation of Lin-TT1 and ANP peptides.[246] They were loaded with two compounds, CHIR and SB, for the stimulation of CMs proliferation.[160] In publication (**II**) instead, spermine-modified acetalated dextran NPs, abbreviated as AcDXSp NPs, were used to deliver the same compounds, CHIR and SB. The system was then coated with a coordination complex made of TA and Fe^{3+} ions.[248]

5.1.1 Size, PDI, surface charge, KBr-FTIR, elemental analysis and morphology of Putre-AcDX and AcDXSp NPs (I, II)

The Putre-AcDX and AcDXSp NPs were prepared by single o/w emulsion technique, as previously described,[247] and drugs (CHIR and SB) were dissolved in the organic phase together with the polymers. Putre-AcDX NPs were then conjugated with PEG and the peptides, lin-TT1 and ANP in different conjugation steps (**I**). AcDXSp NPs were instead coated by simply mixing and vortexing TA and Fe^{3+} ions, similar to what reported in literature (**II**).[397] The formation of a coating film was obtained by formation of coordination bonds between TA and Fe^{3+} in a pH-depended manner,[390] resulting in a change of color of the suspension, from white to grey (images can be found in the Supplementary Information (SI) of publication **II**). The coating was obtained in a fast (few seconds time) and easy way, representing a more advantageous approach compared to the different and time-consuming conjugation steps usually used to conjugate moieties on the NPs surface. Fe^{3+} was selected because of its adhesive properties after coordination with polyphenolic materials.[398] Moreover, the presence of Fe^{3+} in the coating can also be exploited for magnetic resonance imaging purposes in the future, enabling to follow the NPs fate inside the body.[399] The size, PDI and surface charge of the different NPs was evaluated by dynamic light scattering (DLS) and electrophoretic light scattering (ELS). The size of Putre-AcDX NPs encountered a significant increase after conjugation with peptides (**Figure 6A**). However, encapsulation with compounds, CHIR and SB, had a stabilizing effect on the NPs, since drug-loaded NPs experienced only a slight increase in size upon peptides conjugations. For AcDXSp NPs, there was a small increase of size after coating with TA, but the encapsulation of drugs inside the NPs, did not affect significantly their size (**Figure 6A**).
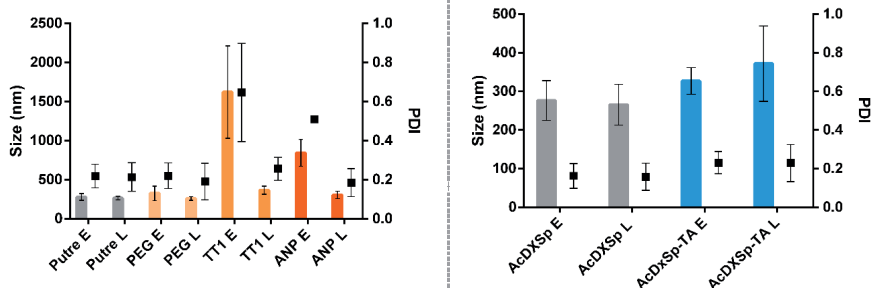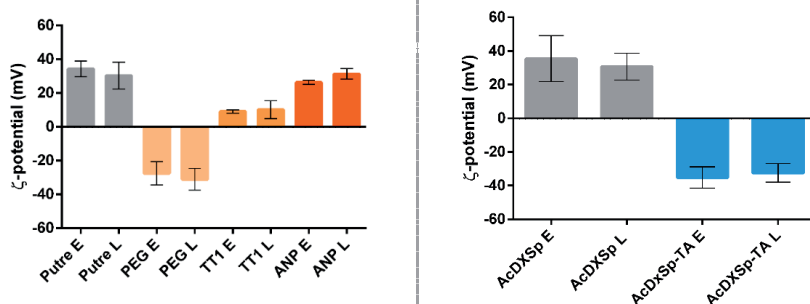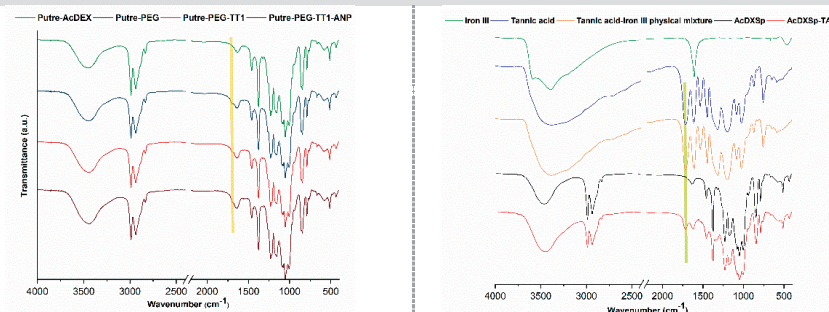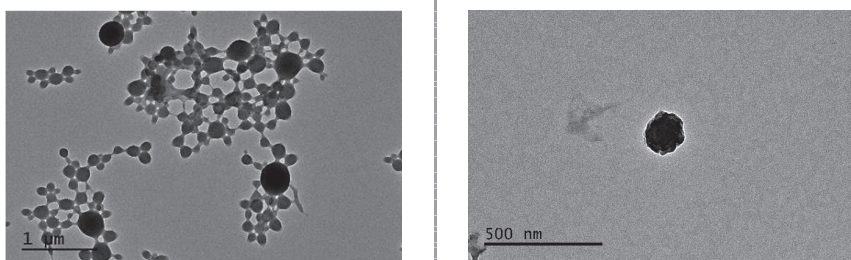
Figure 6. Physicochemical characterization of Putre-AcDX and AcDXSp NPs. (**A**) Size, PDI values and (**B**) ζ-potential (mV) of bare and surface modified Putre-AcDX (left panel) and AcDXSp NPs (right panel). (**C**) KBr FTIR spectra of bare and surface modified Putre-AcDX (left panel) and AcDXSp NPs (right panel). (**D**) Representative TEM images of Putre-AcDX-

PEG-TT1-ANP NPs (left panel) and AcDXSp-TA NPs (right panel). Abbreviations: E, empty; L, loaded; Putre, Putre-AcDX NPs; PEG, Putre-AcDX-PEG NPs; TT1, Putre-AcDX-PEG-TT1 NPs; ANP, Putre-AcDX-PEG-TT1-ANP NPs. Adapted and reprinted with permission from publications **(I)** and **(II)**.

Both bare Putre-AcDX and AcDXSp NPs showed positive charge due to the amine groups of putrescine and spermine, but upon conjugation with branched PEG and coating with TA respectively, the ζ-potential shifted to negative values (**Figure 6B**), suggesting their successful surface modification. In publication **(I)**, further conjugation with TT1 and ANP peptides led to a progressive increase of ζ-potential to positive values (**Figure 6B**). Evidence of successful PEGylation of Putre-AcDX NPs was seen also in the KBr-FTIR spectra, where the presence of the amide-indicative bands at 1565–1570 cm^{-1} (in-plane N–H bending and C–N stretching) and 1630–1640 cm^{-1} (amide C=O stretching) confirmed the formation of a covalent amide bond between the Putre-AcDX and PEG, and the appearance of a shoulder at 1735 cm^{-1} (C=O stretching from –COOH belonging to PEG and maleimide groups), underlined by the yellow band in **Figure 6C**, denotes the presence of free carboxyl groups.

For AcDXSp-TA NPs instead, KBr-FTIR showed appearance in the spectrum of bands corresponding to the carbonyl groups C=O stretching (1714 cm^{-1}), as well as a broadening of the band corresponding to the stretching of the hydrogen bonds established by the hydroxyl groups (O–H) (**Figure 6C**).[400]

The presence of TT1 on the NPs surface was further confirmed by the fluorescence of the FAM moiety conjugated to the peptide, and TT1-binding assay, shown in publication **(I)**. ANP conjugation was further confirmed by elemental analysis, according to which there are 14.14 µg of ANP in 1 mg of Putre-AcDX-PEG-TT1-ANP NPs (table shown in SI of publication **(I)**).

Morphology of the different NPs was evaluated by TEM. Images shown in **Figure 6D**, demonstrate that Putre-AcDX-PEG-TT1-ANP NPs had a spherical shape, while TA-coated AcDXSp NPs presented an irregular coating, due to deposition of the complex between TA and Fe^{3+} ions on the AcDXSp NPs (which are also spherical, as shown in publication **(II)**).

Overall, the physicochemical characterization of both systems suggested the successful achievement of NPs with desired characteristics.

5.1.2   Drug loading and evaluation of drug release profiles from the NPs

The encapsulation of CHIR and SB in NPs helped improving their solubility and pharmacokinetic profile. The encapsulation of the drug molecules was done at a molar ratio CHIR : SB of 1 : 2, which is the optimal ratio, according to the literature, in order to induce CMs proliferation.[159,206] Before studying the drugs release profile from the NPs, the EE and LD of the drugs in the NPs were calculated by determining CHIR and SB quantities with HPLC (**Table 6**).

After functionalization, there is a loss of encapsulated drugs, more evident for Putre-AcDX NPs compared to AcDXSp NPs. This loss could be attributed to the fact that some of the compounds might still be on the surface of the NPs, even though they were washed thoroughly, or to system saturation due to the high amount of compounds loaded at the beginning of the preparation process. However, the amount of encapsulated drugs was still enough to produce an effect on cells.[401,402]

Table 6. EE and LD values for Putre-AcDX and AcDXSp NPs.

Formulation	LD% (CHIR99021)	LD% (SB203580)	EE% (CHIR99021)	EE% (SB203580)
Putre-AcDX NPs	1.62 ± 0.39	3.73 ± 1.01	88.70 ± 3.32	81.30 ± 1.61
Putre-AcDX-PEG NPs	1.35 ± 0.69	2.87 ± 1.72	72.34 ± 4.39	56.36 ± 11.21
Putre-AcDX-PEG-TT1 NPs	1.04 ± 0.19	1.96 ± 0.36	48.25 ± 2.98	31.22 ± 1.33
Putre-AcDX-PEG-TT1-ANP NPs	0.97 ± 0.60	1.67 ± 1.14	33.08 ± 16.06	25.29 ± 9.46
AcDXSp NPs	2.4 ± 0.2	3.9 ± 0.1	79.9 ± 3.1	51.1 ± 1.2
AcDXSp-TA NPs	1.5 ± 0.3	3.2 ± 0.4	67.6 ± 4.6	41.0 ± 6.4

The release profile of CHIR and SB was evaluated in PBS (pH 7.4) and acetate (pH 5.0) buffers, in order to mimic the physiological extracellular environment and the conditions found in acidic intracellular compartments after internalization in the cells, respectively.[403] The release of the drugs was evaluated over 24 h, considering that this is the maximum incubation time with the NPs during the *in vitro* evaluation of CMs proliferation. As expected, the release of the drugs from both AcDXSp and Putre-AcDX NPs was enhanced at pH:5 (**Figure 7**).
Upon conjugation with PEG and the peptides (named CS@Putre-AcDEX-PEG-TT1-ANP in the plot), the release of drugs was faster compared to the bare NPs (named CS@Putre-AcDEX in the plot). This can be explained by the possible increased interaction with the solvent molecules, resulting from the higher hydrophilicity of the nanosystem after surface modifications, which allows the release of the drugs entrapped in the polymer matrix close to the surface of the NPs.[404,405] The coating of AcDXSp NPs with TA instead, resulted in a slower release for both the compounds and this can be attributed to the pH-dependent disassembly of the TA–Fe^{3+} capsules.[390] At pH 2 most of the hydroxyl groups of TA are protonated and this results in rapid destabilization of cross-links and disassembly of the films and capsules. At pH 5 and 7.4, instead, ~70% and 90% of the capsules, respectively, remain intact after 10 days of incubation.[390] However, if a faster release is desired, it can be obtained by just changing the metal used to form complexes with the TA.[397]
Free drugs were used as control and, especially for CHIR, the acidic pH increased its solubility (**Figure 7A** and **7B**). For SB instead (**Figure 7C** and **7D**), encapsulation in NPs improved its stability at pH 5.0, as the free drug started degrading after 8 h, whereas the drug-loaded NPs showed a release of the drug concentration up to 24 h.
Considering also that inflammation occurring in the ischemic myocardium lowers the interstitial pH to 6–6.5,[406,407] these NPs could be used for the sustained release of cargos into the infarcted myocardium under these conditions.
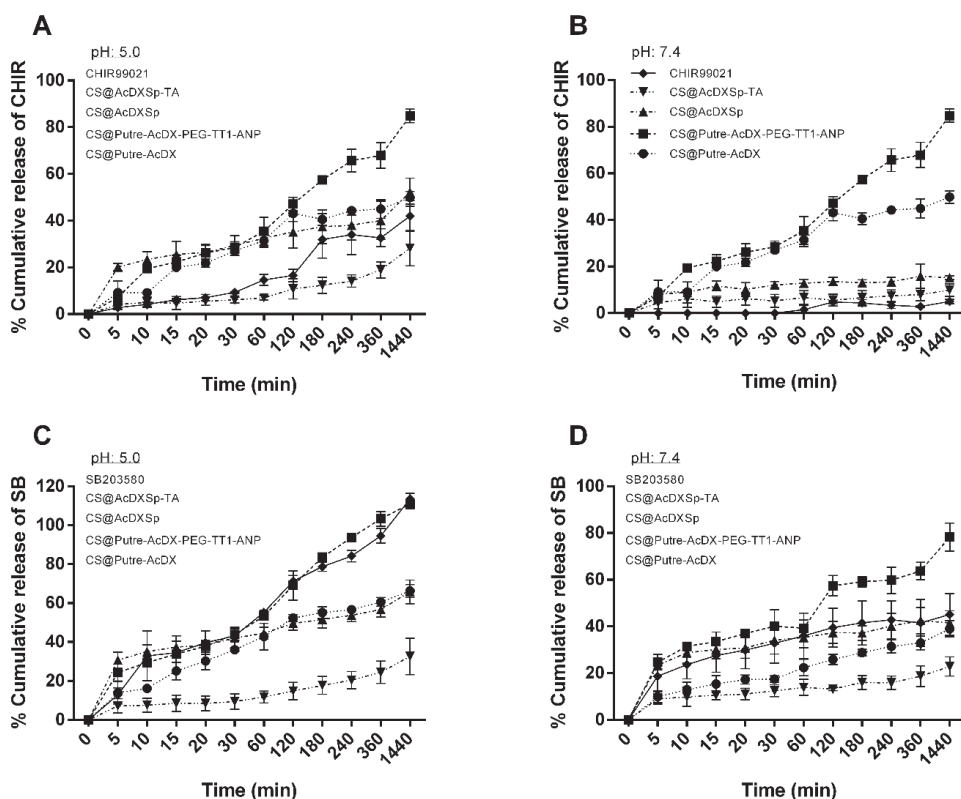
Figure 7. Drug release profiles of Putre-AcDX and AcDXSp NPs. Release profiles of (**A, B**) CHIR and (**C, D**) SB from bare and surface modified Putre-AcDX and AcDXSp NPs at pH: 5.0 and 7.4. Data represented as mean ± s.d. (n ≥ 3 biological replicates in which each time three technical replicates have been used). Abbreviations: C, CHIR99021; S, SB203580. Adapted and reprinted with permission from publications **(I)** and **(II)**.

5.1.3   Stability of the NPs in different media

Since all *in vitro* studies were performed in cell medium, the colloidal stability of the nanosystems was determined by incubation in DMEM/F-12 containing FBS. Stability in human plasma was also evaluated. When NPs were incubated in medium containing serum for 2 h, both bare Putre-AcDX NPs and uncoated AcDXSp NPs showed an increase of size (**Figure 8A**) and PDI (**Figure 8B**) over time, while the surface modification with PEG and the TA-coating NPs made NPs more stable. The same trend was recorded when the stability was performed in human plasma (**Figure 8C**). The stability was monitored also in an isotonic sucrose solution, considered as a vehicle to re-suspend the NPs during injections for future *in vivo* applications. Also in isotonic sucrose solution, the NPs showed very good stability in terms of size and PDI (**Figure 8D,E**), validating its potential use as NPs resuspension media for injections. Altogether, these results showed the increased stability of NPs after PEGylation and TA coating. In particular, TA coating reduced the interaction of coated AcDXSp NPs with plasma proteins and serum *in vitro*, showing similar properties to PEG.[24,308]
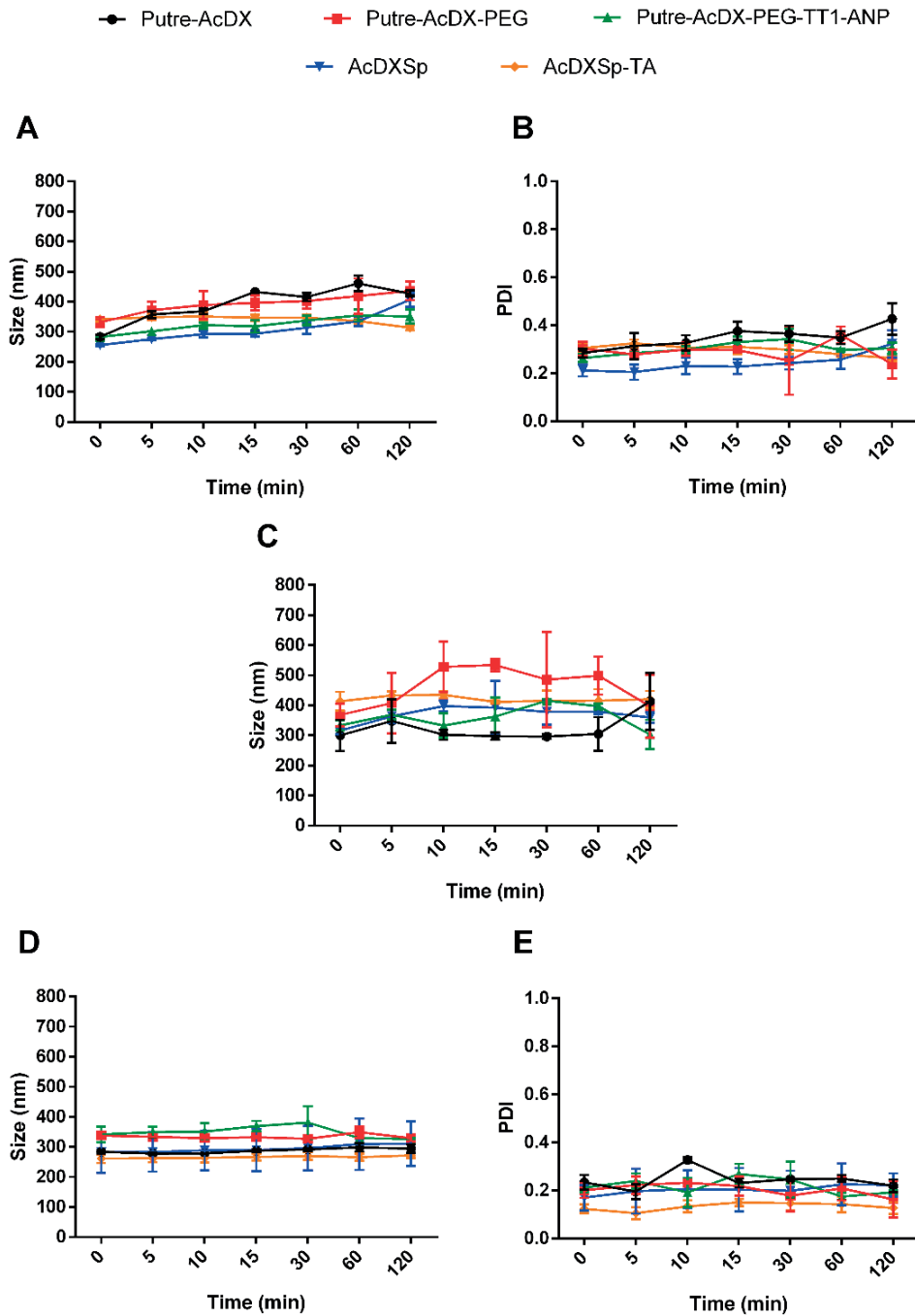
Figure 8. Colloidal stability of Putre-AcDX and AcDXSp NPs in different media. Stability of bare and surface modified Putre-AcDX and AcDXSp NPs in DMEM/F-12 supplemented with 10% FBS in terms of (**A**) size and (**B**) PDI. Changes in size of the NPs were evaluated also upon (**C**) human plasma incubation. (**D**) Size and (**E**) PDI values of the different Putre-AcDX

and AcDXSp NPs incubated in isotonic sucrose. Data represented as mean ± s.d. (n ≥ 3 biological replicates in which each time three technical replicates have been used). Adapted and reprinted with permission from publication **(II)**. Part of the data is also from publication **(III)**.

As previously discussed, it has been demonstrated that in order to extravasate in the infarct site, the optimal size of NPs should be between 20 and 200 nm.[226] In the same study, it was shown that also NPs with size of 500 nm resulted in higher accumulation in infarcted sites, but they had also higher retention in spleen and liver.[226] Since the systems here developed, when incubated in physiological conditions, present bigger sizes, ranging between 250 and 300 nm, they will probably still benefit of improved accumulation in infarcted sites due to their size, but they might also accumulate in liver and spleen.

5.2   *In vitro* screening of the NPs (I–III)

Once the physicochemical features of NPs, as well as their drug release profiles and stability in relevant media have been assessed, investigation of their *in vitro* behaviour was evaluated in different cell lines and primary cells. The first aspect screened was the biocompatibility of the developed systems towards their first contact cells. Then, the interaction between the NPs and cardiac cells and/or macrophages was studied to understand their affinity for specific cells and have insight on their mechanism of uptake. Finally, the biological effects of the compounds encapsulated and of the materials themselves were evaluated on cardiac cells and macrophages.

5.2.1   *In vitro* biocompatibility of Putre-AcDX and AcDXSp (I-III)

The aim of both Putre-AcDX and AcDXSp NPs was to interact with CMs to stimulate their proliferation. However, the heart is composed not only by CMs, but also non-myocytes and once injected, NPs might interact, even to less extent, with those cells. Moreover, in the case of Putre-AcDX NPs, the interaction is extended to macrophages, since their aim is to achieve heart targeting by hitchhiking those cells. It is then of great importance to know if those NPs have any toxic effects on those cells. The cytotoxicity of the NPs was thus investigated using an ATP-based luminescence assay by the quantification of metabolically active cells.[408] Different NPs concentrations and both empty and drug-loaded NPs were screened, with incubation times ranging between 24−48 h, in order to study both concentration and time-dependent toxic effects, as well as to identify the highest concentration of NPs that can be safely used in *in vitro* tests.

The biocompatibility of Putre-AcDX NPs was first studied in macrophages cell lines and primary M1− and M2−like macrophages of both human and murine origin **(I)**. Results for the continuous cell lines can be found in publication **(I)**. The investigation on primary macrophages revealed a concentration- and time-dependent toxicity of the bare empty NPs, attributable to their positive charge (**Figure 9**). Toxicity of positively charged NPs is due to disruption of the plasma-membrane integrity, production of a high number of autophagosomes and damage to cellular organelles, in particular mitochondria and lysosomes, resulting from the increased cell−NP interactions.[233] In addition, murine cells were more sensitive to this toxicity compared to the human counterpart.
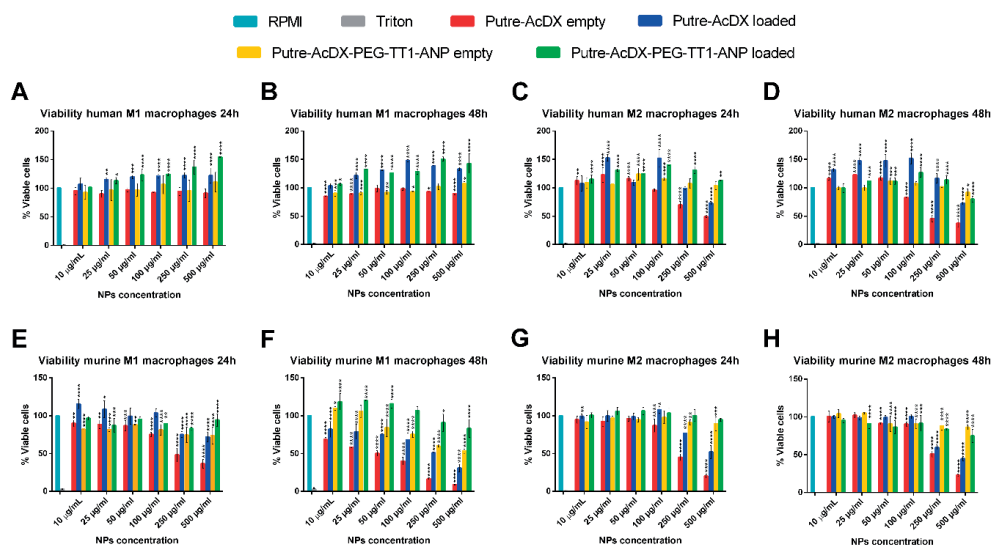
Figure 9. Viability of primary macrophages treated with Putre-AcDX NPs. Cell viability studies were performed on both human (**A–D**) and murine (**E–H**) M1-/M2-like macrophages. NPs were incubated with the cells for both 24 (**A, C, E, G**) and 48 h (**B, D, F, H**). Values are represented as mean ± s.d. (n = 3 biological replicates in which each time 3 technical replicates have been used). A one-way ANOVA followed by a Tukey–Kramer post hoc test was used for the statistical analysis. The significance levels of the differences were set at probabilities of *p < 0.05, **p < 0.01, ***p < 0.001 and ****p < 0.0001 for comparison with the medium, which was used as the control in all the tests. Adapted and reprinted with permission from publication (**I**).

After surface functionalization, the toxicity was reduced and the NPs were more biocompatible because the charge of the nanosystems was not highly positive anymore. Moreover, the encapsulation of drugs corresponded to a significant increase in cell viability, suggesting a protective effect of the two compounds. It is indeed known that the activation of canonical Wnt signaling and inhibition of p38 MAPK pathways are implicated not only in the cytokine production of stimulated macrophages, but also in their proliferation.[409–411] SB203580 increases the stability of granulocyte-colony stimulating factor (G-CSF) mRNA, and enhances its expression at the post transcriptional level, thus stimulating cell proliferation.[409] CHIR99021, on the other hand, upregulates cyclin D1 protein expression, resulting in a proliferative effect.[411]

In publication **III**, the biocompatibility of Putre-AcDX NPs was assessed also on primary rat CMs and FBs (**Figure 10**). Similar results were found for those cells, with bare empty NPs showing a dose- and time-dependent toxicity due to their positive charge. Viability was investigated also on primary murine CMs and hiPSC-CMs to see if results were comparable between species. Results can be seen in the SI of publication **III** and they showed that NPs are safe towards CMs, with exception for Putre-AcDX NPs in murine CMs for 48h. Also in that case, toxicity was due to positive charge of the NPs. Overall, the studies showed that the Putre-AcDX NPs, especially after surface functionalization and when loaded with drugs, were biocompatible towards both macrophages and cardiac cells.
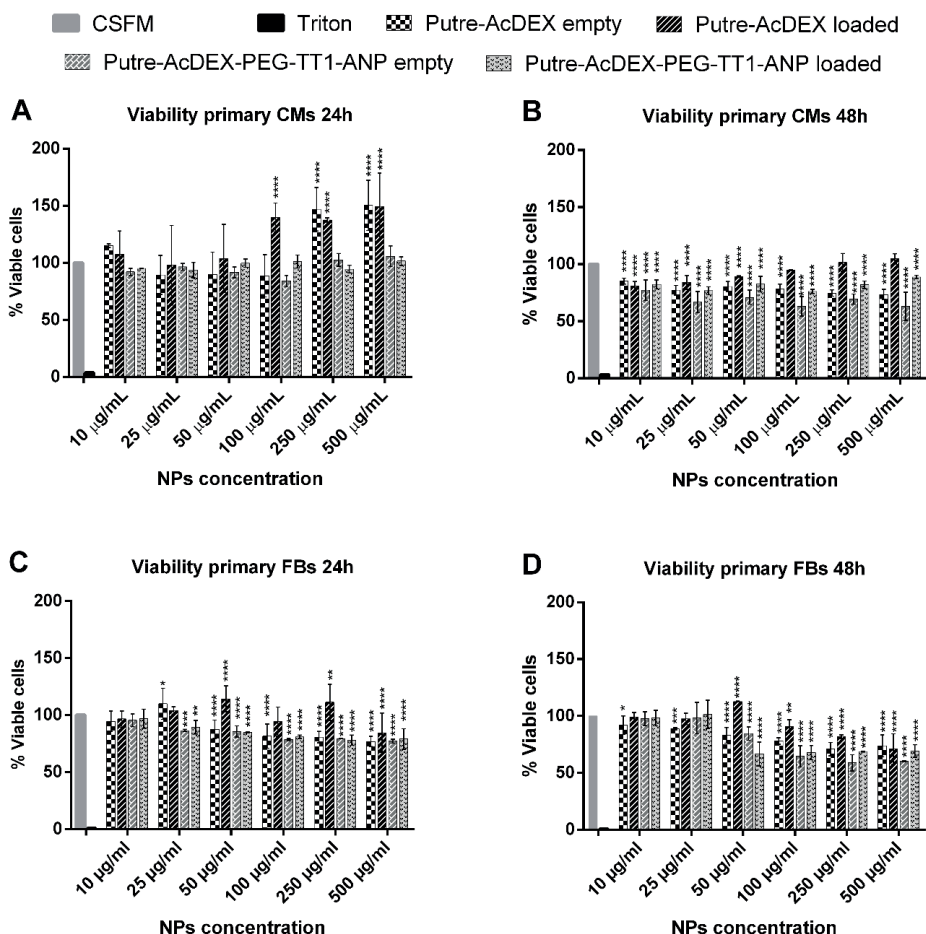
Figure 10. Biocompatibility of Putre-AcDX NPs on primary rat cardiac cells. The safety of bare and modified Putre-AcDX NPs was assessed in both (**A, B**) CMs and (**C,D**) FBs. Values are represented as mean ± s.d. (n = 3 biological replicates in which each time three technical replicates have been used). A one-way ANOVA followed by a Tukey–Kramer post hoc test was used for the statistical analysis. The significance levels of the differences were set at the probabilities of *p < 0.05, **p < 0.01, ***p < 0.001 and ****p < 0.0001 for comparison with the medium, which was used as a control in all the tests. From publication (**III**).

The cytotoxicity of AcDXSp-TA NPs was evaluated in rat cardiac cells (CMs and FBs) for 24 and 48 h and in HCAEC for 6 and 24 h. HCAEC were chosen considering that ideally these are the first cells encountered by the NPs when arriving to the cardiac tissue. As shown in the SI of publication (**II**), empty AcDXSp and AcDXSp-TA NPs reduced the viability of HCAEC, especially after 24 h and at higher doses. Also here, the cytotoxicity was recovered by loaded NPs, probably due to the protective effect of the drugs. In a similar way, AcDXSp NPs exhibited a dose- and time-dependent toxicity, as well as a protective effects of drugs, towards both primary CMs (**Figure 11A** and **11B**) and FBs (**Figure 11C** and **11D**). Coating with TA did not change the biocompatibility of the system, but FBs exhibited a higher sensitivity

compared to CMs (for the effects of Fe^{3+} and TA alone see SI of publication **(II)**), probably due to the anti-fibrotic properties of TA.[412]

In summary, both the developed systems, Putre-AcDX and AcDXSp NPs, showed high biocompatibility towards different cell types, especially when loaded with drugs and after surface modifications.
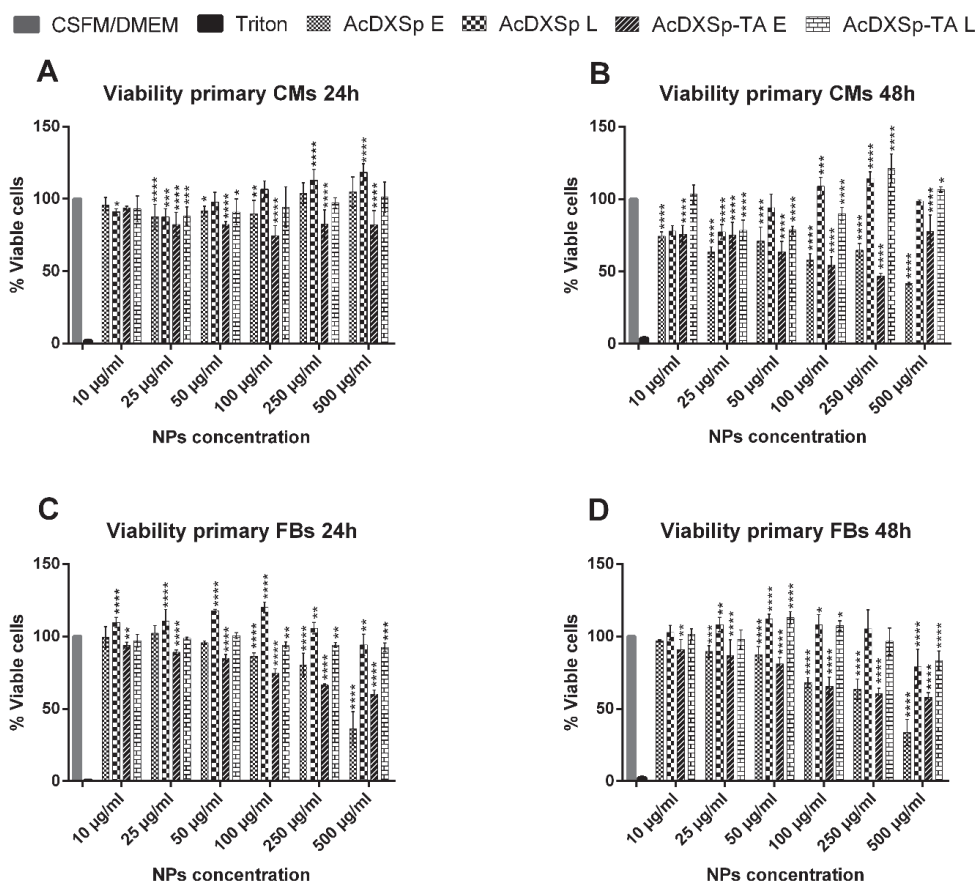
Figure 11. Biocompatibility of AcDXSp-TA NPs on primary rat cardiac cells. The viability of primary rat (**A, B**) CMs and (**C, D**) FBs was assessed after incubation of bare and TA coated NPs for both (**A, C**) 24 and (**B, D**) 48h. Values are represented as mean ± s.d. (n = 3 biological replicates in which each time three technical replicates have been used). A one-way ANOVA followed by a Tukey–Kramer post hoc test was used for the statistical analysis. The significance levels of the differences were set at the probabilities of *p < 0.05, **p < 0.01, ***p < 0.001 and ****p < 0.0001 for comparison with the medium, which was used as a control in all the tests. Reprinted with permission from publication **(II)**.

5.2.1 *In vitro* cell−NP interactions

In vitro cell−NP interactions were evaluated with different cells both quantitatively and qualitatively after incubation with fluorescently labelled NPs. For Putre-AcDX NPs, the cell−NP

interactions were studied with both macrophage cell lines and primary macrophages (**I**), and cardiac cells (**III**). Data concerning the cell–NPs interactions with macrophages cell lines can be found in publication (**I**). Considering that the aim of those NPs was to hitchhike macrophages to reach the infarcted myocardium, their ideal behaviour would consist in being associated on the macrophage surface without being taken up. For this purpose, both M1– and M2–like macrophages from human and murine origin were incubated with both bare and surface modified Putre-AcDX NPs for 1 h, and then cells were analyzed by flow cytometry. Data showed that Putre-AcDX-PEG-TT1-ANP NPs generally interacted more with M2-like macrophages compared to M1-like ones, and their interaction with cells was higher compared to NPs without the peptides (**Figure 12**).

Most importantly, the cell–NP association *vs.* uptake ratio was higher for M2-like macrophages in both human and murine cells, suggesting that M2 macrophages can act as more efficient carriers of NPs into the infarcted heart. Considering the bi-phasic macrophage recruitment in the infarcted heart,[85] these NPs showed putatively to reach the heart in an optimal time frame for the delivery of CHIR and SB, which can then inhibit the fibrotic remodeling of the tissue by stimulating CMs proliferation.
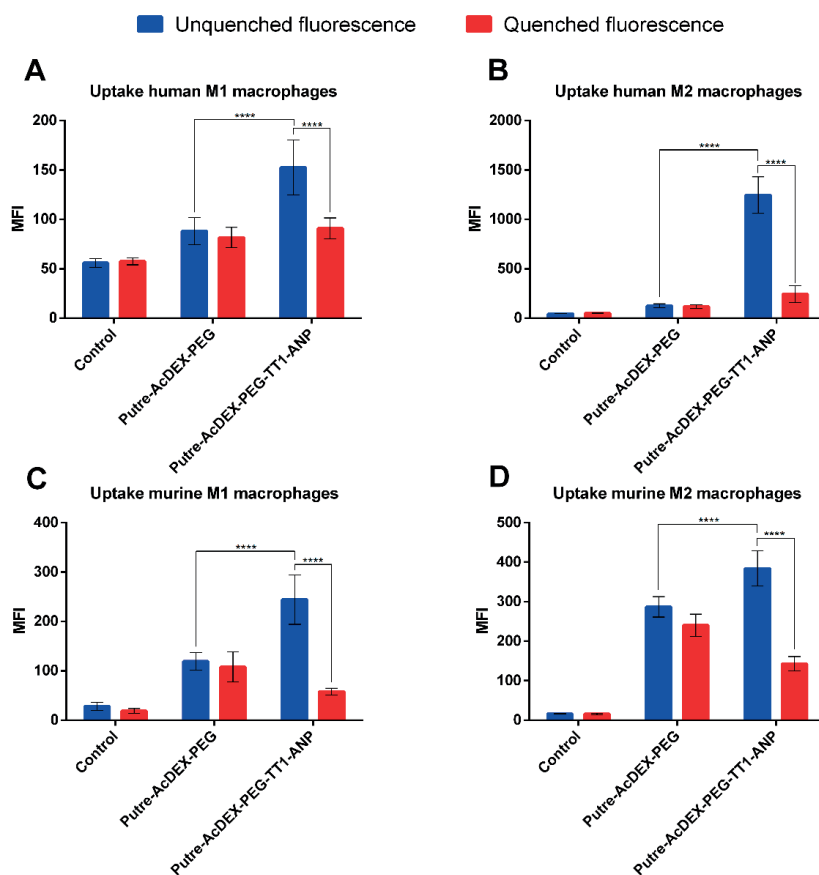
Figure 12. Interaction of Putre-AcDX NPs with primary macrophages of both human and murine origin. The uptake of Putre-AcDX NPs before and after conjugation with TT1 and ANP was quantitatively evaluated by flow cytometry on human (**A**) M1– and (**B**) M2–like

macrophages, as well as murine macrophages of murine origin, respectively with (**C**) M1– and (**D**) M2–like phenotype. The results are represented as MFI values ± s.d. (n = 3 biological replicates in which each time 3 technical replicates have been used). A one-way ANOVA followed by a Tukey–Kramer post hoc test was used for the statistical analysis. The significance levels of the differences were set at probabilities of *p < 0.05 and ****p < 0.0001 for comparison between Putre-AcDX-PEG and the Putre-AcDX-PEG-TT1-ANP (both before fluorescence quenching with TB), and for Putre-AcDX-PEG-TT1-ANP, before and after fluorescence quenching. Reprinted with permission from publication (**I**).

Quantitative results were confirmed also by qualitative cell uptake studies, using fluorescence confocal microscopy. Images can be found in SI of publication (**I**) and they show an augmented cell–NP interactions when treated with Putre-AcDX-PEG-TT1-ANP NPs. Furthermore, studies on the mechanism of internalization revealed that Putre-AcDX-PEG-TT1-ANP NPs are internalized by the macrophages by micropinocytosis. The highest inhibition of internalization was obtained when cells were pre-treated with Cytochalasin D, demonstrating that actin filaments were the cytoskeleton components involved in the uptake mechanism of the Putre-AcDX-PEG-TT1-ANP NPs (data can be found in publication (**I**)).

Overall, results suggested the engagement of energy dependent pathways in the endocytosis of the produced NPs, justifying the high association *vs*. cell uptake ratio observed in **Figure 12**.

The uptake of Putre-AcDX NPs was evaluated also in primary rat cardiac cells (**III**). In this case, both CMs and FBs were incubated with the fluorescently labelled NPs for 2 h and then uptake was evaluated both quantitatively, by flow cytometry, and qualitatively, by confocal microscopy. Flow cytometry data showed that Putre-AcDX-PEG-TT1-ANP NPs interacted more with CMs compared to NPs without peptides (Putre-AcDX-PEG NPs) (**Figure 13**).
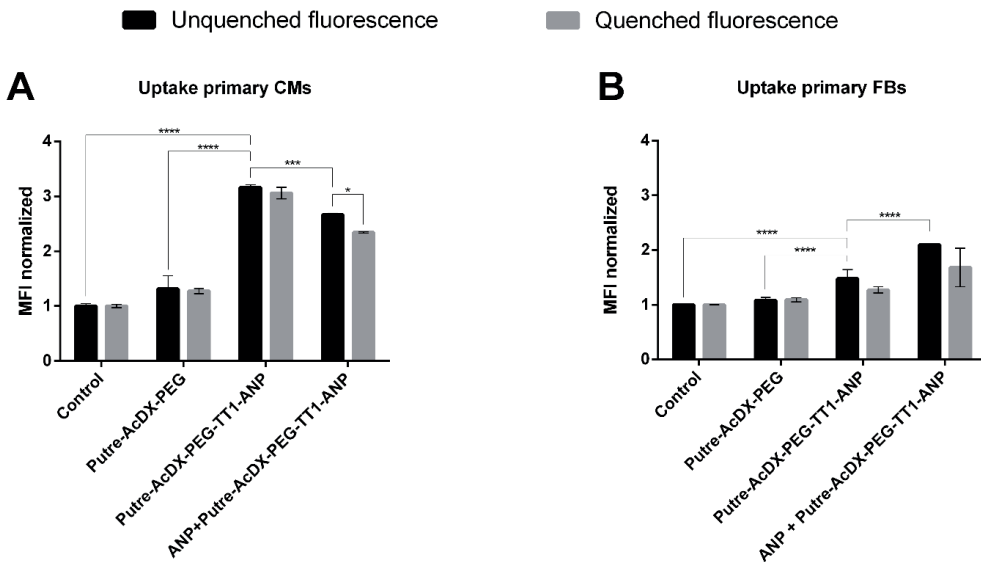
Figure 13. Uptake of Putre-AcDX NPs on primary rat cardiac cells. Quantitative uptake of Putre-AcDX NPs was investigated by flow-cytometry on both primary rat (**A**) CMs and (**B**) FBs. Results are represented as MFI values normalized to the control ± s.d. (n = 3 biological

replicates in which each time 3 technical replicates have been used). A one-way ANOVA followed by a Tukey–Kramer post hoc test was used for the statistical analysis. The significance levels of the differences in uptake studies were set at probabilities of ****$p <$ 0.0001 for comparison between Putre-AcDX-PEG NPs and the control and Putre-AcDX-PEG-TT1-ANP NPs for both CMs and FBs, ****$p <$ for comparison between internalized unquenched fluorescence with or without treatment with ANP in FBs, ***$p < 0.001$ for comparison between internalized unquenched fluorescence with or without treatment with ANP in CMs, and *$p <$ 0.05 for comparison between fluorescently unquenched and quenched Putre-AcDX-PEG-TT1-ANP NPs with ANP pre-treatment. From publication **(III)**.

This difference of interaction can be explained by both the positive charge of Putre-AcDX-PEG-TT1-ANP NPs and their presence on the surface of ANP peptide. Pre-treatment with ANP for 30 min, was used to saturate the ANP receptors and avoid their turn-over in order to study the contribution of the interaction between ANP and its receptors on the NPs internalization.[413] Reduction of uptake of NPs conjugated with the peptides in presence of NP pre-treatment demonstrated that the boosted interaction of Putre-AcDX-PEG-TT1-ANP NPs with CMs was dictated by the presence of ANP on the NPs' surface. For FBs, the presence of peptides on the NPs' surface also increased the interaction of the NPs with the cells. However, pre-treatment with ANP, did not reduce the uptake of the NPs, suggesting that NPs were taken up by the FBs non-specifically. Interestingly, NPs interacted more with primary CMs (**Figure 13A**) compared to FBs (**Figure 13B**), as shown by the 3-fold increase of MFI compared to the control, against the 2-fold, obtained for CMs and FBs, respectively. Confocal images, that can be found in the SI of publication **(III)**, confirmed the results obtained by flow cytometry, showing an increased cell–NP interactions when cells were conjugated with both the peptides.

The uptake of AcDXSp NPs modified with TA **(II)** was evaluated also with both macrophages and primary cardiac cells. In this case, interaction between NPs and macrophages was studied to demonstrate the similarity between TA and PEG in reducing the interaction of NPs with cells of the MPS. Flow cytometry data (they can be found in publication **(II)**) showed that the TA coating can reduce the interaction between both M1– and M2–like macrophages and AcDXSp-TA NPs, probably due to their negative surface charge, as well as increased hydrophilicity due to high presence of hydroxyl groups.[24,399] In this way, the TA coating can reduce the interaction with MPS cells and increase the circulation time of the NPs in the bloodstream. With cardiac cells, TA coating decreased the interaction between NPs and both CMs and FBs compared to AcDXSp NPs, probably due to the negative charge it imparts to the otherwise positively charged AcDXSp NPs (**Figure 14**).
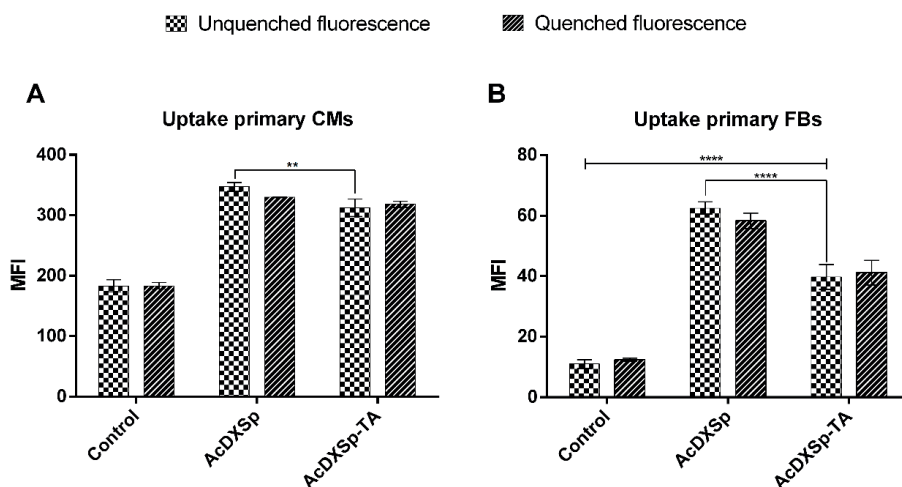
Figure 14. Quantitative uptake of AcDXSp NPs on primary cardiac cells. The uptake of bare and TA-coated AcDXSp was quantified by flow cytometry on both primary rat (**A**) CMs and (**B**) FBs. Results are represented as MFI values ± s.d. (n = 3 biological replicates in which each time three technical replicates have been used). A one-way ANOVA followed by a Tukey–Kramer post hoc test was used for the statistical analysis. The significance levels of the differences in uptake studies were set at the probabilities of $**p < 0.01$ and $****p < 0.0001$ for comparison between associated and internalized AcDXSp NPs, before and after fluorescence quenching with trypan blue and between AcDXSp and AcDXSp-TA NPs, respectively. Adapted and reprinted with permission from publication **(II)**.

However, TA-coated NPs still exhibited a statistically significant interaction with cells, demonstrating that the TA coating is not preventing the uptake of NPs by the cells. Moreover, NPs were mainly taken up by the cells, since there were no statistically significant differences between MFI values before and after surface fluorescence quenching with trypan blue. Importantly, both TA coated and uncoated AcDXSp NPs exhibited preferential interaction with primary CMs, considering the higher MFI values. Inhibition of different uptake mechanisms by different compounds, revealed the engagement of energy-dependent pathways for the internalization of AcDXSp-TA NPs (data can be found in publication **(II)**). The qualitative interaction between TA-coated AcDXSp NPs and cardiac cells was evaluated in primary cultures of CMs, FBs and their co-cultures as such or after treatment with TGF-β for stimulation of ECM production. Increased collagen I production and hypertrophy signals in cells treated with TGF-β were supported by characterization images taken on control cells without NPs treatment (see SI of publication **(II)**). Confocal images (**Figure 15**) showed that TA-coated NPs interacted more than bare AcDXSp NPs with the cells, especially after treatment with TGF-β. These considerations were expected, since it is known that TA can achieve heart targeting due to its high affinity for components of the ECM.[24] Interestingly, CMs cultures, which are characterized by less production of collagen I, compared to FBs and co-cultures, showed a relatively high amount of TA-coated NPs interacting with the culture and this could be in accordance with flow cytometry data showing that the TA-coated NPs were more interacting with CMs compared to FBs. Altogether, results showed that the TA coating could enhance the NP-cell interaction especially when there is stimulation of ECM production, due to TA high affinity for collagen and elastin.
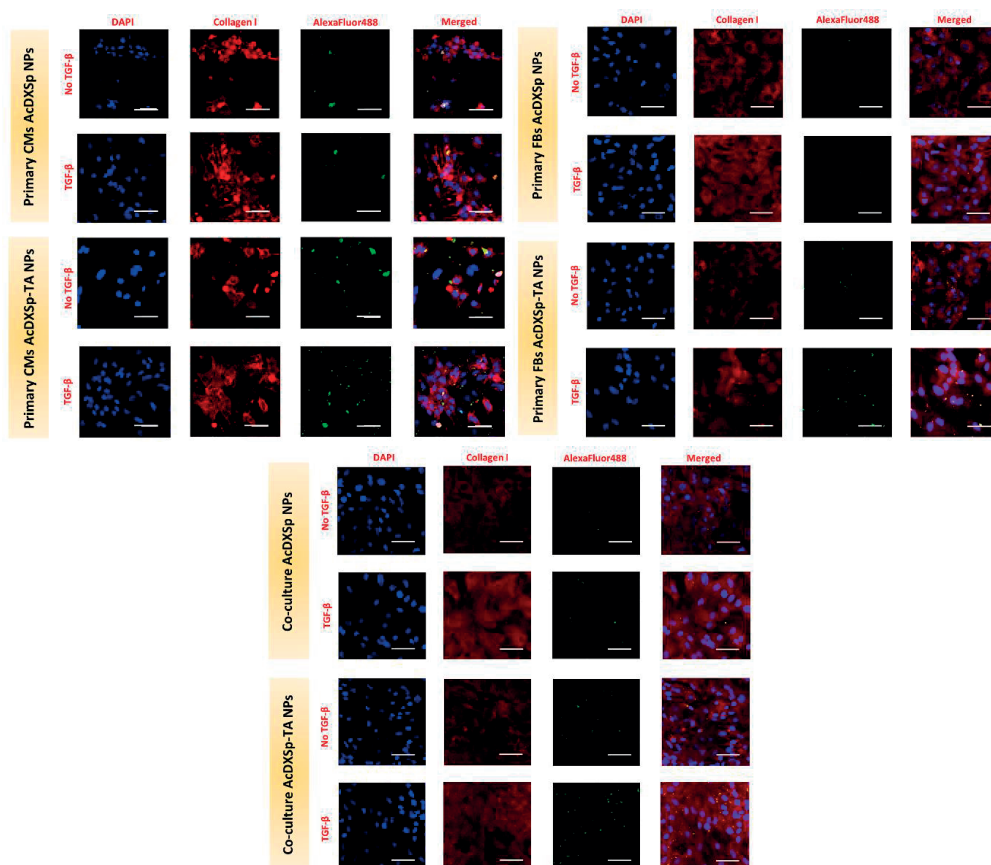
Figure 15. Qualitative uptake studies on primary rat CMs, FBs, and cell co-cultures stimulated and non-stimulated with TGFβ. The cell uptake was evaluated by confocal fluorescence microscopy after incubation with the fluorescently labelled NPs (AlexaFluor488®) for 2 h at 37 °C. The cells were stained with DAPI (nuclei) and anti-Collagen I antibody (collagen/ECM). Scale bars are equal to 50 µm. Reprinted with permission from publication **(II)**.

5.2.3 Biological actions exerted by the materials used

Besides the therapeutical effects exerted by the drugs encapsulated, CHIR and SB, which will be described in the next section, the material themselves have shown to induce biological changes in different cells. For instance, TA has heart targeting abilities,[24] but also anti-fibrotic properties,[412] which can be advantageous in preventing the fibrotic remodeling taking place after MI. Biocompatibility studies had already shown a higher sensitivity of FBs compared to CMs towards TA, giving a hint of the anti-fibrotic properties of TA. Those properties were further investigated by RT-qPCR aimed at quantifying the expression of pro-fibrotic genes, such as Col1a1, Tgfb, Fos, Myc, osteopontin (Spp1) and Tnfa in primary FBs treated with NPs and drugs corresponding to a concentration of CHIR of 3×10^{-6} M (concentrations of SB were approximately double) for 24 h. The 18s gene was used as control housekeeping gene, while DMSO and cell medium were used as controls for the drugs and the NPs, respectively. An increase of Col1a1 gene expression has been highly correlated to

fibrosis and HF and it has been recently recognized as marker in human HF progression.[414] Similarly, increased expression of Spp1 and Fos genes has been directly linked to fibrosis.[415,416] TGF-β and TNF-α instead, are respectively, the principal cytokine/growth factor secreted during fibrosis, which activates fibroblasts in producing more ECM,[417] and a pro-inflammatory cytokine secreted after MI and regulating the remodeling of the heart, promoting the advent of the pro-fibrotic response.[418] The Myc oncogene is a transcription factor affecting cellular activities, such as cell cycle, proliferation, and hypertrophy.[419]

Results showed that the loaded TA-coated AcDXSp NPs were able to reduce the expression of Col1a1, Tgfb, Spp1, Myc, and Fos genes (data can be found in publication **(II)**). In particular, there was a decrease of ~80% in the expression of genes such as Col1a1 and Spp1 when cells were treated with drugs loaded AcDXSp-TA NPs. For Tnfa data showed an unexpected increase of gene expression, whilst it has been reported that both TA and compounds encapsulated have anti-inflammatory properties. According to some reports though, TA has the ability to induce an increase of TNF-α in keratinocytes in patients affected by pemphigus vulgaris.[420]

The ability of NPs to induce macrophage repolarization was investigated for Putre-AcDX NPs. It is known that both ANP and the compounds encapsulated, CHIR and SB, have an immunomodulatory effect.[207,368,409] ANP has exhibited ability to modulate the secretion of inflammatory mediators in macrophages, by inhibiting the LPS-induced expression of inducible nitric oxide synthase (iNOS), and the secretion of TNF-α and IL-1β in macrophages.[368] CHIR also demonstrated an anti-inflammatory effect by reducing the serum levels of TNF-α and increasing the expression of IL-10. It also decreased the expression of markers genes, such as CD11c, CD68, and F4/80 and the pro-inflammatory cytokine/chemokine genes, such as Tnfa, IL1b, Mcp1 and 3.[207] Similarly, treatment with SB resulted in a decrease of the LPS-induced secretion of TNF-α and IL-6.[409] Overall the system was expected to have anti-inflammatory properties and thus, repolarization of M1-like macrophages was investigated by studying the markers expression of the cells after incubation with the NPs at different time-points. Results showed that after incubation with drug loaded Putre-AcDX-PEG-TT1-ANP for 1 h, the expression of CD86 in M1-like macrophages was significantly reduced, while their CD206 expression increased. Treatment with empty Putre-AcDX-PEG-TT1-ANP NPs has also shown a similar effect, but less remarkable, suggesting the synergistic anti-inflammatory effect of ANP and the encapsulated compounds (**Figure 16**).
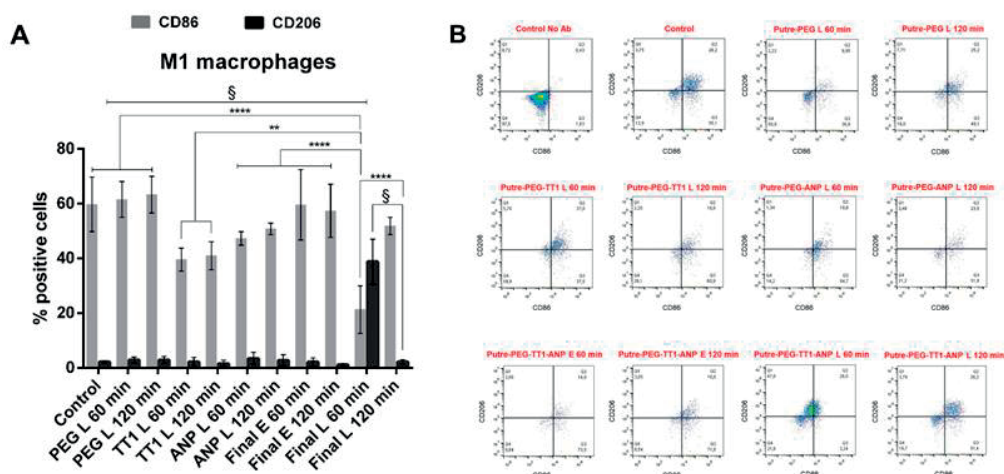
Figure 16. Repolarization studies on murine M1-like macrophages treated with Putre-AcDX NPs. Given the anti-inflammatory properties of both ANP and drugs encapsulated, the investigation of repolarization of M1-like macrophages was carried out by (**A**) quantifying the expression of CD86 and CD206 by flow cytometry. In (**B**) there are the populations for each condition. Results are represented as number of positive cells ± s.d. (n = 3 biological replicates in which each time three technical replicates have been used). The significance levels of the differences were set at probabilities of ****$p < 0.0001$ and ***$p < 0.001$ for comparison between the control and drug loaded Putre-AcDX-PEG (PEG L), Putre-AcDX-PEG-TT1 (TT1 L), Putre-AcDX-PEG-ANP (ANP L), and empty and loaded Putre-AcDX-PEG-TT1-ANP (Final E and Final L respectively). The significance levels of the differences were set at probabilities of *$p < 0.1$ for comparison between empty and loaded Putre-AcDX-PEG-TT1-ANP incubated with the cells for 1h. Abbreviations: E, empty; L, loaded; PEG, Putre-AcDX-PEG NPs; TT1, Putre-AcDX-PEG-TT1 NPs; ANP, Putre-AcDX-PEG-ANP NPs; Final: Putre-AcDX-PEG-TT1-ANP NPs. From publication (**III**).

Also, the effect was reduced when the incubation time was increased to 2 h, and this can be explained by the fact that probably NPs are taken up by the cells when incubated for longer times. NPs conjugated with only either one of the peptides (Putre-AcDX-PEG-TT1 and Putre-AcDX-PEG-ANP) were less efficient reducing the inflammatory phenotype of M1-like macrophages, with Putre-AcDX-PEG-ANP NPs performing better compared to NPs conjugated with only TT1, demonstrating that both compounds encapsulated and ANP have some influence in reducing inflammation. Ultimately, PEGylated NPs did not show any ability in modulating the markers expression of M1-like macrophages. The immunomodulatory of the system was also evaluated in M2-like macrophages and results showed that there were no remarkable changes between the different conditions (data can be found in SI of publication (**III**)).

Overall, the results suggested that the NPs conjugated with both peptides (Putre-AcDX-PEG-TT1-ANP NPs) and loaded with CHIR and SB can exert an immunomodulatory effect on M1-like macrophages, by reducing their pro-inflammatory phenotype.

5.2.4 Stimulation of cardiomyocytes proliferation upon treatment with Putre-AcDX and AcDXSp NPs

The main aim of both the Putre-AcDX and the AcDXSp NPs developed in this thesis was to deliver CHIR and SB and to stimulate the proliferation of CMs to achieve regeneration of the damaged tissue. The ability of the NPs to induce such an effect was evaluated on CMs by different immunostainings: For Putre-AcDX NPs, BrdU, β-catenin (downstream effector of CHIR) and Phospho-MAPKAPK2 (downstream effector of p38 inhibition by SB) immunostainings were performed on primary rat and murine CMs and hiPSC-CMs; and for AcDXSp NPs, Ki67, phospho-histone H3 and aurora B immunostainings were performed on primary rat CMs. In both cases, cells were treated for 24 h with NPs concentrations corresponding to 1×10^{-6}, 3×10^{-6}, 5×10^{-6} , and 10×10^{-6} M of CHIR99021 (concentrations of SB were approximately double), calculated from the LD values of the NPs and corresponding to a safe dose of NPs. The biological effect was then evaluated by immunostainings, quantifying the intensity of the selected markers in the nuclei or in the cytoplasm. DAPI staining was used to identify the nuclear area and a cardiac specific marker (cardiac troponin T, cTnT) was employed to select the cells of interest from the primary culture (though we tried to separate cell types, cultures always contained some non-myocytes). A 5-pixel ring immediately outside the nucleus was considered to represent cytoplasm in β-catenin stainings.

When CMs were treated with drug-loaded Putre-AcDX-PEG-TT1-ANP NPs corresponding to concentration of CHIR 5×10^{-6} M, the percentage of BrdU positive cells was significantly higher than control, empty NPs before and after surface conjugations and loaded Putre-AcDX NPs (data can be found in publication **III**). Since the concentration of CHIR 5×10^{-6} M was the one showing the highest increase in BrdU incorporating cells after treatment with loaded in Putre-AcDX-PEG-TT1-ANP NPs in rat CMs (4-fold higher compared to control), it was then chosen for the treatment of murine primary CMs and hiPSC-CMs. Moreover it was corresponding to a still safe dose of NPs. Similarly, murine CMs and hiPSC-CMs exhibited an increase of BrdU positive cells when treated with drug-loaded NPs conjugated with both peptides (data can be found in SI of publication **(III)**). Modulation of downstream effectors of Wnt activation by CHIR and p38 inhibition by SB were also investigated. The downstream effector of Wnt activation by CHIR is β-catenin. Inhibition of GSK3 by CHIR prevents phosphorylation of β-catenin and it is further degradation, leading to its increased concentration in cytoplasm and translocation in nucleus, where it can regulate the expression of target genes.[204] The efficient delivery of CHIR to primary rat CMs *via* Putre-AcDX NPs, resulted in increased presence of β-catenin in both nucleus and cytoplasm (data can be found in publication **(III)**), compared to empty NPs and drug-loaded Putre-AcDX, especially when cells were treated with drug-loaded Putre-AcDX-PEG-TT1-ANP NPs at concentrations 3×10^{-6} M and 5×10^{-6} M. Inhibition of p38 by SB leads to inhibition of phosphorylation and activation of MAPKs, which are then unable to translocate in the nucleus. The decrease of Phospho-MAPKAPK2 in the nucleus was then detected to study the effects of SB delivery. As shown in publication **(III)**, there was no significant decrease of MAPKAPK2 expression in the nucleus between the different conditions. However, this can be due to the fact that cells were fixed after 24 h incubation, while phosphorylation of proteins it is a relative fast process. Probably shorter time points would have allowed to discriminate greater differences in the results. Similar results were obtained for both CMs of murine and human origin, as showed in SI of publication **(III)**.

Treatment of primary rat CMs with drug-loaded AcDXSp-TA NPs resulted in increased numbers of Ki67 (**Figure 17A** and **17B**) and phospho-histone H3 (**Figure 17C**) positive nuclei

in a concentration-dependent manner. Since Ki67 is usually used as proliferation marker for cells in active cell cycle,[421] while phospho-histone H3 is a mitotic index marker,[422] results validate the ability of drug-loaded TA-coated AcDXSp NPs to stimulate cell cycle re-entry in primary CMs. Administration of empty NPs had an inhibitory effect instead, underlining the importance of CHIR and SB delivery for the stimulation of CMs proliferation. Ki67 immunostainings were performed also on hiPSC-CMs and they showed an increase of Ki67 with treatment of drug-loaded AcDXSp-TA NPs, confirming that the system has a pro-proliferative effect on CMs of different origin (data can be found in SI of publication **(II)**).

Further confirmation of the ability of treated CMs to enter cell-cycle and go towards actual cell division was obtained by aurora B immunostainings (**Figure 17D**).[206,423] Aurora B has a different cellular localization based on which cell-cycle phase a cell is.[424] When a cell enters the cell-cycle and is in interphase or prophase, aurora B has a nuclear localization, while in the final phases of cell-cycle, telophase and cytokinesis, it localize between the two dividing cells.[424] For the confirmation of cell division upon treatment with AcDXSp-TA NPs, the presence of aurora B was first detected in the nucleus. Data showed that similarly to Ki67 and phospho-histone H3 immunostainings, treatment with drug-loaded AcDXSp-TA NPs increases the percentage of aurora B positive nuclei (**Figure 17E**), demonstrating that the system can induce primary CMs to enter the cell cycle. However, especially in the case of CMs, it is known that cells might not physically divide, *i.e.*, complete cytokinesis, giving origin to bi-/poly-nucleated cells.[425]

Thus, in order to evaluate whether the NPs induced actual cell division, a double-blinded study, in which the cells that were in telophase were manually counted to quantify cytokinesis, was performed. **Figure 17F** shows that when cells were treated with drug-loaded TA-coated NPs, a higher percentage of cells in cytokinesis was observed, and in particular, at the concentration of CHIR of 3×10^{-6} M, the delivery of the compounds CHIR and SB doubled the percentage of dividing CMs compared to the control (**Figure 17F**). Further evidence of the pro-proliferative properties of the system were obtained by analysis of the surface area of the CMs and RT-qPCR aimed at quantifying the expression of cyclin D, E, A and B. The smaller mean surface area of the CMs treated with drug-loaded AcDXSp NPs coated with TA compared to the ones that received other treatments, reflected their ability to divide, as the relative surface area of cells decreases when entering cell-cycle, due to a rounding-up phase[426] (data can be found in SI of publication **(II)**). RT-qPCR analysis displayed an increase of all the studied cyclins, and in particular a doubling in cyclin B expression, when cells were administered AcDXSp-TA NPs loaded with CHIR and SB, further confirming the ability of the drug delivery system to promote cell-cycle entry and progression in CMs (data can be found in SI of publication **(II)**).
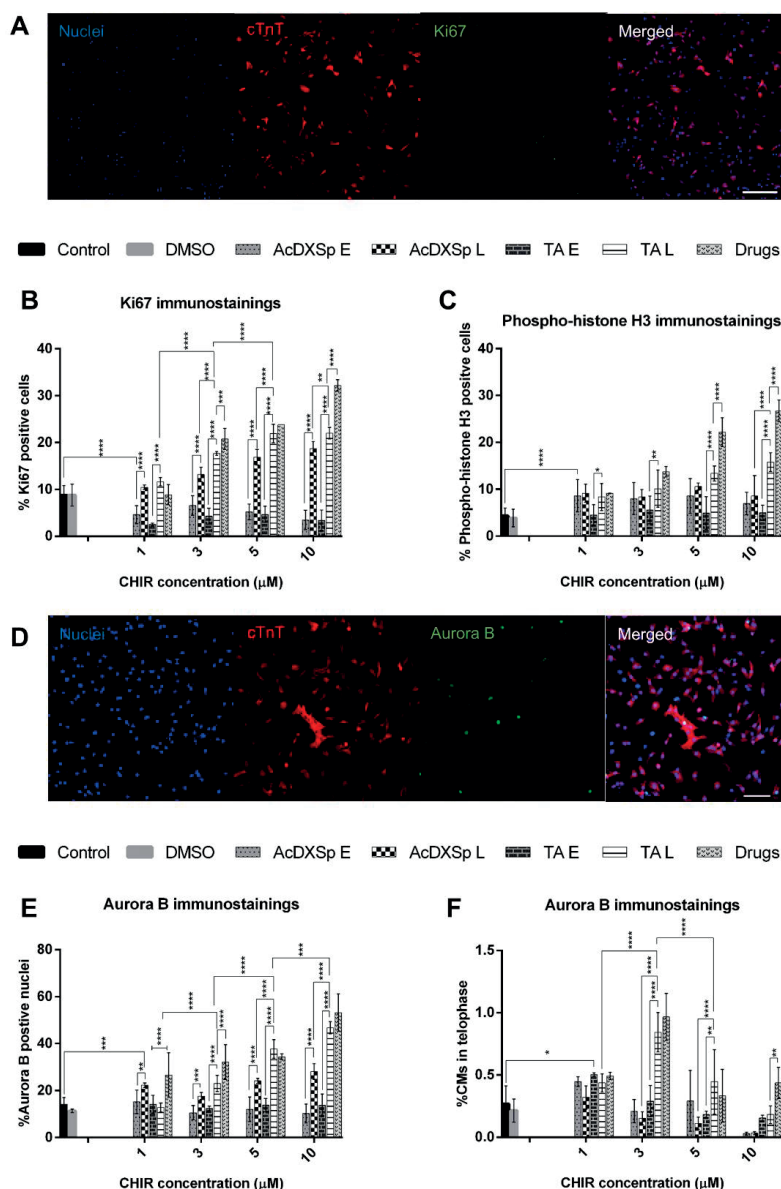
Figure 17. High-content cell imaging and quantification of Ki67, phospho-histone H3, and aurora B staining intensity. Representative images of (**A**) Ki67 immunostainings performed on CMs treated with empty (E) and loaded (L) AcDXSp-TA NPs at the concentrations of 1×10^{-6} M of CHIR99021 and 2.2×10^{-6} M of SB203580, and stained for nuclei (DAPI, blue), cardiac troponin T (cTnt, red) and Ki67 (green), with a 10 × magnification objective. Scale bars are 200 µm. Quantification of (**B**) Ki67 and (**C**) phospho-histone H3 staining intensity in the nucleus. Representative images of (**D**) Aurora B immunostainings of CMs treated with loaded AcDXSp-TA NPs at the dose of 1×10^{-6} M of CHIR99021 and 2.2×10^{-6} M of SB203580, and stained for nuclei (DAPI, blue), cardiac troponin T (cTnT, red) and aurora B (green), with a 20 × magnification objective. Scale bars are 100 µm. Quantification of aurora B staining intensity in (**E**) the nucleus and (**F**) percentage of CMs in telophase. The

different treatment conditions are stated in the legend. Values represent the mean ± s.d. (n = 3). A one-way ANOVA followed by a Tukey-Kramer post hoc test was used for the statistical analysis. The significance levels of the differences were set at the probabilities of *$p < 0.05$, **$p < 0.01$, ***$p < 0.001$, and ****$p < 0.0001$ for comparison with the medium, which was used as control, with the compounds alone, between empty and loaded NPs, as well as bare and TA coated NPs. Reprinted with permission from publication **II**.

Overall, both the systems prepared in this thesis showed efficient delivery of CHIR and SB and ability to stimulate proliferation of CMs, holding potential to regenerate the damaged cardiac tissue when infarction occurs. The encapsulation of CHIR and SB in the nanosystems, improved their solubility and ability to be delivered intracellularly, representing an advantageous approach for potential clinical translation of regenerative strategies. Together with the ability of reducing the pro-inflammatory phenotype of macrophages owned by Putre-AcDX NPs and the anti-fibrotic properties of the TA coating, the systems here presented constitute multifunctional systems for drug-delivery to the infarcted heart.

5.3 *In vivo* studies (III)

The ability of Putre-AcDX NPs to reach the infarcted heart was studied on a rat model of MI, obtained by permanent ligation of the left descending coronary artery. Fluorescent imaging by confocal microscopy was used to study the accumulation of bare and peptides-modified NPs in different organs. The immunological profile of animals injected with the NPs was also evaluated by studying the markers expression of cells isolated from blood and spleen.

5.3.1 *Ex vivo* biodistribution of Putre-AcDX NPs and immunoprofile studies

For the study of biodistribution of Putre-AcDX NPs, rats underwent surgery and were divided into four groups (n= 3–5 animals per group), namely isotonic sucrose (control), Putre-AcDX-PEG NPs, Putre-AcDX-PEG-ANP NPs and Putre-AcDX-PEG-TT1-ANP NPs. Considering the potential macrophage-hitchhiking properties of the system, NPs were injected i.v. at both day 3 post-MI, corresponding to the peak of M1-like macrophages recruitment, and day 7 post-MI, which is instead the time in which M2-like macrophages are peaking after MI.[85] After 1h, animals were sacrificed and organs collected to study the *ex-vivo* accumulation of the NPs. As expected, some NPs accumulated in spleens and liver, suggesting that they were captured by cells of the MPS.[221] Lungs were also collected and stained, and images showed none or little presence of NPs in them, demonstrating that the formulation was stable upon i.v. administration. Interestingly, confocal images (**Figure 18**), show the presence of Putre-AcDX-PEG-TT1-ANP NPs in the heart, especially when they were injected 7 days post-MI. Results are thus suggesting that the NPs with both peptides accumulate in the infarcted heart in concomitance with the recruitment of M2-like macrophages (images showed also more expression of CD163 vs CD86), confirming the hypothesis generated from the *in vitro* data collected in publication **(I)**. Moreover, NPs modified with just ANP (Putre-AcDX-PEG-ANP), used as main comparison due to the wide known heart targeting abilities of ANP, and PEGylated NPs, showed no tendency to accumulate in the heart in the same extent, demonstrating that macrophage hitchhiking can improve the heart targeting abilities of ANP. SHAM controls (images can be found in SI of publication **(III)**) also showed little or no NPs accumulation and inflammatory cells infiltration.

In addition, immunoprofiling studies were performed to study the safety of the NPs *in vivo*. Considering that inflammation plays a critical role in the outcome of the pathology, NPs should not induce any inflammation in the body or alter the physiological immunological state of the patient.
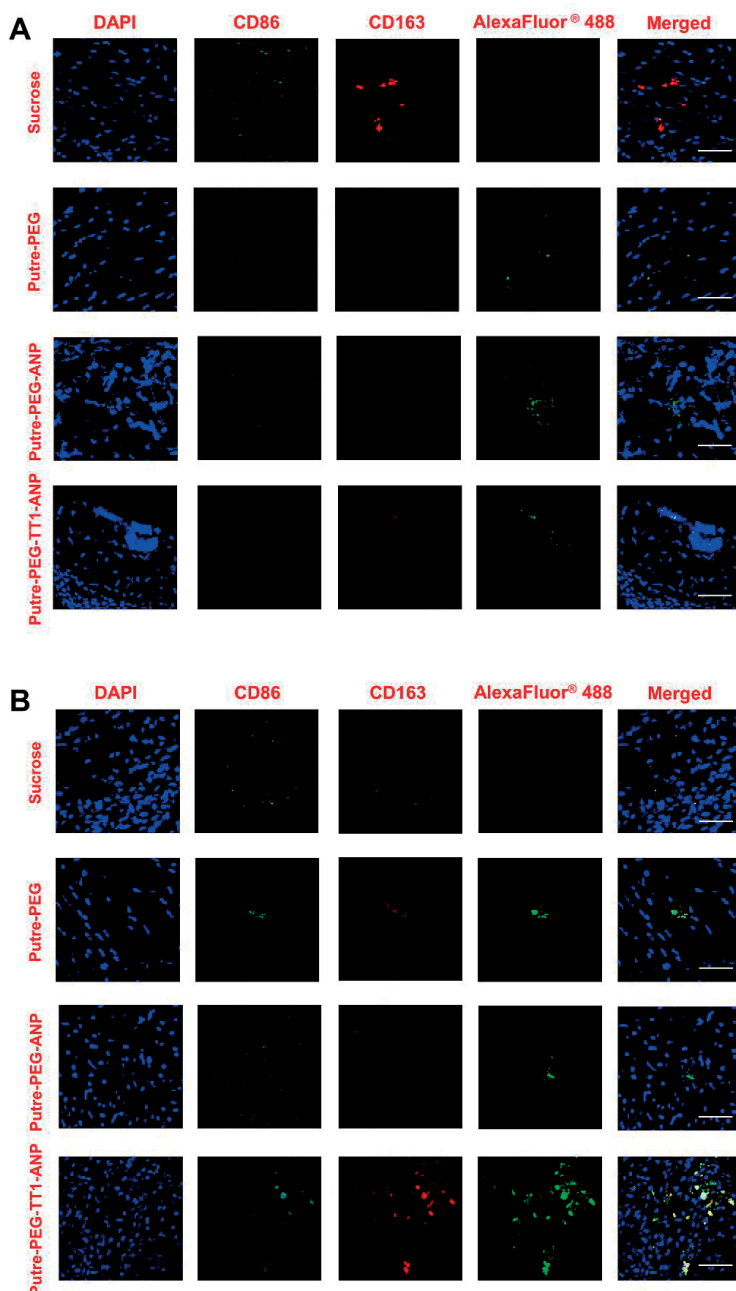
Figure18. *Ex vivo* biodistribution studies of Putre-AcDX NPs. Heart sections deriving from animals injected with Putre-AcDX NPs at (**A**) day 3 and (**B**) 7 post-MI were stained and imaged by confocal microscopy. Scale bars are corresponding to 200 μm. From publication **III**.

Hence, both spleens and blood were screened to determine the populations of M1− and M2−like macrophages, as well as $CD4^+$ and $CD8^+$ T-cells. Determination of the markers expression by flow cytometry was used for this purpose. Results can be found in publication **(III)** and they showed that the NPs do not induce consistent changes in the immunoprofile of blood and spleens collected from the animals. In some cases, there was reduction of the expression of CD86 when animals were injected with NPs modified with ANP, suggesting an anti-inflammatory effect of those NPs. This effect is in accordance with the *in vitro* data presented previously, and it can have an influence in improving the cardiac function, as it is known that reducing inflammation in the infarcted area has a beneficial effect.[427]

Overall, the *in vivo* immunoprofile and biodistribution studies demonstrated that Putre-AcDX-PEG-TT1-ANP NPs are not inducing changes in the immunological state of the animals upon *i.v.* administration, they can increase the heart targeting abilities of ANP and they accumulate in the infarcted heart preferentially 7 days post-MI, probably due to their preferential interaction with M2-like macrophages.

6 Conclusions

Despite the recent advances in pharmacological therapies, there is still a urgent need for effective therapies for MI patients. Nanomedicines can provide solutions to the problems encountered by innovative strategies, filling the gap between research and clinical translation. However, successful heart targeting still represents a challenge, and thus, investigation of superior heart targeting strategies is crucial for the development of nanomedicines for the treatment of MI. To date, both passive and active strategies have been used to achieve heart targeting. Among them, conjugation of particles with ANP has been widely used and it is regarded as a conventional strategy to delivery therapeutics to the infarcted myocardium. Yet, it is known that the ANP receptors are not only expressed in sites of infarction, but also in other organs, posing a risk of off target effects. In particular, if not properly addressed, delivery of molecules able to stimulate cell proliferation, can potentially induce tumorigenesis in sites not affected by the disease. It is then crucial to selectively deliver such therapeutics only to the infarcted myocardium.

Therefore, main aim of this thesis was to explore different heart targeting strategies to improve the selectivity of nanocarriers for the heart. This work resulted in the development of two different systems, made of AcDX-based polymers for the delivery of two small hydrophobic compounds able to stimulate cardiomyocytes proliferation.

In the first system, the heart targeting properties of ANP were improved by co-conjugation of lin-TT1 peptide on the surface of Putre-AcDX NPs. The presence of lin-TT1 endowed the system with ability to target inflammatory cells and resulted in increased heart accumulation due to the hitchhike effect on macrophages accumulating in the infarcted myocardium. In particular, the system showed both *in vitro* and *in vivo* the ability to preferentially target M2-like macrophages, resulting in boosted *in vivo* biodistribution in infarcted hearts 7 days post-MI. Moreover, immunoprofiling of spleens and blood collected from *in vivo* studies showed no significant alterations of the macrophages and T-cells populations, demonstrating that the system here developed is not presenting toxicity or immunomodulatory effect towards cells of the immune system.

In the second system, spermine modified-AcDX NPs were coated with TA, which has shown heart targeting abilities due to high affinity for components of the ECM, in particular collagen and elastin. *In vitro* data confirmed the increased interaction of TA coated NPs with cardiac cells cultures stimulated with TGF-β to induce production of ECM.

Both systems above resulted in biocompatible towards rat and murine primary cardiac cells and hiPS-CMs, and for the Putre-AcDX NPs safety was assessed also of primary macrophages of both human and murine origin. Moreover, both systems successfully deliver the encapsulated compounds in a pH-dependent manner and induce CMs proliferation *in vitro*.

Overall, the work presented in this thesis consisted in the development of two acetalated dextran based nanocarriers with the aim to improve the heart targeting abilities of nanomedicines. The encapsulation of two therapeutically relevant small hydrophobic compounds able to stimulate CMs proliferation, improved their delivery to cells and culminated in efficient CMs division *in vitro*, holding potential for successful regeneration of the cardiac tissue.

Despite the advances brought by the investigations carried out in this thesis, the *in vivo* biodistribution of AcDXSp-TA still need to be investigated in animal models of MI, as well as the *in vivo* therapeutical potential of both systems. Also, a deeper investigation on the immunomodulatory and toxic effects of such systems as well as carcinogenesis studies should be carried out to exclude any potential long-term carcinogenetic and toxic effects. Future work

would cover these aspects and provide better insights on the potential and safety of these systems.

The development of therapies able to restore the function of injured hearts would save the life of millions of patients all over the world and eliminate the burden imposed by them on our society. Nanomedicines have developed throughout the years as a great multifunctional tool, able to solve drawbacks affecting conventional drug therapies and they offer options addressing the undruggable target space. However, the clinical development of nanoparticulate carriers is not straightforward and it is affected by reproducibility and scalability issues, as well as need for time-consuming and complex surface conjugation steps. Also, limitations posed by biological barriers need to be overcome for successful delivery in specific sites of the body. In addition to these limiting aspects, the lack of specific heart targeting moieties pones a great challenge to the development of nanomedicines for the treatment of MI. Regardless, this thesis offers insights on the application of dextran based NPs in the treatment of MI and can be regarded as a starting point for the development of future treatments for heart diseases.

References

1. Cardiovascular diseases (CVDs). https://www.who.int/news-room/fact-sheets/detail/cardiovascular-diseases-(cvds).
2. Kikuchi, K. & Poss, K. D. Cardiac regenerative capacity and mechanisms. *Annu. Rev. Cell Dev. Biol.* **28**, 719–741 (2012).
3. Nguyen, P. D., de Bakker, D. E. M. & Bakkers, J. Cardiac regenerative capacity: an evolutionary afterthought? *Cell. Mol. Life Sci.* **78**, 5107–5122 (2021).
4. Talman, V. & Ruskoaho, H. Cardiac fibrosis in myocardial infarction-from repair and remodeling to regeneration. *Cell Tissue Res.* **365**, 563–581 (2016).
5. Opie, L. H., Commerford, P. J., Gersh, B. J. & Pfeffer, M. A. Controversies in ventricular remodelling. *Lancet (London, England)* **367**, 356–367 (2006).
6. Krum, H. & Teerlink, J. R. Medical therapy for chronic heart failure. *Lancet (London, England)* **378**, 713–721 (2011).
7. Lin, Z. & Pu, W. T. Strategies for cardiac regeneration and repair. *Sci. Transl. Med.* **6**, 239rv1-239rv1 (2014).
8. Ferreira, M. P. A., Balasubramanian, V., Hirvonen, J. & Santos, H. R. and H. A. Advanced Nanomedicines for the Treatment and Diagnosis of Myocardial Infarction and Heart Failure. *Current Drug Targets* vol. 16 1682–1697 at https://doi.org/http://dx.doi.org/10.2174/1389450115999141030143923 (2015).
9. He, L. & Zhou, B. Cardiomyocyte proliferation: remove brakes and push accelerators. *Cell Res.* **27**, 959–960 (2017).
10. Ghiroldi, A. *et al.* Cell-Based Therapies for Cardiac Regeneration: A Comprehensive Review of Past and Ongoing Strategies. *Int. J. Mol. Sci.* **19**, 3194 (2018).
11. Liew, L. C., Ho, B. X. & Soh, B.-S. Mending a broken heart: current strategies and limitations of cell-based therapy. *Stem Cell Res. Ther.* **11**, 138 (2020).
12. Liu, C., Han, D., Liang, P., Li, Y. & Cao, F. The Current Dilemma and Breakthrough of Stem Cell Therapy in Ischemic Heart Disease. *Front. Cell Dev. Biol.* **9**, (2021).
13. Ye, L., Zimmermann, W.-H., Garry, D. J. & Zhang, J. Patching the heart: cardiac repair from within and outside. *Circ. Res.* **113**, 922–932 (2013).
14. Peña, B. *et al.* Injectable Hydrogels for Cardiac Tissue Engineering. *Macromol. Biosci.* **18**, e1800079–e1800079 (2018).
15. Tenreiro, M. F., Louro, A. F., Alves, P. M. & Serra, M. Next generation of heart regenerative therapies: progress and promise of cardiac tissue engineering. *npj Regen. Med.* **6**, 30 (2021).
16. Lou, L., Lopez, K. O., Nautiyal, P. & Agarwal, A. Integrated Perspective of Scaffold Designing and Multiscale Mechanics in Cardiac Bioengineering. *Adv. NanoBiomed Res.* **1**, 2100075 (2021).
17. Mitchell, M. J. *et al.* Engineering precision nanoparticles for drug delivery. *Nat. Rev. Drug Discov.* **20**, 101–124 (2021).
18. Galagudza, M. *et al.* Passive targeting of ischemic-reperfused myocardium with adenosine-loaded silica nanoparticles. *Int. J. Nanomedicine* **7**, 1671–1678 (2012).
19. Ferreira, M. P. A. *et al.* Drug-Loaded Multifunctional Nanoparticles Targeted to the Endocardial Layer of the Injured Heart Modulate Hypertrophic Signaling. *Small* **13**, 1701276 (2017).
20. Skelton, R. J. P. *et al.* SIRPA, VCAM1 and CD34 identify discrete lineages during early human cardiovascular development. *Stem Cell Res.* **13**, 172–179 (2014).
21. Yu, J., Li, W. & Yu, D. Atrial natriuretic peptide modified oleate adenosine prodrug lipid nanocarriers for the treatment of myocardial infarction: in vitro and in vivo evaluation. *Drug Des. Devel. Ther.* **12**, 1697–1706 (2018).
22. Potter, L. R., Yoder, A. R., Flora, D. R., Antos, L. K. & Dickey, D. M. Natriuretic peptides: their structures, receptors, physiologic functions and therapeutic applications. *Handb. Exp. Pharmacol.* 341–366 (2009) doi:10.1007/978-3-540-68964-5_15.
23. Wang, S., Fontana, F., Shahbazi, M.-A. & Santos, H. A. Acetalated dextran based nano- and microparticles: synthesis{,} fabrication{,} and therapeutic applications. *Chem. Commun.* **57**, 4212–4229 (2021).
24. Shin, M. *et al.* Targeting protein and peptide therapeutics to the heart via tannic acid modification. *Nat. Biomed. Eng.* **2**, 304–317 (2018).
25. Prabhu, S. D. & Frangogiannis, N. G. The Biological Basis for Cardiac Repair After Myocardial Infarction. *Circ. Res.* **119**, 91–112 (2016).
26. Frangogiannis, N. G. & Rosenzweig, A. Regulation of the Inflammatory Response in Cardiac Repair. *Circ. Res.* **110**, 159–173 (2012).
27. Fogal, V., Zhang, L., Krajewski, S. & Ruoslahti, E. Mitochondrial/cell-surface protein p32/gC1qR as a molecular target in tumor cells and tumor stroma. *Cancer Res.* **68**, 7210–7218 (2008).
28. Hamzah, J. *et al.* Specific penetration and accumulation of a homing peptide within atherosclerotic plaques of apolipoprotein E-deficient mice. *Proc. Natl. Acad. Sci. U. S. A.* **108**, 7154–7159 (2011).
29. Paasonen, L. *et al.* New p32/gC1qR Ligands for Targeted Tumor Drug Delivery. *Chembiochem* **17**, 570–575 (2016).
30. European Cardiovascular Disease Statistics 2017. https://ehnheart.org/cvd-statistics/cvd-statistics-2017.html.
31. No major changes in causes of death compared to the previous year. https://www.stat.fi/til/ksyyt/2020/ksyyt_2020_2021-12-10_tie_001_en.html.
32. Yang, F. *et al.* Myocardial Infarction and Cardiac Remodelling in Mice. *Exp. Physiol.* **87**, 547–555 (2002).

References

33. D., P. K., G., W. L. & T., K. M. Heart Regeneration in Zebrafish. *Science (80-.).* **298**, 2188–2190 (2002).

34. Lafontant, P. J. *et al.* The Giant Danio (D. Aequipinnatus) as A Model of Cardiac Remodeling and Regeneration. *Anat. Rec.* **295**, 234–248 (2012).

35. Grivas, J. *et al.* Cardiac repair and regenerative potential in the goldfish (Carassius auratus) heart. *Comp. Biochem. Physiol. Part C Toxicol. Pharmacol.* **163**, 14–23 (2014).

36. Laube, F., Heister, M., Scholz, C., Borchardt, T. & Braun, T. Re-programming of newt cardiomyocytes is induced by tissue regeneration. *J. Cell Sci.* **119**, 4719–4729 (2006).

37. Oberpriller, J. O. & Oberpriller, J. C. Response of the adult newt ventricle to injury. *J. Exp. Zool.* **187**, 249–259 (1974).

38. Godwin, J. W., Debuque, R., Salimova, E. & Rosenthal, N. A. Heart regeneration in the salamander relies on macrophage-mediated control of fibroblast activation and the extracellular landscape. *npj Regen. Med.* **2**, 22 (2017).

39. Cano-Martínez, A. *et al.* Functional and structural regeneration in the axolotl heart (Ambystoma mexicanum) after partial ventricular amputation. *Arch. Cardiol. Mex.* **80**, 79–86 (2010).

40. R., P. E. *et al.* Transient Regenerative Potential of the Neonatal Mouse Heart. *Science (80-.).* **331**, 1078–1080 (2011).

41. Porrello, E. R. *et al.* Regulation of neonatal and adult mammalian heart regeneration by the miR-15 family. *Proc. Natl. Acad. Sci.* **110**, 187 LP – 192 (2013).

42. Mario, N. *et al.* The local microenvironment limits the regenerative potential of the mouse neonatal heart. *Sci. Adv.* **4**, eaao5553 (2021).

43. Haubner, B. J. *et al.* Functional Recovery of a Human Neonatal Heart After Severe Myocardial Infarction. *Circ. Res.* **118**, 216–221 (2016).

44. Papneja, K., Chan, A. K., Mondal, T. K. & Paes, B. Myocardial Infarction in Neonates: A Review of an Entity with Significant Morbidity and Mortality. *Pediatr. Cardiol.* **38**, 427–441 (2017).

45. Cannon, R. O. *et al.* Early degradation of collagen after acute myocardial infarction in the rat. *Am. J. Cardiol.* **52**, 390–395 (1983).

46. Whittaker, P., Boughner, D. R. & Kloner, R. A. Role of collagen in acute myocardial infarct expansion. *Circulation* **84**, 2123–2134 (1991).

47. Dobaczewski, M. *et al.* Extracellular matrix remodeling in canine and mouse myocardial infarcts. *Cell Tissue Res.* **324**, 475–488 (2006).

48. Brown, L. F. *et al.* Expression of vascular permeability factor (vascular endothelial growth factor) by epidermal keratinocytes during wound healing. *J. Exp. Med.* **176**, 1375–1379 (1992).

49. Ignotz, R. A. & Massagué, J. Transforming growth factor-beta stimulates the expression of fibronectin and collagen and their incorporation into the extracellular matrix. *J. Biol. Chem.* **261**, 4337–4345 (1986).

50. Ulrich, M. M. W. *et al.* Increased Expression of Fibronectin Isoforms After Myocardial Infarction in Rats. *J. Mol. Cell. Cardiol.* **29**, 2533–2543 (1997).

51. Brown, L. F. *et al.* Macrophages and fibroblasts express embryonic fibronectins during cutaneous wound healing. *Am. J. Pathol.* **142**, 793–801 (1993).

52. Cleutjens, J. P., Verluyten, M. J., Smiths, J. F. & Daemen, M. J. Collagen remodeling after myocardial infarction in the rat heart. *Am. J. Pathol.* **147**, 325–338 (1995).

53. Wei, S., Chow, L. T. C., Shum, I. O. L., Qin, L. & Sanderson, J. E. Left and right ventricular collagen type I/III ratios and remodeling post-myocardial infarction. *J. Card. Fail.* **5**, 117–126 (1999).

54. Lepilina, A. *et al.* A Dynamic Epicardial Injury Response Supports Progenitor Cell Activity during Zebrafish Heart Regeneration. *Cell* **127**, 607–619 (2006).

55. Sánchez-Iranzo, H. *et al.* Transient fibrosis resolves via fibroblast inactivation in the regenerating zebrafish heart. *Proc. Natl. Acad. Sci.* **115**, 4188 LP – 4193 (2018).

56. Münch, J., Grivas, D., González-Rajal, Á., Torregrosa-Carrión, R. & de la Pompa, J. L. Notch signalling restricts inflammation and serpine1 expression in the dynamic endocardium of the regenerating zebrafish heart. *Development* **144**, 1425–1440 (2017).

57. Sanz-Morejón, A. *et al.* Wilms Tumor 1b Expression Defines a Pro-regenerative Macrophage Subtype and Is Required for Organ Regeneration in the Zebrafish. *Cell Rep.* **28**, 1296-1306.e6 (2019).

58. Hui, S. P. *et al.* Zebrafish Regulatory T Cells Mediate Organ-Specific Regenerative Programs. *Dev. Cell* **43**, 659-672.e5 (2017).

59. Desmoulière, A., Redard, M., Darby, I. & Gabbiani, G. Apoptosis mediates the decrease in cellularity during the transition between granulation tissue and scar. *Am. J. Pathol.* **146**, 56–66 (1995).

60. Nelissen-Vrancken, H. J. M. G., Debets, J. J. M., Snoeckx, L. H. E. H., Daemen, M. J. A. P. & Smits, J. F. M. Time-Related Normalization of Maximal Coronary Flow in Isolated Perfused Hearts of Rats With Myocardial Infarction. *Circulation* **93**, 349–355 (1996).

61. Baudino, T. A., Carver, W., Giles, W. & Borg, T. K. Cardiac fibroblasts: friend or foe? *Am. J. Physiol. Circ. Physiol.* **291**, H1015–H1026 (2006).

62. Travers, J. G., Kamal, F. A., Robbins, J., Yutzey, K. E. & Blaxall, B. C. Cardiac Fibrosis. *Circ. Res.* **118**, 1021–1040 (2016).

63. Sharov, V. G. *et al.* Abnormalities of cardiocytes in regions bordering fibrous scars of dogs with heart failure. *Int. J. Cardiol.* **60**, 273–279 (1997).

64. Dispersyn, G. D. *et al.* Dissociation of cardiomyocyte apoptosis and dedifferentiation in infarct border zones. *Eur. Heart J.* **23**, 849–857 (2002).

65. Kikuchi, K. *et al.* Primary contribution to zebrafish heart regeneration by gata4+ cardiomyocytes. *Nature*

464, 601–605 (2010).

66. Jopling, C. *et al.* Zebrafish heart regeneration occurs by cardiomyocyte dedifferentiation and proliferation. *Nature* **464**, 606–609 (2010).
67. Honkoop, H. *et al.* Single-cell analysis uncovers that metabolic reprogramming by ErbB2 signaling is essential for cardiomyocyte proliferation in the regenerating heart. *Elife* **8**, (2019).
68. Fukuda, R. *et al.* Stimulation of glycolysis promotes cardiomyocyte proliferation after injury in adult zebrafish. *EMBO Rep.* **21**, e49752 (2020).
69. González-Rosa, J. M. *et al.* Myocardial Polyploidization Creates a Barrier to Heart Regeneration in Zebrafish. *Dev. Cell* **44**, 433-446.e7 (2018).
70. Patterson, M. *et al.* Frequency of mononuclear diploid cardiomyocytes underlies natural variation in heart regeneration. *Nat. Genet.* **49**, 1346–1353 (2017).
71. Windmueller, R. *et al.* Direct Comparison of Mononucleated and Binucleated Cardiomyocytes Reveals Molecular Mechanisms Underlying Distinct Proliferative Competencies. *Cell Rep.* **30**, 3105-3116.e4 (2020).
72. Eltzschig, H. K. & Eckle, T. Ischemia and reperfusion—from mechanism to translation. *Nat. Med.* **17**, 1391–1401 (2011).
73. Vandervelde, S. *et al.* Increased inflammatory response and neovascularization in reperfused vs. nonreperfused murine myocardial infarction. *Cardiovasc. Pathol.* **15**, 83–90 (2006).
74. Kain, V., Prabhu, S. D. & Halade, G. V. Inflammation revisited: inflammation versus resolution of inflammation following myocardial infarction. *Basic Res. Cardiol.* **109**, 444 (2014).
75. Timmers, L. *et al.* The innate immune response in reperfused myocardium. *Cardiovasc. Res.* **94**, 276–283 (2012).
76. Arslan, F., de Kleijn, D. P. & Pasterkamp, G. Innate immune signaling in cardiac ischemia. *Nat. Rev. Cardiol.* **8**, 292–300 (2011).
77. de Haan, J. J., Smeets, M. B., Pasterkamp, G. & Arslan, F. Danger Signals in the Initiation of the Inflammatory Response after Myocardial Infarction. *Mediators Inflamm.* **2013**, 206039 (2013).
78. Mann, D. L. & Kirschenbaum, L. The Emerging Role of Innate Immunity in the Heart and Vascular System. *Circ. Res.* **108**, 1133–1145 (2011).
79. Yan, X. *et al.* Temporal dynamics of cardiac immune cell accumulation following acute myocardial infarction. *J. Mol. Cell. Cardiol.* **62**, 24–35 (2013).
80. Mantovani, A., Cassatella, M. A., Costantini, C. & Jaillon, S. Neutrophils in the activation and regulation of innate and adaptive immunity. *Nat. Rev. Immunol.* **11**, 519–531 (2011).
81. Serhan, C. N., Chiang, N. & Van Dyke, T. E. Resolving inflammation: dual anti-inflammatory and pro-resolution lipid mediators. *Nat. Rev. Immunol.* **8**, 349–361 (2008).
82. Soehnlein, O. & Lindbom, L. Phagocyte partnership during the onset and resolution of inflammation. *Nat. Rev. Immunol.* **10**, 427–439 (2010).
83. Williams, M. R., Azcutia, V., Newton, G., Alcaide, P. & Luscinskas, F. W. Emerging mechanisms of neutrophil recruitment across endothelium. *Trends Immunol.* **32**, 461–469 (2011).
84. Boufenzer, A. *et al.* TREM-1 Mediates Inflammatory Injury and Cardiac Remodeling Following Myocardial Infarction. *Circ. Res.* **116**, 1772–1782 (2015).
85. Matthias, N. *et al.* The healing myocardium sequentially mobilizes two monocyte subsets with divergent and complementary functions . *J. Exp. Med.* **204**, 3037–3047 (2007).
86. Dewald, O. *et al.* CCL2/Monocyte Chemoattractant Protein-1 Regulates Inflammatory Responses Critical to Healing Myocardial Infarcts. *Circ. Res.* **96**, 881–889 (2005).
87. Nahrendorf, M., Pittet, M. J. & Swirski, F. K. Monocytes: Protagonists of Infarct Inflammation and Repair After Myocardial Infarction. *Circulation* **121**, 2437–2445 (2010).
88. K., S. F. *et al.* Identification of Splenic Reservoir Monocytes and Their Deployment to Inflammatory Sites. *Science (80-.).* **325**, 612–616 (2009).
89. Hilgendorf, I. *et al.* Ly-6Chigh Monocytes Depend on Nr4a1 to Balance Both Inflammatory and Reparative Phases in the Infarcted Myocardium. *Circ. Res.* **114**, 1611–1622 (2014).
90. Hofmann, U. *et al.* Activation of CD4+ T Lymphocytes Improves Wound Healing and Survival After Experimental Myocardial Infarction in Mice. *Circulation* **125**, 1652–1663 (2012).
91. Homma, T. *et al.* Activation of invariant natural killer T cells by α-galactosylceramide ameliorates myocardial ischemia/reperfusion injury in mice. *J. Mol. Cell. Cardiol.* **62**, 179–188 (2013).
92. Sobirin, M. A. *et al.* Activation of Natural Killer T Cells Ameliorates Postinfarct Cardiac Remodeling and Failure in Mice. *Circ. Res.* **111**, 1037–1047 (2012).
93. Weirather, J. *et al.* Foxp3+ CD4+ T Cells Improve Healing After Myocardial Infarction by Modulating Monocyte/Macrophage Differentiation. *Circ. Res.* **115**, 55–67 (2014).
94. Yan, X. *et al.* Deleterious Effect of the IL-23/IL-17A Axis and γδT Cells on Left Ventricular Remodeling After Myocardial Infarction. *J. Am. Heart Assoc.* **1**, e004408 (2021).
95. Hofmann, U. & Frantz, S. Role of Lymphocytes in Myocardial Injury, Healing, and Remodeling After Myocardial Infarction. *Circ. Res.* **116**, 354–367 (2015).
96. Santos-Zas, I. *et al.* Cytotoxic CD8+ T cells promote granzyme B-dependent adverse post-ischemic cardiac remodeling. *Nat. Commun.* **12**, 1483 (2021).
97. Ilatovskaya, D. V *et al.* CD8(+) T-cells negatively regulate inflammation post-myocardial infarction. *Am. J. Physiol. Heart Circ. Physiol.* **317**, H581–H596 (2019).
98. Curato, C. *et al.* Identification of noncytotoxic and IL-10-producing CD8+AT2R+ T cell population in response to ischemic heart injury. *J. Immunol.* **185**, 6286–6293 (2010).

99. Mann, D. L. Inflammatory Mediators and the Failing Heart. *Circ. Res.* **91**, 988–998 (2002).
100. Prabhu, S. D. It Takes Two to Tango. *Circ. Res.* **114**, 1558–1560 (2014).
101. Bui, A. L., Horwich, T. B. & Fonarow, G. C. Epidemiology and risk profile of heart failure. *Nat. Rev. Cardiol.* **8**, 30–41 (2011).
102. Ponikowski, P. *et al.* Heart failure: preventing disease and death worldwide. *ESC Hear. Fail.* **1**, 4–25 (2014).
103. Conrad, N. *et al.* Temporal trends and patterns in heart failure incidence: a population-based study of 4 million individuals. *Lancet (London, England)* **391**, 572–580 (2018).
104. van den Borne, S. W. M. *et al.* Myocardial remodeling after infarction: the role of myofibroblasts. *Nat. Rev. Cardiol.* **7**, 30–37 (2010).
105. Shinde, A. V & Frangogiannis, N. G. Fibroblasts in myocardial infarction: a role in inflammation and repair. *J. Mol. Cell. Cardiol.* **70**, 74–82 (2014).
106. Sweeney, M., Corden, B. & Cook, S. A. Targeting cardiac fibrosis in heart failure with preserved ejection fraction: mirage or miracle? *EMBO Mol. Med.* **12**, e10865 (2020).
107. Francis Stuart, S. D., De Jesus, N. M., Lindsey, M. L. & Ripplinger, C. M. The crossroads of inflammation, fibrosis, and arrhythmia following myocardial infarction. *J. Mol. Cell. Cardiol.* **91**, 114–122 (2016).
108. Schaper, J., Meiser, E. & Stämmler, G. Ultrastructural morphometric analysis of myocardium from dogs, rats, hamsters, mice, and from human hearts. *Circ. Res.* **56**, 377–391 (1985).
109. Kostin, S., Hein, S., Arnon, E., Scholz, D. & Schaper, J. The cytoskeleton and related proteins in the human failing heart. *Heart Fail. Rev.* **5**, 271–280 (2000).
110. Sharov, V. G., Kostin, S., Todor, A., Schaper, J. & Sabbah, H. N. Expression of cytoskeletal, linkage and extracellular proteins in failing dog myocardium. *Heart Fail. Rev.* **10**, 297–303 (2005).
111. Rienks, M., Papageorgiou, A.-P., Frangogiannis, N. G. & Heymans, S. Myocardial Extracellular Matrix. *Circ. Res.* **114**, 872–888 (2014).
112. Hall, M. L. & Ogle, B. M. Cardiac Extracellular Matrix Modification as a Therapeutic Approach. *Adv. Exp. Med. Biol.* **1098**, 131–150 (2018).
113. Frangogiannis, N. G. The Extracellular Matrix in Ischemic and Nonischemic Heart Failure. *Circ. Res.* **125**, 117–146 (2019).
114. Weber, K. T. Cardiac interstitium in health and disease: the fibrillar collagen network. *J. Am. Coll. Cardiol.* **13**, 1637–1652 (1989).
115. Brilla, C. G., Zhou, G., Rupp, H., Maisch, B. & Weber, K. T. Role of angiotensin II and prostaglandin E2 in regulating cardiac fibroblast collagen turnover. *Am. J. Cardiol.* **76**, 8D-13D (1995).
116. Weber, K. T. Extracellular Matrix Remodeling in Heart Failure . *Circulation* **96**, 4065–4082 (1997).
117. Weber, K. T. Targeting pathological remodeling: concepts of cardioprotection and reparation. *Circulation* vol. 102 1342–1345 at https://doi.org/10.1161/01.cir.102.12.1342 (2000).
118. Badenhorst, D. *et al.* Cross-linking influences the impact of quantitative changes in myocardial collagen on cardiac stiffness and remodelling in hypertension in rats. *Cardiovasc. Res.* **57**, 632–641 (2003).
119. Norton, G. R. *et al.* Myocardial stiffness is attributed to alterations in cross-linked collagen rather than total collagen or phenotypes in spontaneously hypertensive rats. *Circulation* **96**, 1991–1998 (1997).
120. Willems, I. E., Havenith, M. G., De Mey, J. G. & Daemen, M. J. The alpha-smooth muscle actin-positive cells in healing human myocardial scars. *Am. J. Pathol.* **145**, 868–875 (1994).
121. Sun, Y. & Weber, K. T. Infarct scar: a dynamic tissue. *Cardiovasc. Res.* **46**, 250–256 (2000).
122. Sun, Y., Kiani, M. F., Postlethwaite, A. E. & Weber, K. T. Infarct scar as living tissue. *Basic Res. Cardiol.* **97**, 343–347 (2002).
123. Segura, A. M., Frazier, O. H. & Buja, L. M. Fibrosis and heart failure. *Heart Fail. Rev.* **19**, 173–185 (2014).
124. Leask, A. TGFbeta, cardiac fibroblasts, and the fibrotic response. *Cardiovasc. Res.* **74**, 207–212 (2007).
125. Villarreal, F. J., Kim, N. N., Ungab, G. D., Printz, M. P. & Dillmann, W. H. Identification of functional angiotensin II receptors on rat cardiac fibroblasts. *Circulation* **88**, 2849–2861 (1993).
126. Anker, S. D. & von Haehling, S. Inflammatory mediators in chronic heart failure: an overview. *Heart* **90**, 464–470 (2004).
127. El-Menyar, A. A. Cytokines and myocardial dysfunction: state of the art. *J. Card. Fail.* **14**, 61–74 (2008).
128. Hedayat, M., Mahmoudi, M. J., Rose, N. R. & Rezaei, N. Proinflammatory cytokines in heart failure: double-edged swords. *Heart Fail. Rev.* **15**, 543–562 (2010).
129. Satoh, M., Minami, Y., Takahashi, Y. & Nakamura, M. Immune modulation: role of the inflammatory cytokine cascade in the failing human heart. *Curr. Heart Fail. Rep.* **5**, 69–74 (2008).
130. Siwik, D. A. & Colucci, W. S. Regulation of matrix metalloproteinases by cytokines and reactive oxygen/nitrogen species in the myocardium. *Heart Fail. Rev.* **9**, 43–51 (2004).
131. Sivasubramanian, N. *et al.* Left ventricular remodeling in transgenic mice with cardiac restricted overexpression of tumor necrosis factor. *Circulation* **104**, 826–831 (2001).
132. Yamauchi-Takihara, K. & Kishimoto, T. Cytokines and their receptors in cardiovascular diseases--role of gp130 signalling pathway in cardiac myocyte growth and maintenance. *Int. J. Exp. Pathol.* **81**, 1–16 (2000).
133. Shioi, T. *et al.* Increased expression of interleukin-1 beta and monocyte chemotactic and activating factor/monocyte chemoattractant protein-1 in the hypertrophied and failing heart with pressure overload. *Circ. Res.* **81**, 664–671 (1997).
134. Dai, R. P., Dheen, S. T., He, B. P. & Tay, S. S. W. Differential expression of cytokines in the rat heart in response to sustained volume overload. *Eur. J. Heart Fail.* **6**, 693–703 (2004).
135. Chandrasekar, B., Mummidi, S., Claycomb, W. C., Mestril, R. & Nemer, M. Interleukin-18 is a pro-hypertrophic cytokine that acts through a   phosphatidylinositol 3-kinase-phosphoinositide-dependent

kinase-1-Akt-GATA4 signaling pathway in cardiomyocytes. *J. Biol. Chem.* **280**, 4553–4567 (2005).

136. Tsutsui, H., Kinugawa, S. & Matsushima, S. Mitochondrial oxidative stress and dysfunction in myocardial remodelling. *Cardiovasc. Res.* **81**, 449–456 (2009).

137. Tsutsui, H., Kinugawa, S. & Matsushima, S. Oxidative stress and mitochondrial DNA damage in heart failure. *Circ. J.* **72 Suppl A**, A31-7 (2008).

138. Zimmet, J. M. & Hare, J. M. Nitroso–Redox Interactions in the Cardiovascular System. *Circulation* **114**, 1531–1544 (2006).

139. Sandoval, Y. & Jaffe, A. S. Type 2 Myocardial Infarction: JACC Review Topic of the Week. *J. Am. Coll. Cardiol.* **73**, 1846–1860 (2019).

140. Ryan, T. J. *et al.* ACC/AHA Guidelines for the Management of Patients With Acute Myocardial Infarction:Executive Summary. *Circulation* **94**, 2341–2350 (1996).

141. Bauersachs, J. Heart failure drug treatment: the fantastic four. *Eur. Heart J.* **42**, 681–683 (2021).

142. McDonagh, T. A. *et al.* 2021 ESC Guidelines for the diagnosis and treatment of acute and chronic heart failure. *Eur. Heart J.* **42**, 3599–3726 (2021).

143. Treatment, heart failure. https://www.nhs.uk/conditions/heart-failure/treatment/.

144. Heart failure - Diagnosis and Treatment. https://www.mayoclinic.org/diseases-conditions/heart-failure/diagnosis-treatment/drc-20373148#:~:text=Beta blockers.,%2C Kapspargo Sprinkle) and bisoprolol.

145. Jessup, M. & Brozena, S. Heart failure. *N. Engl. J. Med.* **348**, 2007–2018 (2003).

146. Devices and Surgical Procedures to Treat Heart Failure. https://www.heart.org/en/health-topics/heart-failure/treatment-options-for-heart-failure/devices-and-surgical-procedures-to-treat-heart-failure.

147. Cao, F. *et al.* Long-term myocardial functional improvement after autologous bone marrow mononuclear cells transplantation in patients with ST-segment elevation myocardial infarction: 4 years follow-up. *Eur. Heart J.* **30**, 1986–1994 (2009).

148. Garikapati, K. *et al.* Outcomes of patients with left ventricular diastolic dysfunction in adult hematopoietic stem cell transplantation. at (2013).

149. Babin-Ebell, J. *et al.* Transmyocardial laser revascularization combined with intramyocardial endothelial progenitor cell transplantation in patients with intractable ischemic heart disease ineligible for conventional revascularization: preliminary results in a highly selected s. *Thorac. Cardiovasc. Surg.* **58**, 11–16 (2010).

150. Aghajanian, H. *et al.* Targeting cardiac fibrosis with engineered T cells. *Nature* **573**, 430–433 (2019).

151. G., R. J. *et al.* CAR T cells produced in vivo to treat cardiac injury. *Science (80-.).* **375**, 91–96 (2022).

152. Machaj, F. *et al.* New therapies for the treatment of heart failure: a summary of recent accomplishments. *Ther. Clin. Risk Manag.* **15**, 147–155 (2019).

153. Cleland, J. G. F., Pellicori, P. & González, A. A novel treatment for heart failure targets myocardial fibrosis. *Nat. Med.* **27**, 1343–1344 (2021).

154. Lewis, G. A. *et al.* Pirfenidone in heart failure with preserved ejection fraction: a randomized phase 2 trial. *Nat. Med.* **27**, 1477–1482 (2021).

155. Magadum, A. *et al.* Live cell screening platform identifies PPARδ as a regulator of cardiomyocyte proliferation and cardiac repair. *Cell Res.* **27**, 1002–1019 (2017).

156. Chen, W. *et al.* TT-10-loaded nanoparticles promote cardiomyocyte proliferation and cardiac repair in a mouse model of myocardial infarction. *JCI insight* **6**, (2021).

157. Hara, H. *et al.* Discovery of a Small Molecule to Increase Cardiomyocytes and Protect the Heart After Ischemic Injury. *JACC. Basic to Transl. Sci.* **3**, 639–653 (2018).

158. Bersell, K., Arab, S., Haring, B. & Kühn, B. Neuregulin1/ErbB4 signaling induces cardiomyocyte proliferation and repair of heart injury. *Cell* **138**, 257–270 (2009).

159. Tseng, A.-S., Engel, F. B. & Keating, M. T. The GSK-3 Inhibitor BIO Promotes Proliferation in Mammalian Cardiomyocytes. *Chem. Biol.* **13**, 957–963 (2006).

160. Uosaki, H. *et al.* Identification of chemicals inducing cardiomyocyte proliferation in developmental stage-specific manner with pluripotent stem cells. *Circ. Cardiovasc. Genet.* **6**, 624–633 (2013).

161. Kocabas, F. *et al.* The Hypoxic Epicardial and Subepicardial Microenvironment. *J. Cardiovasc. Transl. Res.* **5**, 654–665 (2012).

162. Längle, D., Halver, J., Rathmer, B., Willems, E. & Schade, D. Small Molecules Targeting in Vivo Tissue Regeneration. *ACS Chem. Biol.* **9**, 57–71 (2014).

163. Firestone, A. J. & Chen, J. K. Controlling Destiny through Chemistry: Small-Molecule Regulators of Cell Fate. *ACS Chem. Biol.* **5**, 15–34 (2010).

164. Sadek, H. *et al.* Cardiogenic small molecules that enhance myocardial repair by stem cells. *Proc. Natl. Acad. Sci.* **105**, 6063–6068 (2008).

165. Qin, H., Zhao, A. & Fu, X. Small molecules for reprogramming and transdifferentiation. *Cell. Mol. Life Sci.* **74**, 3553–3575 (2017).

166. Engel, F. B., Hsieh, P. C. H., Lee, R. T. & Keating, M. T. FGF1/p38 MAP kinase inhibitor therapy induces cardiomyocyte mitosis, reduces scarring, and rescues function after myocardial infarction. *Proc. Natl. Acad. Sci. U. S. A.* **103**, 15546–15551 (2006).

167. Pouliquin, P. & Dulhunty, A. F. Homer and the ryanodine receptor. *Eur. Biophys. J.* **39**, 91 (2009).

168. Liang, D. *et al.* miRNA-204 drives cardiomyocyte proliferation via targeting Jarid2. *Int. J. Cardiol.* **201**, 38–48 (2015).

169. Arif, M. *et al.* MicroRNA-210-mediated proliferation, survival, and angiogenesis promote cardiac repair post myocardial infarction in rodents. *J. Mol. Med. (Berl).* **95**, 1369–1385 (2017).

170. Wang, B. *et al.* miR-25 Promotes Cardiomyocyte Proliferation by Targeting FBXW7. *Mol. Ther. Nucleic*

Acids **19**, 1299–1308 (2020).

171. Jayawardena, T. M. *et al.* MicroRNA-mediated in vitro and in vivo direct reprogramming of cardiac fibroblasts to cardiomyocytes. *Circ. Res.* **110**, 1465–1473 (2012).

172. Paoletti, C. *et al.* MicroRNA-Mediated Direct Reprogramming of Human Adult Fibroblasts Toward Cardiac Phenotype. *Front. Bioeng. Biotechnol.* **8**, 529 (2020).

173. Melissa, V. *et al.* Repression of Osmr and Fgfr1 by miR-1/133a prevents cardiomyocyte dedifferentiation and cell cycle entry in the adult heart. *Sci. Adv.* **7**, eabi6648 (2022).

174. Kim, Y., Jeong, J. & Choi, D. Small-molecule-mediated reprogramming: a silver lining for regenerative medicine. *Exp. Mol. Med.* **52**, 213–226 (2020).

175. Yanpu, C. *et al.* Reversible reprogramming of cardiomyocytes to a fetal state drives heart regeneration in mice. *Science (80-.).* **373**, 1537–1540 (2021).

176. Qian, L., Berry, E. C., Fu, J., Ieda, M. & Srivastava, D. Reprogramming of mouse fibroblasts into cardiomyocyte-like cells in vitro. *Nat. Protoc.* **8**, 1204–1215 (2013).

177. Song, K. *et al.* Heart repair by reprogramming non-myocytes with cardiac transcription factors. *Nature* **485**, 599–604 (2012).

178. Addis, R. C. *et al.* Optimization of direct fibroblast reprogramming to cardiomyocytes using calcium activity as a functional measure of success. *J. Mol. Cell. Cardiol.* **60**, 97–106 (2013).

179. Cho, J. *et al.* Regeneration of infarcted mouse hearts by cardiovascular tissue formed via the direct reprogramming of mouse fibroblasts. *Nat. Biomed. Eng.* **5**, 880–896 (2021).

180. Zhang, G., Hu, Q., Braunlin, E. A., Suggs, L. J. & Zhang, J. Enhancing efficacy of stem cell transplantation to the heart with a PEGylated fibrin biomatrix. *Tissue Eng. Part A* **14**, 1025–1036 (2008).

181. Christman, K. L. *et al.* Injectable fibrin scaffold improves cell transplant survival, reduces infarct expansion, and induces neovasculature formation in ischemic myocardium. *J. Am. Coll. Cardiol.* **44**, 654–660 (2004).

182. Yu, J. *et al.* The use of human mesenchymal stem cells encapsulated in RGD modified alginate microspheres in the repair of myocardial infarction in the rat. *Biomaterials* **31**, 7012–7020 (2010).

183. Li, J. *et al.* A chitosan-glutathione based injectable hydrogel for suppression of oxidative stress damage in cardiomyocytes. *Biomaterials* **34**, 9071–9081 (2013).

184. Zhang, Y. *et al.* Collagen-based matrices improve the delivery of transplanted circulating progenitor cells: development and demonstration by ex vivo radionuclide cell labeling and in vivo tracking with positron-emission tomography. *Circ. Cardiovasc. Imaging* **1**, 197–204 (2008).

185. Ajdary, R. *et al.* Multifunctional 3D-Printed Patches for Long-Term Drug Release Therapies after Myocardial Infarction. *Adv. Funct. Mater.* **30**, 2003440 (2020).

186. Contessotto, P. *et al.* Elastin-like recombinamers-based hydrogel modulates post-ischemic remodeling in a non-transmural myocardial infarction in sheep. *Sci. Transl. Med.* **13**, (2021).

187. Liu, B. *et al.* Cardiac recovery via extended cell-free delivery of extracellular vesicles secreted by cardiomyocytes derived from induced pluripotent stem cells. *Nat. Biomed. Eng.* **2**, 293–303 (2018).

188. Yao, J. *et al.* A Minimally Invasive Exosome Spray Repairs Heart after Myocardial Infarction. *ACS Nano* **15**, 11099–11111 (2021).

189. Soonpaa, M. H., Kim, K. K., Pajak, L., Franklin, M. & Field, L. J. Cardiomyocyte DNA synthesis and binucleation during murine development. *Am. J. Physiol.* **271**, H2183-9 (1996).

190. Li, F., Wang, X., Capasso, J. M. & Gerdes, A. M. Rapid transition of cardiac myocytes from hyperplasia to hypertrophy during postnatal development. *J. Mol. Cell. Cardiol.* **28**, 1737–1746 (1996).

191. Bergmann, O. *et al.* Evidence for cardiomyocyte renewal in humans. *Science* **324**, 98–102 (2009).

192. Poolman, R. A., Gilchrist, R. & Brooks, G. Cell cycle profiles and expressions of p21CIP1 AND P27KIP1 during myocyte development. *Int. J. Cardiol.* **67**, 133–142 (1998).

193. Evans-Anderson, H. J., Alfieri, C. M. & Yutzey, K. E. Regulation of cardiomyocyte proliferation and myocardial growth during development by FOXO transcription factors. *Circ. Res.* **102**, 686–694 (2008).

194. Rochais, F. *et al.* FGF10 promotes regional foetal cardiomyocyte proliferation and adult cardiomyocyte cell-cycle re-entry. *Cardiovasc. Res.* **104**, 432–442 (2014).

195. Kühn, B. *et al.* Periostin induces proliferation of differentiated cardiomyocytes and promotes cardiac repair. *Nat. Med.* **13**, 962–969 (2007).

196. Fan, X. *et al.* Matrix metalloproteinase-2 in oncostatin M-induced sarcomere degeneration in cardiomyocytes. *Am. J. Physiol. Heart Circ. Physiol.* **311**, H183-9 (2016).

197. Payan, S. M., Hubert, F. & Rochais, F. Cardiomyocyte proliferation, a target for cardiac regeneration. *Biochim. Biophys. Acta - Mol. Cell Res.* **1867**, 118461 (2020).

198. Williams, C., Quinn, K. P., Georgakoudi, I. & Black, L. D. 3rd. Young developmental age cardiac extracellular matrix promotes the expansion of neonatal cardiomyocytes in vitro. *Acta Biomater.* **10**, 194–204 (2014).

199. Ieda, M. *et al.* Cardiac fibroblasts regulate myocardial proliferation through beta1 integrin signaling. *Dev. Cell* **16**, 233–244 (2009).

200. Morikawa, Y., Heallen, T., Leach, J., Xiao, Y. & Martin, J. F. Dystrophin–glycoprotein complex sequesters Yap to inhibit cardiomyocyte proliferation. *Nature* **547**, 227–231 (2017).

201. Bassat, E. *et al.* The extracellular matrix protein agrin promotes heart regeneration in mice. *Nature* **547**, 179–184 (2017).

202. Turan, R. D., Aslan, G. S., Yücel, D., Döğer, R. & Kocabaş, F. Evolving approaches to heart regeneration by therapeutic stimulation of resident cardiomyocyte cell cycle. *Anatol. J. Cardiol.* **16**, 881–886 (2016).

203. Gessert, S. & Kühl, M. The multiple phases and faces of wnt signaling during cardiac differentiation and

development. *Circ. Res.* **107**, 186–199 (2010).

204. Ozhan, G. & Weidinger, G. Wnt/β-catenin signaling in heart regeneration. *Cell Regen. (London, England)* **4**, 3 (2015).
205. Titmarsh, D. M. *et al.* Induction of Human iPSC-Derived Cardiomyocyte Proliferation Revealed by Combinatorial Screening in High Density Microbioreactor Arrays. *Sci. Rep.* **6**, 24637 (2016).
206. Engel, F. B. *et al.* p38 MAP kinase inhibition enables proliferation of adult mammalian cardiomyocytes. *Genes Dev.* **19**, 1175–1187 (2005).
207. Wang, L. *et al.* Inhibiting Glycogen Synthase Kinase 3 Reverses Obesity-Induced White Adipose Tissue Inflammation by Regulating Apoptosis Inhibitor of Macrophage/CD5L-Mediated Macrophage Migration. *Arterioscler. Thromb. Vasc. Biol.* **38**, 2103–2116 (2018).
208. Schindler, J. F., Monahan, J. B. & Smith, W. G. p38 pathway kinases as anti-inflammatory drug targets. *J. Dent. Res.* **86**, 800–811 (2007).
209. Strebhardt, K. & Ullrich, A. Paul Ehrlich's magic bullet concept: 100 years of progress. *Nature reviews. Cancer* vol. 8 473–480 at https://doi.org/10.1038/nrc2394 (2008).
210. Suarez, S., Almutairi, A. & Christman, K. L. Micro- and Nanoparticles for Treating Cardiovascular Disease. *Biomater. Sci.* **3**, 564–580 (2015).
211. Borrelli, M. A., Turnquist, H. R. & Little, S. R. Biologics and their delivery systems: Trends in myocardial infarction. *Adv. Drug Deliv. Rev.* **173**, 181–215 (2021).
212. Eniola-Adefeso, O., Heslinga, M. J. & Porter, T. M. Design of nanovectors for therapy and imaging of cardiovascular diseases. *Methodist Debakey Cardiovasc. J.* **8**, 13–17 (2012).
213. Bor, G., Mat Azmi, I. D. & Yaghmur, A. Nanomedicines for cancer therapy: current status, challenges and future prospects. *Ther. Deliv.* **10**, 113–132 (2019).
214. Fang, R. H. *et al.* Cancer Cell Membrane-Coated Nanoparticles for Anticancer Vaccination and Drug Delivery. *Nano Lett.* **14**, 2181–2188 (2014).
215. Spanjers, J. M. & Städler, B. Cell Membrane Coated Particles. *Adv. Biosyst.* **4**, 2000174 (2020).
216. Doshi, N., Zahr, A. S., Bhaskar, S., Lahann, J. & Mitragotri, S. Red blood cell-mimicking synthetic biomaterial particles. *Proc. Natl. Acad. Sci.* **106**, 21495–21499 (2009).
217. Fontana, F. *et al.* Multistaged Nanovaccines Based on Porous Silicon@Acetalated Dextran@Cancer Cell Membrane for Cancer Immunotherapy. *Adv. Mater.* **29**, (2017).
218. Rahikkala, A. *et al.* Hybrid red blood cell membrane coated porous silicon nanoparticles functionalized with cancer antigen induce depletion of T cells. *RSC Adv.* **10**, 35198–35205 (2020).
219. Li, J. *et al.* Multifunctional Biomimetic Nanovaccines Based on Photothermal and Weak-immunostimulatory Nanoparticulate Cores for the Immunotherapy of Solid Tumors. *Adv. Mater.* **n/a**, 2108012 (2021).
220. Martins, J. P. *et al.* Neonatal Fc receptor-targeted lignin-encapsulated porous silicon nanoparticles for enhanced cellular interactions and insulin permeation across the intestinal epithelium. *Bioact. Mater.* **9**, 299–315 (2022).
221. Blanco, E., Shen, H. & Ferrari, M. Principles of nanoparticle design for overcoming biological barriers to drug delivery. *Nat. Biotechnol.* **33**, 941–951 (2015).
222. Soo Choi, H. *et al.* Renal clearance of quantum dots. *Nat. Biotechnol.* **25**, 1165–1170 (2007).
223. Zhang, Y.-N., Poon, W., Tavares, A. J., McGilvray, I. D. & Chan, W. C. W. Nanoparticle-liver interactions: Cellular uptake and hepatobiliary elimination. *J. Control. Release* **240**, 332–348 (2016).
224. Sun, W., Hu, Q., Ji, W., Wright, G. & Gu, Z. Leveraging Physiology for Precision Drug Delivery. *Physiol. Rev.* **97**, 189–225 (2016).
225. Jain, R. K. & Stylianopoulos, T. Delivering nanomedicine to solid tumors. *Nat. Rev. Clin. Oncol.* **7**, 653–664 (2010).
226. Lundy, D. J., Chen, K.-H., Toh, E. K.-W. & Hsieh, P. C.-H. Distribution of Systemically Administered Nanoparticles Reveals a Size-Dependent Effect Immediately following Cardiac Ischaemia-Reperfusion Injury. *Sci. Rep.* **6**, 25613 (2016).
227. Petros, R. A. & DeSimone, J. M. Strategies in the design of nanoparticles for therapeutic applications. *Nat. Rev. Drug Discov.* **9**, 615–627 (2010).
228. Zhao, J. & Stenzel, M. H. Entry of nanoparticles into cells: the importance of nanoparticle properties. *Polym. Chem.* **9**, 259–272 (2018).
229. Foroozandeh, P. & Aziz, A. A. Insight into Cellular Uptake and Intracellular Trafficking of Nanoparticles. *Nanoscale Res. Lett.* **13**, 339 (2018).
230. Toy, R., Peiris, P. M., Ghaghada, K. B. & Karathanasis, E. Shaping cancer nanomedicine: the effect of particle shape on the in vivo journey of nanoparticles. *Nanomedicine (Lond).* **9**, 121–134 (2014).
231. Champion, J. A. & Mitragotri, S. Role of target geometry in phagocytosis. *Proc. Natl. Acad. Sci.* **103**, 4930–4934 (2006).
232. Huang, X., Teng, X., Chen, D., Tang, F. & He, J. The effect of the shape of mesoporous silica nanoparticles on cellular uptake and cell function. *Biomaterials* **31**, 438–448 (2010).
233. Fröhlich, E. The role of surface charge in cellular uptake and cytotoxicity of medical nanoparticles. *Int. J. Nanomedicine* **7**, 5577–5591 (2012).
234. Nel, A. E. *et al.* Understanding biophysicochemical interactions at the nano–bio interface. *Nat. Mater.* **8**, 543–557 (2009).
235. Zhang, L. *et al.* Microfluidic Synthesis of Hybrid Nanoparticles with Controlled Lipid Layers: Understanding Flexibility-Regulated Cell–Nanoparticle Interaction. *ACS Nano* **9**, 9912–9921 (2015).
236. Guo, P. *et al.* Nanoparticle elasticity directs tumor uptake. *Nat. Commun.* **9**, 130 (2018).

237. Thu Trang, T. T. *et al.* Surface Roughness, Hydrophilicity and Encapsulation Efficiency of Gentamicin Loaded Surface Engineered PLA Microspheres. *J. Phys. Conf. Ser.* **1082**, 12068 (2018).

238. Kim, H.-J., Kim, S. H., Kim, H.-M., Kim, Y. S. & Oh, J.-M. Surface roughness effect on the cellular uptake of layered double hydroxide nanoparticles. *Appl. Clay Sci.* **202**, 105992 (2021).

239. Chen, H., Langer, R. & Edwards, D. A. A Film Tension Theory of Phagocytosis. *J. Colloid Interface Sci.* **190**, 118–133 (1997).

240. Jokerst, J. V, Lobovkina, T., Zare, R. N. & Gambhir, S. S. Nanoparticle PEGylation for imaging and therapy. *Nanomedicine (Lond).* **6**, 715–728 (2011).

241. Gustafson, H. H., Holt-Casper, D., Grainger, D. W. & Ghandehari, H. Nanoparticle Uptake: The Phagocyte Problem. *Nano Today* **10**, 487–510 (2015).

242. Bachelder, E. M., Beaudette, T. T., Broaders, K. E., Dashe, J. & Fréchet, J. M. J. Acetal-derivatized dextran: an acid-responsive biodegradable material for therapeutic applications. *J. Am. Chem. Soc.* **130**, 10494–10495 (2008).

243. Mehvar, R. Dextrans for targeted and sustained delivery of therapeutic and imaging agents. *J. Control. Release* **69**, 1–25 (2000).

244. Gannimani, R., Walvekar, P., Naidu, V. R., Aminabhavi, T. M. & Govender, T. Acetal containing polymers as pH-responsive nano-drug delivery systems. *J. Control. Release* **328**, 736–761 (2020).

245. Cohen, J. L. *et al.* Acid-degradable cationic dextran particles for the delivery of siRNA therapeutics. *Bioconjug. Chem.* **22**, 1056–1065 (2011).

246. Torrieri, G. *et al.* Dual-peptide functionalized acetalated dextran-based nanoparticles for sequential targeting of macrophages during myocardial infarction. *Nanoscale* **12**, 2350–2358 (2020).

247. Ferreira, M. P. A. *et al.* Dual-Drug Delivery Using Dextran-Functionalized Nanoparticles Targeting Cardiac Fibroblasts for Cellular Reprogramming. *Adv. Funct. Mater.* **28**, 1705134 (2018).

248. Torrieri, G. *et al.* In Vitro Evaluation of the Therapeutic Effects of Dual-Drug Loaded Spermine-Acetalated Dextran Nanoparticles Coated with Tannic Acid for Cardiac Applications. *Adv. Funct. Mater.* **32**, 2109032 (2022).

249. Liu, Z. *et al.* Close-loop dynamic nanohybrids on collagen-ark with in situ gelling transformation capability for biomimetic stage-specific diabetic wound healing. *Mater. Horiz.* **6**, 385–393 (2019).

250. Broaders, K. E., Cohen, J. A., Beaudette, T. T., Bachelder, E. M. & Fréchet, J. M. J. Acetalated dextran is a chemically and biologically tunable material for particulate immunotherapy. *Proc. Natl. Acad. Sci.* **106**, 5497 LP – 5502 (2009).

251. Yue, X. & Dai, Z. Liposomal Nanotechnology for Cancer Theranostics. *Curr. Med. Chem.* **25**, 1397–1408 (2018).

252. Xing, H., Hwang, K. & Lu, Y. Recent Developments of Liposomes as Nanocarriers for Theranostic Applications. *Theranostics* **6**, 1336–1352 (2016).

253. Miller, A. D. Lipid-Based Nanoparticles in Cancer Diagnosis and Therapy. *J. Drug Deliv.* **2013**, 165981 (2013).

254. Yingchoncharoen, P., Kalinowski, D. S. & Richardson, D. R. Lipid-Based Drug Delivery Systems in Cancer Therapy: What Is Available and What Is Yet to Come. *Pharmacol. Rev.* **68**, 701–787 (2016).

255. Kahraman, E., Güngör, S. & Özsoy, Y. Potential enhancement and targeting strategies of polymeric and lipid-based nanocarriers in dermal drug delivery. *Ther. Deliv.* **8**, 967–985 (2017).

256. Mahapatro, A. & Singh, D. K. Biodegradable nanoparticles are excellent vehicle for site directed in-vivo delivery of drugs and vaccines. *J. Nanobiotechnology* **9**, 55 (2011).

257. Danhier, F. *et al.* PLGA-based nanoparticles: an overview of biomedical applications. *J. Control. Release* **161**, 505–522 (2012).

258. Sarcan, E. T., Silindir-Gunay, M. & Ozer, A. Y. Theranostic polymeric nanoparticles for NIR imaging and photodynamic therapy. *Int. J. Pharm.* **551**, 329–338 (2018).

259. Begines, B. *et al.* Polymeric Nanoparticles for Drug Delivery: Recent Developments and Future Prospects. *Nanomaterials* **10**, (2020).

260. Elsabahy, M. & Wooley, K. L. Design of polymeric nanoparticles for biomedical delivery applications. *Chem. Soc. Rev.* **41**, 2545–2561 (2012).

261. Bolhassani, A. *et al.* Polymeric nanoparticles: potent vectors for vaccine delivery targeting cancer and infectious diseases. *Hum. Vaccin. Immunother.* **10**, 321–332 (2014).

262. Rahikkala, A. *et al.* Mesoporous Silica Nanoparticles for Targeted and Stimuli-Responsive Delivery of Chemotherapeutics: A Review. *Adv. Biosyst.* **2**, 1800020 (2018).

263. Li, W. *et al.* Tailoring Porous Silicon for Biomedical Applications: From Drug Delivery to Cancer Immunotherapy. *Adv. Mater.* **30**, 1703740 (2018).

264. Shahbazi, M.-A. *et al.* The mechanisms of surface chemistry effects of mesoporous silicon nanoparticles on immunotoxicity and biocompatibility. *Biomaterials* **34**, 7776–7789 (2013).

265. Shahbazi, M.-A. *et al.* Surface chemistry dependent immunostimulative potential of porous silicon nanoplatforms. *Biomaterials* **35**, 9224–9235 (2014).

266. Santos, H. A. *et al.* Mesoporous materials as controlled drug delivery formulations. *J. Drug Deliv. Sci. Technol.* **21**, 139–155 (2011).

267. Dulińska-Litewka, J. *et al.* Superparamagnetic Iron Oxide Nanoparticles-Current and Prospective Medical Applications. *Mater. (Basel, Switzerland)* **12**, (2019).

268. Palanisamy, S. & Wang, Y.-M. Superparamagnetic iron oxide nanoparticulate system: synthesis{,} targeting{,} drug delivery and therapy in cancer. *Dalt. Trans.* **48**, 9490–9515 (2019).

References

269. Vallabani, N. V. S. & Singh, S. Recent advances and future prospects of iron oxide nanoparticles in biomedicine and diagnostics. *3 Biotech* **8**, 279 (2018).
270. Singh, P. *et al.* Gold Nanoparticles in Diagnostics and Therapeutics for Human Cancer. *Int. J. Mol. Sci.* **19**, (2018).
271. Almeida, J. P. M., Lin, A. Y., Figueroa, E. R., Foster, A. E. & Drezek, R. A. In vivo gold nanoparticle delivery of peptide vaccine induces anti-tumor immune response in prophylactic and therapeutic tumor models. *Small* **11**, 1453–1459 (2015).
272. Almeida, J. P. M., Figueroa, E. R. & Drezek, R. A. Gold nanoparticle mediated cancer immunotherapy. *Nanomedicine* **10**, 503–514 (2014).
273. Singh, P. *et al.* Organic functionalisation and characterisation of single-walled carbon nanotubes. *Chem. Soc. Rev.* **38**, 2214–2230 (2009).
274. Georgakilas, V. *et al.* Functionalization of Graphene: Covalent and Non-Covalent Approaches, Derivatives and Applications. *Chem. Rev.* **112**, 6156–6214 (2012).
275. Son, K. H., Hong, J. H. & Lee, J. W. Carbon nanotubes as cancer therapeutic carriers and mediators. *Int. J. Nanomedicine* **11**, 5163–5185 (2016).
276. Pleskova, S., Mikheeva, E. & Gornostaeva, E. Using of Quantum Dots in Biology and Medicine. *Adv. Exp. Med. Biol.* **1048**, 323–334 (2018).
277. Wagner, A. M., Knipe, J. M., Orive, G. & Peppas, N. A. Quantum dots in biomedical applications. *Acta Biomater.* **94**, 44–63 (2019).
278. Cheung, A. S., Koshy, S. T., Stafford, A. G., Bastings, M. M. C. & Mooney, D. J. Adjuvant-Loaded Subcellular Vesicles Derived From Disrupted Cancer Cells for Cancer Vaccination. *Small* **12**, 2321–2333 (2016).
279. Liu, D. *et al.* Microfluidic assisted one-step fabrication of porous silicon@acetalated dextran nanocomposites for precisely controlled combination chemotherapy. *Biomaterials* **39**, 249–259 (2015).
280. Wang, S. *et al.* Intracellular Delivery of Budesonide and Polydopamine Co-Loaded in Endosomolytic Poly(butyl methacrylate-co-methacrylic acid) Grafted Acetalated Dextran for Macrophage Phenotype Switch from M1 to M2. *Adv. Ther.* **4**, 2000058 (2021).
281. Bertoni, S. *et al.* pH and Reactive Oxygen Species-Sequential Responsive Nano-in-Micro Composite for Targeted Therapy of Inflammatory Bowel Disease. *Adv. Funct. Mater.* **28**, 1806175 (2018).
282. Dai, B. *et al.* Encapsulating maytansinoid in pH-sensitive nanocarriers: The importance of using extremely potent cytotoxic agents and fast release for nanomedicine to achieve tumor elimination. *Nano Res.* **12**, 1959–1966 (2019).
283. Fontana, F., Figueiredo, P., Bauleth-Ramos, T., Correia, A. & Santos, H. A. Immunostimulation and Immunosuppression: Nanotechnology on the Brink. *Small Methods* **2**, 1700347 (2018).
284. Chen, N. *et al.* Co-Delivery of Disease Associated Peptide and Rapamycin via Acetalated Dextran Microparticles for Treatment of Multiple Sclerosis. *Adv. Biosyst.* **1**, 1700022 (2017).
285. Watkins-Schulz, R. *et al.* A microparticle platform for STING-targeted immunotherapy enhances natural killer cell- and CD8+ T cell-mediated anti-tumor immunity. *Biomaterials* **205**, 94–105 (2019).
286. Fontana, F. *et al.* Biohybrid Vaccines for Improved Treatment of Aggressive Melanoma with Checkpoint Inhibitor. *ACS Nano* **13**, 6477–6490 (2019).
287. V., H. K. *et al.* Needle-Free Delivery of Acetalated Dextran-Encapsulated AR-12 Protects Mice from Francisella tularensis Lethal Challenge. *Antimicrob. Agents Chemother.* **60**, 2052–2062 (2022).
288. Collier, M. A. *et al.* Host-mediated Leishmania donovani treatment using AR-12 encapsulated in acetalated dextran microparticles. *Int. J. Pharm.* **499**, 186–194 (2016).
289. Butzbach, K. *et al.* Receptor-mediated Uptake of Folic Acid-functionalized Dextran Nanoparticles for Applications in Photodynamic Therapy. *Polymers* vol. 11 at https://doi.org/10.3390/polym11050896 (2019).
290. Bertrand, N. *et al.* Mechanistic understanding of in vivo protein corona formation on polymeric nanoparticles and impact on pharmacokinetics. *Nat. Commun.* **8**, 777 (2017).
291. Ke, P. C., Lin, S., Parak, W. J., Davis, T. P. & Caruso, F. A Decade of the Protein Corona. *ACS Nano* **11**, 11773–11776 (2017).
292. Tenzer, S. *et al.* Rapid formation of plasma protein corona critically affects nanoparticle pathophysiology. *Nat. Nanotechnol.* **8**, 772–781 (2013).
293. Hadjidemetriou, M. & Kostarelos, K. Evolution of the nanoparticle corona. *Nat. Nanotechnol.* **12**, 288–290 (2017).
294. Cagliani, R., Gatto, F. & Bardi, G. Protein Adsorption: A Feasible Method for Nanoparticle Functionalization? *Mater. (Basel, Switzerland)* **12**, (2019).
295. Milani, S., Baldelli Bombelli, F., Pitek, A. S., Dawson, K. A. & Rädler, J. Reversible versus Irreversible Binding of Transferrin to Polystyrene Nanoparticles: Soft and Hard Corona. *ACS Nano* **6**, 2532–2541 (2012).
296. Barui, A. K., Oh, J. Y., Jana, B., Kim, C. & Ryu, J.-H. Cancer-Targeted Nanomedicine: Overcoming the Barrier of the Protein Corona. *Adv. Ther.* **3**, 1900124 (2020).
297. Vu, V. P. *et al.* Immunoglobulin deposition on biomolecule corona determines complement opsonization efficiency of preclinical and clinical nanoparticles. *Nat. Nanotechnol.* **14**, 260–268 (2019).
298. Owens, D. E. & Peppas, N. A. Opsonization, biodistribution, and pharmacokinetics of polymeric nanoparticles. *Int. J. Pharm.* **307**, 93–102 (2006).
299. Abuchowski, A., McCoy, J. R., Palczuk, N. C., van Es, T. & Davis, F. F. Effect of covalent attachment of polyethylene glycol on immunogenicity and circulating life of bovine liver catalase. *J. Biol. Chem.* **252**, 3582–3586 (1977).

300. Vllasaliu, D., Fowler, R. & Stolnik, S. PEGylated nanomedicines: recent progress and remaining concerns. *Expert Opin. Drug Deliv.* **11**, 139–154 (2014).

301. Suk, J. S., Xu, Q., Kim, N., Hanes, J. & Ensign, L. M. PEGylation as a strategy for improving nanoparticle-based drug and gene delivery. *Adv. Drug Deliv. Rev.* **99**, 28–51 (2016).

302. Yang, Q. & Lai, S. K. Anti-PEG immunity: emergence, characteristics, and unaddressed questions. *Wiley Interdiscip. Rev. Nanomed. Nanobiotechnol.* **7**, 655–677 (2015).

303. Vonarbourg, A., Passirani, C., Saulnier, P. & Benoit, J.-P. Parameters influencing the stealthiness of colloidal drug delivery systems. *Biomaterials* **27**, 4356–4373 (2006).

304. Barenholz, Y. Doxil®--the first FDA-approved nano-drug: lessons learned. *J. Control. Release* **160**, 117–134 (2012).

305. Guo, S. & Huang, L. Nanoparticles Escaping RES and Endosome: Challenges for siRNA Delivery for Cancer Therapy. *J. Nanomater.* **2011**, 742895 (2011).

306. Rodriguez, P. L. *et al.* Minimal 'Self' peptides that inhibit phagocytic clearance and enhance delivery of nanoparticles. *Science* **339**, 971–975 (2013).

307. Parodi, A. *et al.* Synthetic nanoparticles functionalized with biomimetic leukocyte membranes possess cell-like functions. *Nat. Nanotechnol.* **8**, 61–68 (2013).

308. Xiong, H., Wang, Z., Wang, C. & Yao, J. Correction to "Transforming Complexity to Simplicity: Protein-Like Nanotransformer for Improving Tumor Drug Delivery Programmatically". *Nano Lett.* **20**, 4060 (2020).

309. Anselmo, A. C. & Mitragotri, S. Nanoparticles in the clinic: An update. *Bioeng. Transl. Med.* **4**, e10143–e10143 (2019).

310. Paulis, L. E. *et al.* Distribution of lipid-based nanoparticles to infarcted myocardium with potential application for MRI-monitored drug delivery. *J. Control. Release* **162**, 276–285 (2012).

311. McCarthy, J. R. Nanomedicine and Cardiovascular Disease. *Curr. Cardiovasc. Imaging Rep.* **3**, 42–49 (2010).

312. Martín Giménez, V. M., Kassuha, D. E. & Manucha, W. Nanomedicine applied to cardiovascular diseases: latest developments. *Ther. Adv. Cardiovasc. Dis.* **11**, 133–142 (2017).

313. Bertrand, N., Wu, J., Xu, X., Kamaly, N. & Farokhzad, O. C. Cancer nanotechnology: The impact of passive and active targeting in the era of modern cancer biology. *Adv. Drug Deliv. Rev.* **66**, 2–25 (2014).

314. Matsumura, Y. & Maeda, H. A new concept for macromolecular therapeutics in cancer chemotherapy: mechanism of tumoritropic accumulation of proteins and the antitumor agent smancs. *Cancer Res.* **46**, 6387–6392 (1986).

315. Golombek, S. K. *et al.* Tumor targeting via EPR: Strategies to enhance patient responses. *Adv. Drug Deliv. Rev.* **130**, 17–38 (2018).

316. Iyer, A. K., Khaled, G., Fang, J. & Maeda, H. Exploiting the enhanced permeability and retention effect for tumor targeting. *Drug Discov. Today* **11**, 812–818 (2006).

317. Weis, S. M. Vascular permeability in cardiovascular disease and cancer. *Curr. Opin. Hematol.* **15**, 243–249 (2008).

318. Claesson-Welsh, L. Vascular permeability--the essentials. *Ups. J. Med. Sci.* **120**, 135–143 (2015).

319. Claesson-Welsh, L., Dejana, E. & McDonald, D. M. Permeability of the Endothelial Barrier: Identifying and Reconciling Controversies. *Trends Mol. Med.* **27**, 314–331 (2021).

320. Cheng, Q. *et al.* Selective organ targeting (SORT) nanoparticles for tissue-specific mRNA delivery and CRISPR–Cas gene editing. *Nat. Nanotechnol.* **15**, 313–320 (2020).

321. Dilliard, S. A., Cheng, Q. & Siegwart, D. J. On the mechanism of tissue-specific mRNA delivery by selective organ targeting nanoparticles. *Proc. Natl. Acad. Sci.* **118**, e2109256118 (2021).

322. Lin, Z. P. *et al.* Macrophages Actively Transport Nanoparticles in Tumors After Extravasation. *ACS Nano* **16**, 6080–6092 (2022).

323. Sindhwani, S. *et al.* The entry of nanoparticles into solid tumours. *Nat. Mater.* **19**, 566–575 (2020).

324. Kingston, B. R. *et al.* Specific Endothelial Cells Govern Nanoparticle Entry into Solid Tumors. *ACS Nano* **15**, 14080–14094 (2021).

325. Cuccarese, M. F. *et al.* Heterogeneity of macrophage infiltration and therapeutic response in lung carcinoma revealed by 3D organ imaging. *Nat. Commun.* **8**, 14293 (2017).

326. Miller, M. A. *et al.* Tumour-associated macrophages act as a slow-release reservoir of nano-therapeutic Pt(IV) pro-drug. *Nat. Commun.* **6**, 8692 (2015).

327. Bejerano, T., Etzion, S., Elyagon, S., Etzion, Y. & Cohen, S. Nanoparticle Delivery of miRNA-21 Mimic to Cardiac Macrophages Improves Myocardial Remodeling after Myocardial Infarction. *Nano Lett.* **18**, 5885–5891 (2018).

328. Dvir, T. *et al.* Nanoparticles Targeting the Infarcted Heart. *Nano Lett.* **11**, 4411–4414 (2011).

329. Formiga, F. R. *et al.* Sustained release of VEGF through PLGA microparticles improves vasculogenesis and tissue remodeling in an acute myocardial ischemia-reperfusion model. *J. Control. Release* **147**, 30–37 (2010).

330. Qi, Q. *et al.* Spatiotemporal delivery of nanoformulated liraglutide for cardiac regeneration after myocardial infarction. *Int. J. Nanomedicine* **12**, 4835–4848 (2017).

331. Chang, M.-Y. *et al.* Functionalized nanoparticles provide early cardioprotection after acute myocardial infarction. *J. Control. Release* **170**, 287–294 (2013).

332. Fan, C. *et al.* Myocardial protection by nanomaterials formulated with CHIR99021 and FGF1. *JCI insight* **5**, e132796 (2020).

333. Hwang, H. *et al.* Peptide-loaded nanoparticles and radionuclide imaging for individualized treatment of

myocardial ischemia. *Radiology* **273**, 160–167 (2014).

334.   Binsalamah, Z. M., Paul, A., Khan, A. A., Prakash, S. & Shum-Tim, D. Intramyocardial sustained delivery of placental growth factor using nanoparticles as a vehicle for delivery in the rat infarct model. *Int. J. Nanomedicine* **6**, 2667–2678 (2011).

335.   Sun, B. *et al.* RGD-PEG-PLA Delivers MiR-133 to Infarct Lesions of Acute Myocardial Infarction Model Rats for Cardiac Protection. *Pharmaceutics* vol. 12 at https://doi.org/10.3390/pharmaceutics12060575 (2020).

336.   Michele, M. *et al.* Inhalation of peptide-loaded nanoparticles improves heart failure. *Sci. Transl. Med.* **10**, eaan6205 (2018).

337.   Chen, X. *et al.* A non-invasive nanoparticles for multimodal imaging of ischemic myocardium in rats. *J. Nanobiotechnology* **19**, 82 (2021).

338.   Zheng, Y., Zhang, H., Hu, Y., Bai, L. & Xue, J. MnO nanoparticles with potential application in magnetic resonance imaging and drug delivery for myocardial infarction. *Int. J. Nanomedicine* **13**, 6177–6188 (2018).

339.   Tokutome, M. *et al.* Peroxisome proliferator-activated receptor-gamma targeting nanomedicine promotes cardiac healing after acute myocardial infarction by skewing monocyte/macrophage polarization in preclinical animal models. *Cardiovasc. Res.* **115**, 419–431 (2019).

340.   Vinodhini, A., Govindaraju, K., Singaravelu, G., Mohamed Sadiq, A. & Kumar, V. G. Cardioprotective potential of biobased gold nanoparticles. *Colloids Surfaces B Biointerfaces* **117**, 480–486 (2014).

341.   Cheng, K. *et al.* Magnetic antibody-linked nanomatchmakers for therapeutic cell targeting. *Nat. Commun.* **5**, 4880 (2014).

342.   Nahrendorf, M. *et al.* Dual Channel Optical Tomographic Imaging of Leukocyte Recruitment and Protease Activity in the Healing Myocardial Infarct. *Circ. Res.* **100**, 1218–1225 (2007).

343.   Florian, A. *et al.* Positive effect of intravenous iron-oxide administration on left ventricular remodelling in patients with acute ST-elevation myocardial infarction - a cardiovascular magnetic resonance (CMR) study. *Int. J. Cardiol.* **173**, 184–189 (2014).

344.   Yilmaz, A. *et al.* Imaging of myocardial infarction using ultrasmall superparamagnetic iron oxide nanoparticles: a human study using a multi-parametric cardiovascular magnetic resonance imaging approach. *Eur. Heart J.* **34**, 462–475 (2013).

345.   Weissleder, R., Lee, A. S., Khaw, B. A., Shen, T. & Brady, T. J. Antimyosin-labeled monocrystalline iron oxide allows detection of myocardial infarct: MR antibody imaging. *Radiology* **182**, 381–385 (1992).

346.   Shevtsov, M. A. *et al.* Detection of experimental myocardium infarction in rats by MRI using heat shock protein 70 conjugated superparamagnetic iron oxide nanoparticle. *Nanomedicine* **12**, 611–621 (2016).

347.   Kee, P. H. & Danila, D. CT imaging of myocardial scar burden with CNA35-conjugated gold nanoparticles. *Nanomedicine Nanotechnology, Biol. Med.* **14**, 1941–1947 (2018).

348.   Weissleder, R., Nahrendorf, M. & Pittet, M. J. Imaging macrophages with nanoparticles. *Nat. Mater.* **13**, 125–138 (2014).

349.   Mills, N. L. *et al.* Adverse cardiovascular effects of air pollution. *Nat. Clin. Pract. Cardiovasc. Med.* **6**, 36–44 (2009).

350.   Savi, M. *et al.* Titanium dioxide nanoparticles promote arrhythmias via a direct interaction with rat cardiac tissue. *Part. Fibre Toxicol.* **11**, 63 (2014).

351.   Heijmen, F. H., du Pont, J. S., Middelkoop, E., Kreis, R. W. & Hoekstra, M. J. Cross-linking of dermal sheep collagen with tannic acid. *Biomaterials* **18**, 749–754 (1997).

352.   Lu, Y. & Bennick, A. Interaction of tannin with human salivary proline-rich proteins. *Arch. Oral Biol.* **43**, 717–728 (1998).

353.   Saha, R. N., Vasanthakumar, S., Bende, G. & Snehalatha, M. Nanoparticulate drug delivery systems for cancer chemotherapy. *Mol. Membr. Biol.* **27**, 215–231 (2010).

354.   Gu, F. *et al.* Precise engineering of targeted nanoparticles by using self-assembled biointegrated block copolymers. *Proc. Natl. Acad. Sci. U. S. A.* **105**, 2586–2591 (2008).

355.   Jiang, W., Kim, B. Y. S., Rutka, J. T. & Chan, W. C. W. Nanoparticle-mediated cellular response is size-dependent. *Nature nanotechnology* vol. 3 145–150 at https://doi.org/10.1038/nnano.2008.30 (2008).

356.   Valencia, P. M. *et al.* Effects of ligands with different water solubilities on self-assembly and properties of targeted nanoparticles. *Biomaterials* **32**, 6226–6233 (2011).

357.   Bertrand, N. & Leroux, J. C. The journey of a drug-carrier in the body: an anatomo-physiological perspective. *J. Control. Release* **161 2**, 152–163 (2012).

358.   Monopoli, M. P., Åberg, C., Salvati, A. & Dawson, K. A. Biomolecular coronas provide the biological identity of nanosized materials. *Nat. Nanotechnol.* **7**, 779–786 (2012).

359.   Florence, A. T. 'Targeting' nanoparticles: the constraints of physical laws and physical barriers. *J. Control. Release* **164**, 115–124 (2012).

360.   Kirpotin, D. B. *et al.* Antibody targeting of long-circulating lipidic nanoparticles does not increase tumor localization but does increase internalization in animal models. *Cancer Res.* **66**, 6732–6740 (2006).

361.   Figueiredo, P. *et al.* Peptide-guided resiquimod-loaded lignin nanoparticles convert tumor-associated macrophages from M2 to M1 phenotype for enhanced chemotherapy. *Acta Biomater.* **133**, 231–243 (2021).

362.   Heusch, G. Cardioprotection: chances and challenges of its translation to the clinic. *Lancet (London, England)* **381**, 166–175 (2013).

363.   Dasa, S. S. K. *et al.* Development of target-specific liposomes for delivering small molecule drugs after reperfused myocardial infarction. *J. Control. Release* **220**, 556–567 (2015).

364.   Ferreira, M. P. A. *et al.* In vitro and in vivo assessment of heart-homing porous silicon nanoparticles. *Biomaterials* **94**, 93–104 (2016).

References

365. Kanki, S. *et al.* Identification of targeting peptides for ischemic myocardium by in vivo phage display. *J. Mol. Cell. Cardiol.* **50**, 841–848 (2011).

366. Ruoslahti, E. & MacKenna, D. A. Heart homing peptides and methods of using same. at (2001).

367. Calvieri, C., Rubattu, S. & Volpe, M. Molecular mechanisms underlying cardiac antihypertrophic and antifibrotic effects of natriuretic peptides. *J. Mol. Med.* **90**, 5–13 (2012).

368. Kiemer, A. K. & Vollmar, A. M. The atrial natriuretic peptide regulates the production of inflammatory mediators in macrophages. *Ann. Rheum. Dis.* **60 Suppl 3**, iii68-70 (2001).

369. Nguyen, M. M. *et al.* Enzyme-Responsive Nanoparticles for Targeted Accumulation and Prolonged Retention in Heart Tissue after Myocardial Infarction. *Adv. Mater.* **27**, 5547–5552 (2015).

370. Harel-Adar, T. *et al.* Modulation of cardiac macrophages by phosphatidylserine-presenting liposomes improves infarct repair. *Proc. Natl. Acad. Sci.* **108**, 1827 LP – 1832 (2011).

371. Su, T. *et al.* Platelet-Inspired Nanocells for Targeted Heart Repair After Ischemia/Reperfusion Injury. *Adv. Funct. Mater.* **29**, 1803567 (2019).

372. von Hundelshausen, P. & Weber, C. Platelets as Immune Cells. *Circ. Res.* **100**, 27–40 (2007).

373. Kim, S. H. *et al.* Cardiomyocyte-targeted siRNA delivery by prostaglandin E(2)-Fas siRNA polyplexes formulated with reducible poly(amido amine) for preventing cardiomyocyte apoptosis. *Biomaterials* **29**, 4439–4446 (2008).

374. Zhang, Y. *et al.* TISSUE REGENERATION. Inhibition of the prostaglandin-degrading enzyme 15-PGDH potentiates tissue regeneration. *Science* **348**, aaa2340 (2015).

375. Che, J. *et al.* Neutrophils Enable Local and Non-Invasive Liposome Delivery to Inflamed Skeletal Muscle and Ischemic Heart. *Adv. Mater.* **32**, 2003598 (2020).

376. Muzykantov, V. R., Sakharov, D. V, Smirnov, M. D., Samokhin, G. P. & Smirnov, V. N. Immunotargeting of erythrocytes-bound streptokinase provides local lysis of a fibrin clot. *Biochim. Biophys. Acta (BBA)-General Subj.* **884**, 355–362 (1986).

377. Danielyan, K. *et al.* Cerebrovascular thromboprophylaxis in mice by erythrocyte-coupled tissue-type plasminogen activator. *Circulation* **118**, 1442–1449 (2008).

378. Zaitsev, S. *et al.* Sustained thromboprophylaxis mediated by an RBC-targeted pro-urokinase zymogen activated at the site of clot formation. *Blood, J. Am. Soc. Hematol.* **115**, 5241–5248 (2010).

379. Anselmo, A. C. *et al.* Delivering Nanoparticles to Lungs while Avoiding Liver and Spleen through Adsorption on Red Blood Cells. *ACS Nano* **7**, 11129–11137 (2013).

380. Kolhar, P. *et al.* Using shape effects to target antibody-coated nanoparticles to lung and brain endothelium. *Proc. Natl. Acad. Sci. U. S. A.* **110**, 10753–10758 (2013).

381. Brenner, J. S. *et al.* Red blood cell-hitchhiking boosts delivery of nanocarriers to chosen organs by orders of magnitude. *Nat. Commun.* **9**, 2684 (2018).

382. Jia, H. *et al.* Accessing neuroinflammation sites: Monocyte/neutrophil-mediated drug delivery for cerebral ischemia. *Sci. Adv.* **5**, eaau8301 (2022).

383. Chung, A. S., Gao, Q. & Kao, W. J. Either integrin subunit β1 or β3 is involved in mediating monocyte adhesion, IL-1β protein and mRNA expression in response to surfaces functionalized with fibronectin-derived peptides. *J. Biomater. Sci. Polym. Ed.* **18**, 713–729 (2007).

384. Najmeh, S. *et al.* Neutrophil extracellular traps sequester circulating tumor cells via β1-integrin mediated interactions. *Int. J. cancer* **140**, 2321–2330 (2017).

385. Singh, R. *et al.* Modulation of infection-mediated migration of neutrophils and CXCR 2 trafficking by osteopontin. *Immunology* **150**, 74–86 (2017).

386. Haney, M. J. *et al.* Cell-mediated transfer of catalase nanoparticles from macrophages to brain endothelial, glial and neuronal cells. *Nanomedicine* **6**, 1215–1230 (2011).

387. San-Shan, H. *et al.* Immune cell shuttle for precise delivery of nanotherapeutics for heart disease and cancer. *Sci. Adv.* **7**, eabf2400 (2022).

388. Pang, H.-B. *et al.* An endocytosis pathway initiated through neuropilin-1 and regulated by nutrient availability. *Nat. Commun.* **5**, 4904 (2014).

389. Stevens, R., Stevens, L. & Price, N. C. The stabilities of various thiol compounds used in protein purifications. *Biochem. Educ.* **11**, 70 (1983).

390. Hirotaka, E. *et al.* One-Step Assembly of Coordination Complexes for Versatile Film and Particle Engineering. *Science (80-.).* **341**, 154–157 (2013).

391. Polinger, I. S. Separation of cell types in embryonic heart cell cultures. *Exp. Cell Res.* **63**, 78–82 (1970).

392. Yu, J. *et al.* Induced pluripotent stem cell lines derived from human somatic cells. *Science* **318**, 1917–1920 (2007).

393. Burridge, P. W. *et al.* Human induced pluripotent stem cell–derived cardiomyocytes recapitulate the predilection of breast cancer patients to doxorubicin-induced cardiotoxicity. *Nat. Med.* **22**, 547–556 (2016).

394. Karhu, S. T. *et al.* Stem cells are the most sensitive screening tool to identify toxicity of GATA4-targeted novel small-molecule compounds. *Arch. Toxicol.* **92**, 2897–2911 (2018).

395. Karhu, S. T. *et al.* GATA4-targeted compound exhibits cardioprotective actions against doxorubicin-induced toxicity in vitro and in vivo: establishment of a chronic cardiotoxicity model using human iPSC-derived cardiomyocytes. *Arch. Toxicol.* **94**, 2113–2130 (2020).

396. Zarif, J. C. *et al.* A phased strategy to differentiate human CD14+monocytes into classically and alternatively activated macrophages and dendritic cells. *Biotechniques* **61**, 33–41 (2016).

397. Guo, J. *et al.* Engineering multifunctional capsules through the assembly of metal–phenolic networks. *Angew. Chemie Int. Ed.* **53**, 5546–5551 (2014).

References

398. Andersen, A., Chen, Y. & Birkedal, H. Bioinspired Metal–Polyphenol Materials: Self-Healing and Beyond. *Biomimetics* vol. 4 at https://doi.org/10.3390/biomimetics4020030 (2019).
399. Krungchanuchat, S., Thongtem, T., Thongtem, S. & Pilapong, C. Characterization and cellular studies of molecular nanoparticle of iron (III)-tannic complexes; toward a low cost magnetic resonance imaging agent. *Biointerphases* **12**, 21005 (2017).
400. Aguilera, J. R. *et al.* Targeted multifunctional tannic acid nanoparticles. *RSC Adv.* **6**, 7279–7287 (2016).
401. Callahan, J. F. *et al.* Identification of Novel Inhibitors of the Transforming Growth Factor β1 (TGF-β1) Type 1 Receptor (ALK5). *J. Med. Chem.* **45**, 999–1001 (2002).
402. Ring, D. B. *et al.* Selective Glycogen Synthase Kinase 3 Inhibitors Potentiate Insulin Activation of Glucose Transport and Utilization In Vitro and In Vivo. *Diabetes* **52**, 588 LP – 595 (2003).
403. Kou, L., Sun, J., Zhai, Y. & He, Z. The endocytosis and intracellular fate of nanomedicines: Implication for rational design. *Asian J. Pharm. Sci.* **8**, 1–10 (2013).
404. Frauke Pistel, K., Breitenbach, A., Zange-Volland, R. & Kissel, T. Brush-like branched biodegradable polyesters, part III: Protein release from microspheres of poly(vinyl alcohol)-graft-poly(d,l-lactic-co-glycolic acid). *J. Control. Release* **73**, 7–20 (2001).
405. Ahmad Nor, Y. *et al.* Shaping Nanoparticles with Hydrophilic Compositions and Hydrophobic Properties as Nanocarriers for Antibiotic Delivery. *ACS Cent. Sci.* **1**, 328–334 (2015).
406. Garlick, P. B., Radda, G. K. & Seeley, P. J. Studies of acidosis in the ischaemic heart by phosphorus nuclear magnetic resonance. *Biochem. J.* **184**, 547–554 (1979).
407. Khabbaz, K. R., Zankoul, F. & Warner, K. G. Intraoperative metabolic monitoring of the heart: II. Online measurement of myocardial tissue pH. *Ann. Thorac. Surg.* **72**, S2227-33; discussion S2233-4, S2267-70 (2001).
408. Santos, H. A. *et al.* In vitro cytotoxicity of porous silicon microparticles: Effect of the particle concentration, surface chemistry and size. *Acta Biomater.* **6**, 2721–2731 (2010).
409. Chang, S.-F. *et al.* SB203580 increases G-CSF production via a stem-loop destabilizing element in the 3' untranslated region in macrophages independently of its effect on p38 MAPK activity. *J. Biomed. Sci.* **23**, 3 (2016).
410. Haghighat, A., Weiss, D., Whalin, M. K., Cowan, D. P. & Taylor, W. R. Granulocyte Colony-Stimulating Factor and Granulocyte Macrophage Colony-Stimulating Factor Exacerbate Atherosclerosis in Apolipoprotein E–Deficient Mice. *Circulation* **115**, 2049–2054 (2007).
411. Feng, Y., Liang, Y., Ren, J. & Dai, C. Canonical Wnt Signaling Promotes Macrophage Proliferation during Kidney Fibrosis. *Kidney Dis. (Basel, Switzerland)* **4**, 95–103 (2018).
412. Reed, E. B. *et al.* Anti-fibrotic effects of tannic acid through regulation of a sustained TGF-beta receptor signaling. *Respir. Res.* **20**, 168 (2019).
413. Pandey, K. N. Intracellular trafficking and metabolic turnover ofligand-bound guanylyl cyclase/atrial natriuretic peptide receptor-A into subcellular compartments. *Mol. Cell. Biochem.* **230**, 61–72 (2002).
414. Hua, X. *et al.* Multi-level transcriptome sequencing identifies COL1A1 as a candidate marker in human heart failure progression. *BMC Med.* **18**, 2 (2020).
415. Matsui, Y. *et al.* Role of Osteopontin in Cardiac Fibrosis and Remodeling in Angiotensin II-Induced Cardiac Hypertrophy. *Hypertension* **43**, 1195–1201 (2004).
416. Palomer, X. *et al.* SIRT3-mediated inhibition of FOS through histone H3 deacetylation prevents cardiac fibrosis and inflammation. *Signal Transduct. Target. Ther.* **5**, 14 (2020).
417. Khalil, H. *et al.* Fibroblast-specific TGF-β-Smad2/3 signaling underlies cardiac fibrosis. *J. Clin. Invest.* **127**, 3770–3783 (2017).
418. Duerrschmid, C., Trial, J., Wang, Y., Entman, M. L. & Haudek, S. B. Tumor necrosis factor: a mechanistic link between angiotensin-II-induced cardiac inflammation and fibrosis. *Circ. Heart Fail.* **8**, 352–361 (2015).
419. Luo, W. *et al.* c-Myc inhibits myoblast differentiation and promotes myoblast proliferation and muscle fibre hypertrophy by regulating the expression of its target genes, miRNAs and lincRNAs. *Cell Death Differ.* **26**, 426–442 (2019).
420. Feliciani, C. *et al.* Tannic Acid Induces in vitro Acantholysis of Keratinocytes via IL-1α and TNF-α. *Int. J. Immunopathol. Pharmacol.* **20**, 289–299 (2007).
421. Sun, X. & Kaufman, P. D. Ki-67: more than a proliferation marker. *Chromosoma* **127**, 175–186 (2018).
422. Villani, V. *et al.* Phosphorylated Histone H3 (PHH3) Is a Superior Proliferation Marker for Prognosis of Pancreatic Neuroendocrine Tumors. *Ann. Surg. Oncol.* **23**, 609–617 (2016).
423. Wu, Q., Zhang, W., Mu, T., Song, T. & Li, D. Aurora B kinase is required for cytokinesis through effecting spindle structure. *Cell Biol. Int.* **37**, 436–442 (2013).
424. Crosio, C. *et al.* Mitotic phosphorylation of histone H3: spatio-temporal regulation by mammalian Aurora kinases. *Mol. Cell. Biol.* **22**, 874–885 (2002).
425. Leone, M., Magadum, A. & Engel, F. B. Cardiomyocyte proliferation in cardiac development and regeneration: a guide to methodologies and interpretations. *Am. J. Physiol. Circ. Physiol.* **309**, H1237–H1250 (2015).
426. Clark, A. G. & Paluch, E. Cell Cycle in Development, Results, and Problems in Cell Differentiation 53. (2011).
427. Huang, S. & Frangogiannis, N. G. Anti-inflammatory therapies in myocardial infarction: failures, hopes and challenges. *Br. J. Pharmacol.* **175**, 1377–1400 (2018).